Study on surface modification of RO membrane for improvement of anti-biofouling property

Yang, Zhe

(Degree)
博士（学術）

(Date of Degree)
2020-03-25

(Date of Publication)
2022-03-25

(Resource Type)
doctoral thesis

(Report Number)
甲第7774号

(URL)
https://hdl.handle.net/20.500.14094/D1007774

Doctoral Dissertation

Study on surface modification of RO membrane for improvement of anti-biofouling property

耐バイオファウリング性の向上を目的とした RO 膜の表面修飾に関する研究

January 2020

Graduate School of Engineering

Kobe University

YANG ZHE

Acknowledgment

Firstly, I would like to express my sincere gratitude to my supervisor Professor Hideto Matsuyama of the Department of Chemical Science and Engineering, Kobe University, for his continuous support on my Ph.D study. His gracious supervision strengthened my academic knowledge and confidence so that I was able to complete my research. It would be difficult to be awarded Ph.D degree without his instruction.

I would also like to sincerely thank Professor Ryosuke Takagi for his kind advises throughout this work. He not only provided me with valuable comments and suggestions on academic writing, but also introduced me Japanese culture. I really enjoy discussing with him and have learned many writing skills of academic papers. Without his guidance and support, this thesis would not be possible.

I am pleased to say thank you to Dr. Daisuke Saeki of Shinshu University and Dr. Xinyu Zhang of Soochow University for guiding me well from the selection of research topic to the analysis of results. They gave me enough support, encouragement and motivation to accomplish my Ph.D study.

I would like to thank the examiners: Professor Ogino Chiaki and Professor Mori Atsunori, for their insightful comments and encouragement, but also for the suggestive comments which incented me to improve my research from various perspectives. I also thank Professor Tomohisa Yoshioka and Dr. Hao-Chen Wu for their kind help on simulation analysis during my studies at Kobe University.

I thank the members of Prof. Matsuyama's laboratory. It is my pleasure to know each of them and I have great benefits from them during the stimulating discussions. For studying, they offered me a lot of help and inspiration these years. For life, they brought me a lot of happiness.

Last but not at least, I am grateful to my lovely parents, who have provided me moral and emotional support in my life. I am also grateful to my other family members and friends who have supported me along the way.

YANG ZHE

Graduate School of Engineering

Kobe University, 2020

Table of Contents

Chapter 1

General introduction

1.1. Global crisis of freshwater scarcity

Water resource is essential and valuable on the earth. As water covers 70% of our planet, people always consider that it will be plentiful. However, only 3% of the world's water is fresh water, and two-thirds of that is tucked away in frozen glaciers or otherwise unavailable for our use (Fig. 1.1). Nevertheless, during the last few decades, human activities enhanced freshwater scarcity becoming a threat to sustainable development of human society.

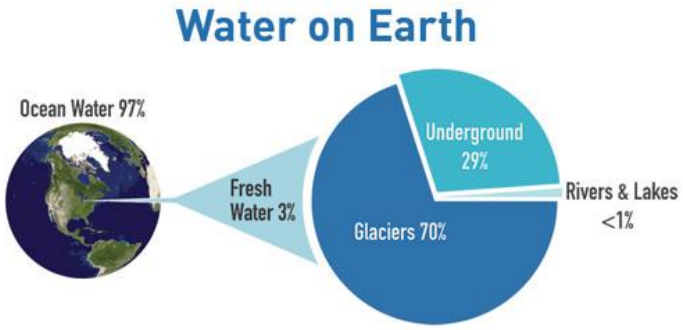

Fig. 1.1. Distribution of water on earth.

The famous Malthusian doctrine states that "population increases in a geometric ratio, whilst the means of subsistence increase in an arithmetic ratio" [1]. This is backed by the fact that the

global fresh water demand increased more than double compared to the concurrent increase in population between 1900 and 1995 [2]. Right now, many developing countries are undergoing rapid industrialization without appropriate wastewater management systems, and are continually facing increasing water scarcity issues (Fig. 1.2). The most serious unresolved water problem is the continued failure to meet basic human needs for water. 4.0 billion people, two-thirds of the world population, are suffering from severe water scarcity [3]; more than 1 billion people worldwide lack access to safe drinking water [4]; 2.4 billion people lack access to adequate sanitation services [5]. Lack of access to safe drinking water causes inadequate sanitation, exposing people to massive health issues, such as cholera and typhoid fever, and other water-borne illnesses. Particularly, it estimated that the diarrhoeal diseases annually cost the lives of 2.18 million people, three-quarters of whom are children younger than 5 years old [6].

Considering the improvement of water availability, the most pressing challenges today include the recovery of clean water from seawater which is the most abundant global water resource, and the treatment and recycle of wastewater.

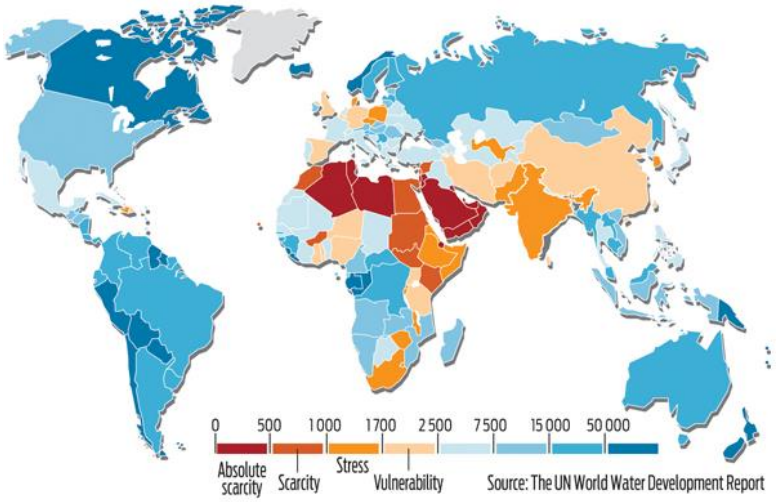

Fig. 1.2. Freshwater availability (m^3 per person, per year, 2013) from The UN World Development Report. (https://www.tes.com/lessons/Cr34uhFf5x0L3Q/water)

1.2. Wastewater treatments

To solve the water scarcity issues, a multitude of techniques classified in conventional methods, established recovery processes and emerging removal methods have been developed to remove solids including colloids, organic matter, nutrients, and soluble contaminants (metals, organics, etc.) from effluents (Fig. 1.3). One of the promising methods for high quality wastewater treatment and resolving water scarcity is membrane technology, which is used to treat wastewater before discharge to environment, to recover materials used in industry before they enter waste streams, and to treat water for potable use. Most importantly, membranes enable us to utilize water resources such as the seawater that was previously inaccessible due to technical or economic considerations [7]. These capabilities of membranes have been significant in driving their use in seawater and wastewater treatments, especially in areas with the shortage of water supplies.

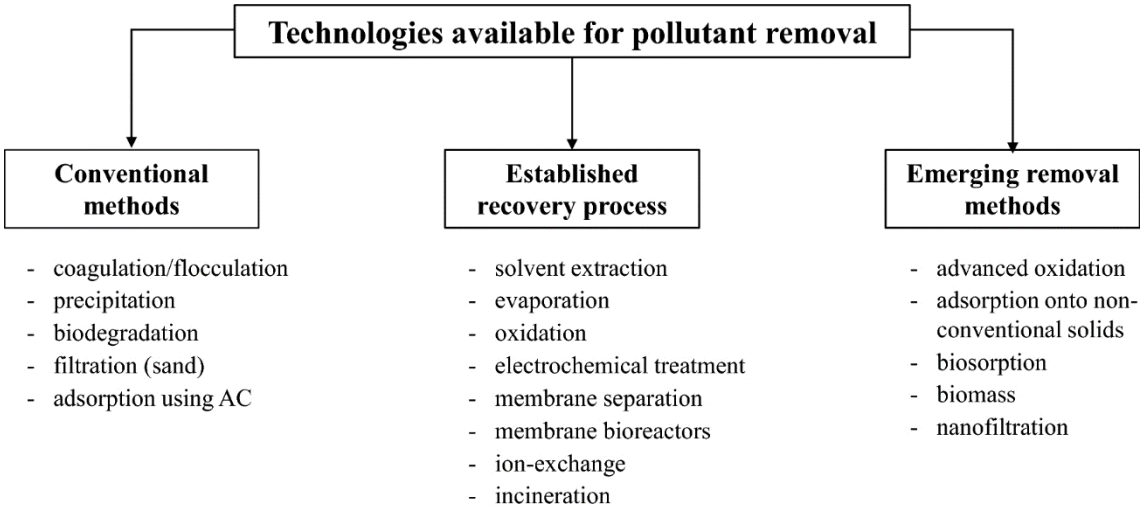

Fig. 1.3. Classification of technologies available for pollutant removal and examples of techniques [8].

1.3. Membrane technology

1.3.1. Water purification principle with membrane

A membrane is a semi-permeable barrier through which one type of substance can pass more readily than others, thus presenting the basis of a separation process. As shown in Fig. 1.4, in wastewater treatment, the membrane rejects pollutants, which may be suspended or dissolved, and produces the purified water [9]. The main advantages of membrane technology for wastewater treatment are: produce of high quality effluent (low turbidity, low total dissolved solids, 90-100% pathogen removal), ease of operation, 50-70% less foot-print than conventional technologies, and less chemicals usage for the process [10, 11].

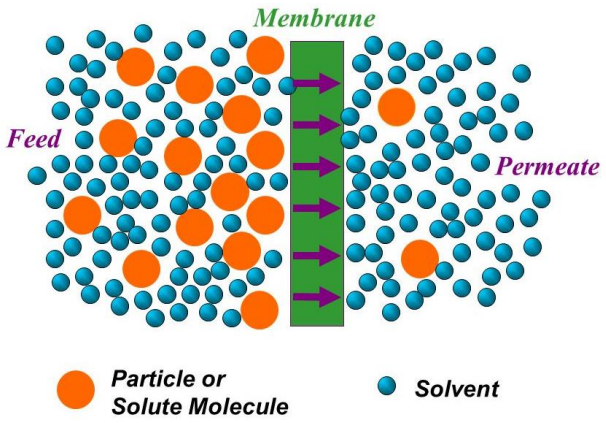

Fig.1.4. Principle of membrane separation process [12].

1.3.2. Membrane classifications

Water treatment membranes are usually pressure driven membranes through which a solvent (usually water) permeates using a pressure difference between the feed and permeate sides as a driving force [13]. Based on the pore size, the membranes are classified into microfiltration (MF), ultrafiltration (UF), nanofiltration (NF), and reverse osmosis (RO) (Fig. 1.5).

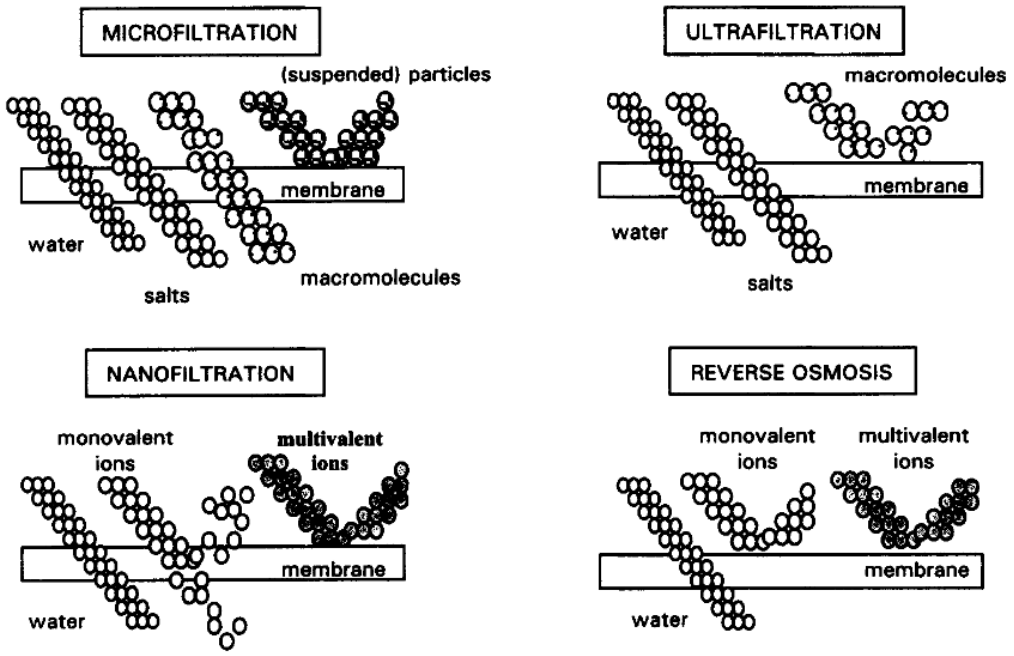

Fig. 1.5. Schematic illustration of microfiltration, ultrafiltration, nanofiltration, and reverse osmosis [13].

Characteristics of all membrane processes are summarized in Table 1.1. MF membranes have the largest pores, ranging from 100 to 10,000 nm, and the highest water permeability, so that a sufficient water flux is obtained at a low pressure. In contrast, UF membranes have smaller pores (2 to 100 nm), and the permeability is considerably lower than that in MF. Then, higher pressure is needed than MF. In both MF and UF processes, components larger than the pore size are removed by a sieving mechanism. In practical applications, MF is an efficient pretreatment to remove particles that may cause problems in further treatment steps, while UF is typically applied to remove large dissolved molecules such as natural organic materials (NOM).

In the case of NF, the pore sizes (0.5 to 2 nm) are smaller than that of UF, which makes NF suitable for the removal of relatively small organics such as organic micropollutants and color from groundwater and surface water. Furthermore, polymeric NF membranes with ionic groups would present a surface charge in the presence of a feed solution. This surface charge makes

possible the removal of coions smaller than the pore size of membrane by the electrostatic repulsion between the membrane charge and the ions in feed (so-called Donnan exclusion).

RO membranes are dense membranes without predefined pores and capable of rejecting nearly all colloidal or dissolved matter from an aqueous solution, producing a concentrate brine and a permeate which is almost pure water [14]. Therefore, RO membrane technology is widely used in seawater desalination, drinking water production, brackish water treatment and wastewater treatment. RO is currently the most energy-efficient technology for desalination, with energy cost about 1.8 kWh/m^3, which is much lower than that of other technologies, such as thermal-based desalination methods [15]. Also, RO membrane has the advantages of high water permeability and salt rejection, as well as fulfillment of the most rigorous rules for public health, environmental protection and separation process [16].

The aim of this thesis is related to the improvement of RO membrane performance. Thus, the development of RO membrane will be discussed as below.

Table 1.1. Classification of pressure-driven membrane processes (MF, UF, NF, and RO) and their characteristics [13].

	Microfiltration (MF)	**Ultrafiltration (UF)**	**Nanofiltration (NF)**	**Reverse Osmosis (RO)**
Permeability (l/h.m^2.bar)	> 1,000	10 – 1,000	1.5 – 30	0.05 – 1.5
Pressure (bar)	0.1 - 2	0.1 – 5	3 – 20	5 – 120
Pore size (nm)	100 – 10,000	2 – 100	0.5 – 2	< 0.5
Rejection				
• Monovalent ions	-	-	-	+
• Multivalent ions	-	-/+	+	+
• Small organic compounds	-	-	-/+	+
• Macromolecules	-	+	+	+
• Particles	+	+	+	+
Separation mechanism	Sieving	Sieving	Sieving Charge effects	Solution - Diffusion
Applications	Clarification; pretreatment; removal of bacteria	Removal of macromolecules, bacteria, viruses	Removal of (multivalent) ions and relatively small organics	Ultrapure water; desalination

1.4. Reverse osmosis membrane

1.4.1. Principle of reverse osmosis process

Osmosis is a natural phenomenon, occurring without any external energy. Osmosis is defined as a process of molecules passing through a semi-permeable membrane from a less-concentrated solution into a more-concentrated solution (Fig. 1.6 (a)).

On the other hand, reverse osmosis, commonly referred to as RO, is a process where water molecules, but not majority of the dissolved salts, organics, bacteria and pathogens, permeate through RO membrane from a more-concentrated solution into a less-concentrated solution (Fig. 1.6 (b)). In RO, an external pressure greater than the osmotic pressure is applied as a driving force. This process allows desalination of feed water permeating pure water while holding back a majority of contaminants.

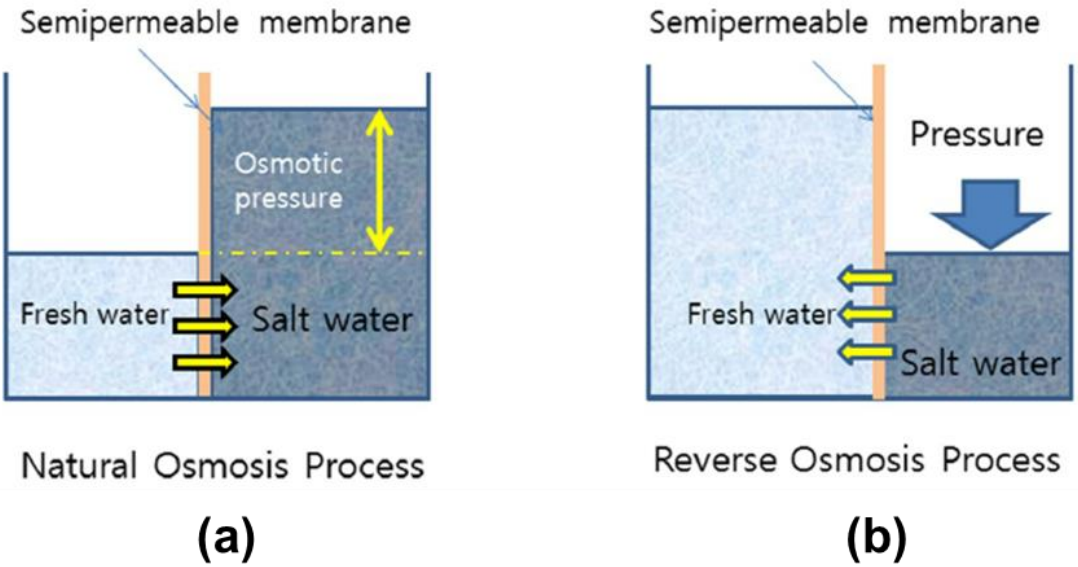

Fig. 1.6. Principles of (a) natural osmosis process and (b) reverse osmosis process.

1.4.2. Development of reverse osmosis membrane

The progress in RO technology is mainly depended on the development of RO membranes because the membrane plays a key role in the technological and economic efficiency of RO process. In the early 1960s, Loeb and Sourirajan developed a method for making asymmetric cellulose acetate membranes with relatively high water flux and separation factor [17]. Especially since the invention of robust thin-film composite (TFC) aromatic polyamide membranes in 1980s [18], RO process became both possible and practical. Further, the energy recovery systems developed in recent years, such as the Pelton wheel, turbocharger, pressure exchanger and Grundfos Pelton wheel [19], have greatly reduced energy consumption and operation costs, making RO technology more competitive.

Commercial interest in RO technology is increasing globally due to continuous improvements in the RO process, which in turn lead to significant cost reductions. These advances include developments in membrane materials, process design, feed pretreatment, and reduction in energy consumption. The beneficial outcomes are shown quantitatively in Figs. 1.7 (a), (b), and (c). During 1978 to 2008, the salt passage seven-fold decreased, which greatly expanded the range of saline feeds that can be treated to meet the stringent potable water standards (Fig. 1.7(a)). Since 1978, the increased water permeability of RO membranes, as well as the enhanced biological, chemical, and mechanical strength, have reduced the membrane cost per unit volume of produced water by more than 10 times (Fig. 1.7(b)). In 2006, the combined efforts to maximize permeate flux and energy recovery , as well as minimizing fouling and concentration polarization, have decreased the energy consumption from 12 kWh m^{-3} in the 1970s to less than 2 kWh m^{-3} in 2006 (Fig. 1.7(c)) [20].

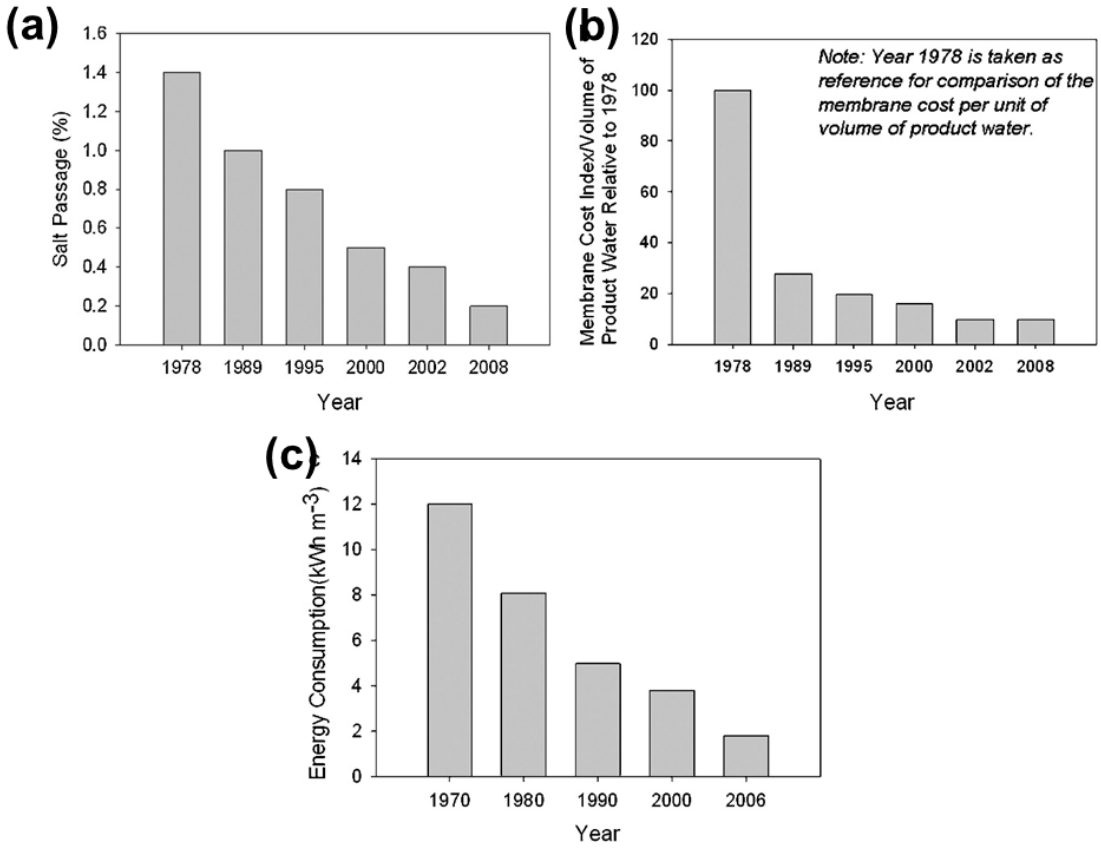

Fig. 1.7. Development of RO membrane in recent decades [20]: (a) Improvement in salt rejection, (b) Reduction in membrane cost, and (c) Reduction in energy consumption.

So far, most commercially available RO membranes are still asymmetric cellulose type (cellulose acetate, triacetate, cellulose diacetate or their blend) and TFC type. The asymmetric cellulose RO membrane is prepared by phase inversion method, while the TFC RO membrane is fabricated by forming a dense aromatic polyamide skin layer on a microporous support such as polysulfone via interfacial polymerization (Fig. 1.8) [14]. Compared with cellulose membrane, the TFC aromatic polyamide membrane exhibits superior water flux and salt rejection, resistance to pressure compaction, wider operating temperature range and pH range, and higher stability to biological attack [21]. Therefore, it dominates RO membrane field nowadays. In this thesis, the TFC polyamide RO membrane was selected as the membrane substrate.

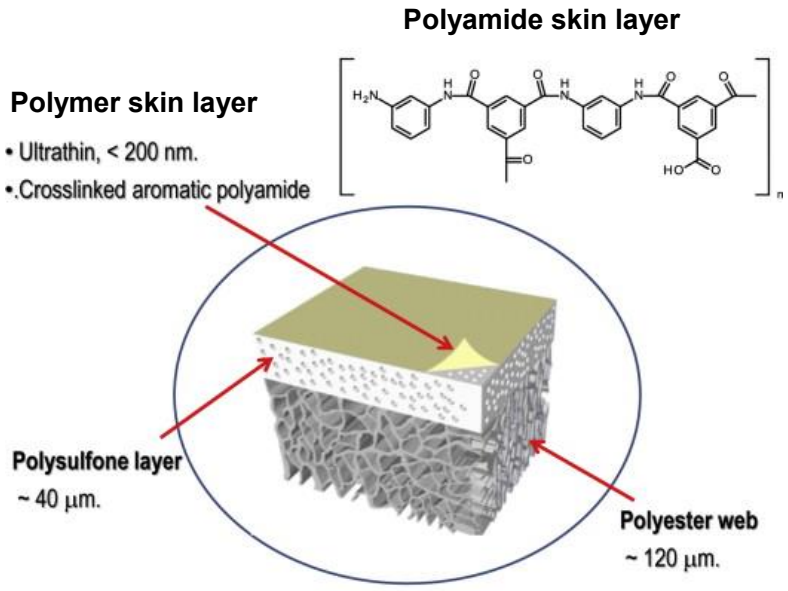

Fig. 1.8. Composition of TFC polyamide RO membrane [22].

1.4.3. Membrane fouling

Despite its many advantages, one of obstacles to the widespread use of TFC polyamide RO membrane is the proneness to fouling [23]. Fouling is a process where solute or particles in feeding water deposit onto RO membrane surface in a way that causes water flux decline and affects the quality of the produced water. Although the performance of fouled RO membranes can be partially restored by appropriate cleaning methods [24, 25], it will inevitably increase operation difficulty and decrease membrane's life time, which will be translated into higher costs.

Membrane fouling occurs as a consequence of interactions between the membrane surface and the various solutes/foulants in the wastewater. There are mainly four types of foulants causing RO membrane fouling (Fig.1.9):

i) colloidal (suspended particles such as silica);

ii) organic (natural organic matters such as humic acid);

iii) scaling (salt precipitations such as metal hydroxides and carbonates);

iv) biological (biofouling, adhesion and accumulation of micro-organisms, forming biofilms).

The first three types of fouling can generally be controlled by reducing the foulant concentration in the water phase. However, biofouling is hard to control by simply reducing the foulant concentration in the water phase [26].

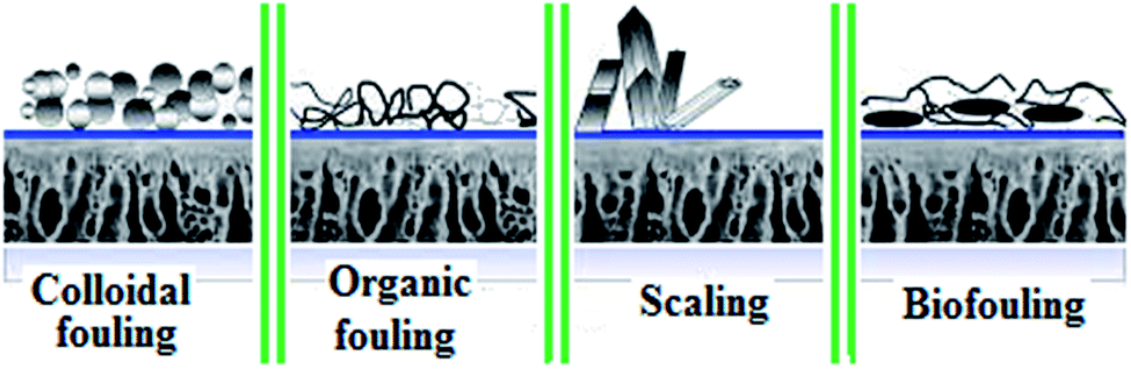

Fig. 1.9. Four types of RO membrane fouling [27].

As descripted in Fig.1.10, biofouling is ascribed to the formation of biofilm, which occurs through a cascade of events including the initial bacterial adhesion followed by extracellular polymeric substances (EPS) production, bacterial growth and proliferation. Even if 99.99% of bacteria are eliminated by pretreatment (e.g. microfiltration or biocide application), a few surviving bacteria will enter the system, adhere to surfaces, and multiply at the expense of biodegradable substances dissolved in the bulk aqueous phase. Therefore, even after significant pretreatment of the feed, membrane biofouling still occurs extensively on RO membranes.

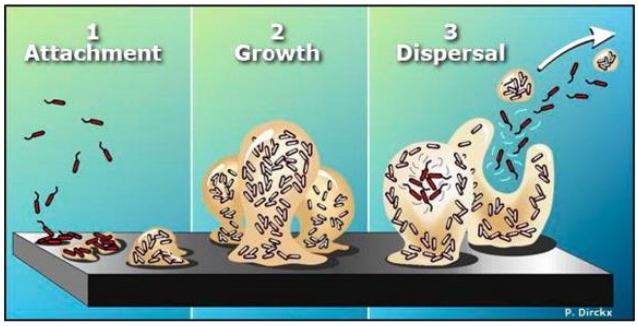

Fig. 1.10. Development of biofilm formation [28].

Effective prevention of microbial growth in membrane filtration is achieved only by treatment with oxidizing agents such as sufficiently high concentration chlorine. However, this method cannot be viewed as an ultimate solution, because of the growth of environmental concerns and the strictive legislative regulations regarding the discharge of chlorinated brines. In addition, the high organic matter concentration in feed water will consume the oxidizing agent and result in by-products [29, 30]. Thus, although RO membrane is considered as an important part in water treatment, the biofouling is still an unsolved problem nowadays. It is clear that there is a great incentive to eliminate biofouling in the RO process.

1.5. Fouling control strategies

Conventionally, fouling can be reduced by pretreatments of the feed solution, chemical cleaning, and back-wash. It can also be minimized by optimizing the module (hydrodynamic conditions) and the process conditions or cleaning the membranes frequently [31]. The main fouling control strategies are discussed as follow.

1.5.1. Pretreatments

Pretreatments have been widely used in RO processes, showing the advantages of improving the feed water quality greatly to ensure reliable RO operation as well as to prolong membrane life.

A statistical analysis in Fig. 1.11 revealed the common RO pretreatment technologies studied in the past 10 years. As shown in Fig. 1.11, coagulation/flocculation, UF, and MF are the three technologies that have been most studied by researchers as RO pretreatments. In fact, UF/MF filtration as a pretreatment of RO is becoming more and more popular in recent years. Coagulation/flocculation has long been used as a pretreatment for not only RO but NF and other technologies as well. Fig. 1.12 shows the flow diagram of RO pretreatment processes with their effects in removing contaminants from feed water and roles in fouling control.

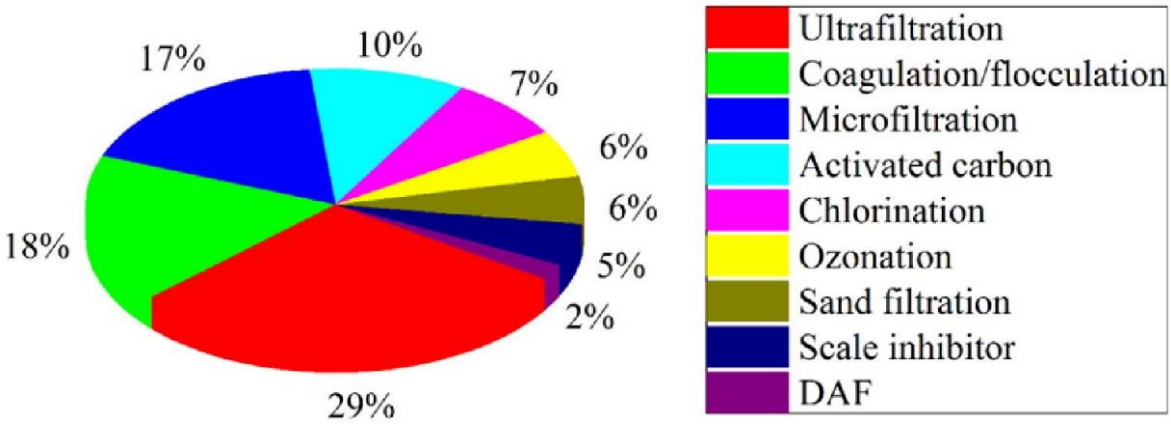

Fig. 1.11. Common studied RO pretreatments in the past 10 years [31].

DAF: dissolved air flotation.

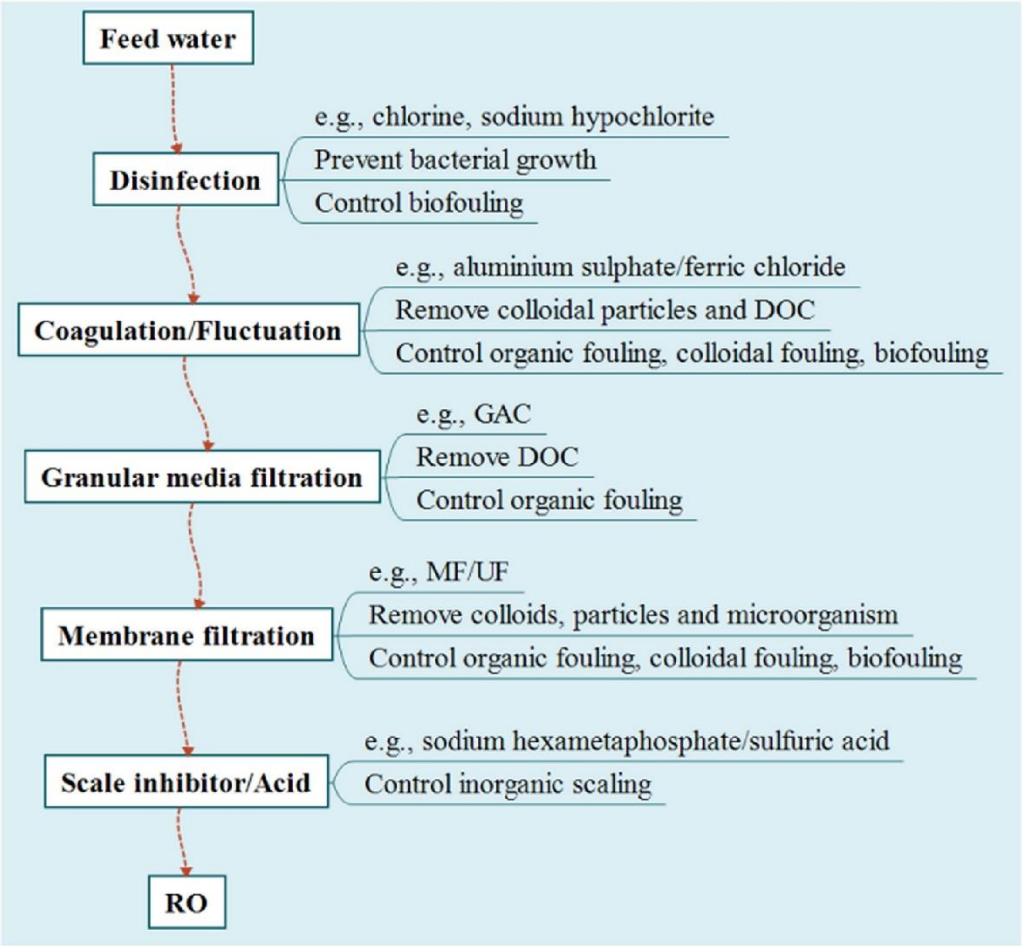

Fig. 1.12. Schematic diagram of RO pretreatment processes and their roles in fouling control. Figure from [31].

1.5.2. Membrane monitoring

In-situ and real-time monitoring of RO performances is necessary to evaluate the severity of fouling on membrane and correspondingly to conduct cleaning timely. Observation of pressure, flow and conductivity is reported to be the most effective way for in-situ and real-time monitoring the RO performances [32]. Early detection of scale formation in RO systems remains challenging. Currently, many monitoring techniques are not sensitive enough to detect the subtle changes occurring on the membrane in an early fouling stage. In other words, the signals delivered by these monitoring parameters only show obvious fouling formation [33].

1.5.3. Membrane cleaning

Periodic membrane cleaning is of great importance during water treatment processes [34, 35]. There are a variety of cleaning methods (e.g., chemical and physical) and their cleaning efficiency could be evaluated by resistance removal and flux recovery [36-38]. For chemical cleaning, selecting proper chemical agents is important, which is usually done by considering the fouling types and foulants components, as well as the chemical properties and economic factors. Also, no chemical damages should be produced by the chemical agents. Chemical agents could react with the foulants and as a result, the cohesion forces between foulants as well as the adhesion of foulants to membrane surface could be reduced, making foulants easy to be removed. The commonly used chemical agents include acids, bases, surfactants and chelating agents [39]. Acids, such as hydrochloric acid, nitric acid and sulfuric acid are effective in removing membrane scaling [40] while alkaline solutions such as sodium hydroxide are more effective in removing organic fouling and biofouling [41, 42]. The commonly used chelating agent is ethylene diamine tetra acetic acid (EDTA) [38]. EDTA cleaning efficiency is very sensitive to solution pH [24]. For physical cleaning, rinsing with water is the most frequent method used in practice. Furthermore, a combination of chemical and physical cleaning can be more efficient, where the former contributing to loosening of the foulant layer while the latter promoting its removal via fluid shear force [43].

1.5.4. Surface modification

Fouling is a surface phenomenon i.e., only the membrane surface properties determine the interaction between the foulant and the membrane surface. Therefore, one attractive way for fouling mitigation is the membrane surface modification. The goal of the modification is to

eliminate the interaction between the membrane surface and the foulant while preserving the other advantageous characteristics of membrane. Specifically, the modification layer can reduce the membrane's fouling propensity by changing the surface roughness, hydrophilicity, and surface charge which are known to be strongly related to fouling and influence the interaction between the membrane surface and the foulants [44, 45] as described as follows:

(i) Roughness: Increase in the surface roughness increases the specific surface area, thus resulting in more available surface for foulants to attach. In addition, since rough surfaces have contours and valleys morphology, they provide locations where foulants can attach without being removed by shear forces. As a result, a membrane with a rougher surface is more favorable for foulants attachment and accelerates fouling rates [46, 47] while a membrane with a smooth surface is not as easily fouled.

(ii) Hydrophilicity: Hydrophilicity of membrane surface is evaluated by water contact angle which is the angle between a water droplet and the membrane surface in the air. A surface is evaluated as hydrophilic when the water contact angle is < 90° and that as hydrophobic when the water contact angle is >90°. It has been well demonstrated that membranes with hydrophilic surfaces are less susceptible to fouling [48, 49]. For example, Nabe et al. found that the water flux decreased with an increase of water contact angle of the membrane surface during filtration of bovine serum albumin (BSA) solution, i.e. an increase in membrane hydrophobicity resulted in an enhancement in membrane fouling [50]. This finding may be explained by the fact that a thin layer of bounded water, also known as hydration layer, exists on the surface of hydrophilic membrane due to the formation of hydrogen bonds. This layer can prevent, or reduce, undesirable adsorption of hydrophobic foulants to the membrane surface (Fig. 1.13a). Therefore, an increase in the hydrophilicity of the membrane surface is often a key goal for reducing membrane fouling including biofouling;

(iii) Surface charge: Charged foulants tend to cause fouling due to electrostatic attraction between the foulants and the membrane surface, if foulants have a counter-charge of membrane. For example, if foulants have a negative charge, the fouling of membranes with positively charged is enhanced due to electrostatic attraction, whereas for negatively charged membrane, fouling is usually hindered because of electrostatic repulsion (Fig. 1.13b) [41, 51]. Therefore, the reducing fouling based only on electrostatic repulsion is not feasible

To summarize, the main goals of membrane surface modification are to increase the membrane hydrophilicity, decrease its surface roughness and introduce of suitable charge groups in order to minimize undesired interactions with potential foulants [52].

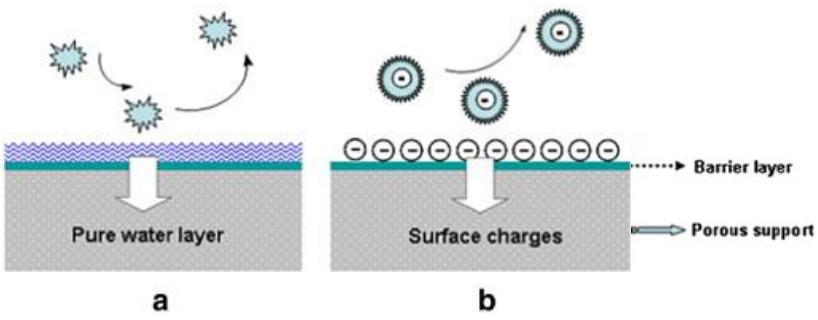

Fig. 1.13. The low fouling mechanism of (a) the hydrophilic surface and (b) the charged surface. Figure from [52].

1.6. Surface modification methods

Membrane surface modification can be achieved using physical or chemical method or a combination of the both. The choice of the specific type of methods depends on the chemical structure of membrane surface and the desired characteristics of the modified surface [53]. The main methods for membrane surface modification are discussed below.

1.6.1. Blending

Blending is a method that addition of additives to the membrane during its fabrication. Blending of polymers with different hydrophilicity is an approach that takes into account both permeability and mechanical stability of the membranes [54-56]. In particular, the polymers with similar structures are more suitable to blend with, in which the compatibility between the polymers may not be an obstacle. Recently, abundant studies have been done about incorporating hydrophilic sulfonated polymers into the membrane matrix, including sulfonated polysulfone (SPSf) [57], sulfonated polyphenylenesulfone (SPPSU) [58], and sulfonated poly(ether ketone) (SPEK) [59]. In addition, the incorporation of inorganic materials into the organic polymer matrix by the blending strategy has attracted great interests due to their completely hydrophilic characteristic [60].

1.6.2. Surface coating

A simple method of surface modification is a coating of membrane surface with polymers which have antifouling properties such as resistance to nonspecific protein adsorption or bacterial adhesion. These polymers can physically adhere to the surface by Van-der Waals interactions. For example, polyelectrolytes can be attached via electrostatic and hydrophobic interactions using the layer-by-layer deposition technique.

1.6.3. Grafting

An attractive and vast studied method is polymer grafting. The grafting of a functional antifouling polymer onto the membrane surface is a beneficial technique because the grafted polymer is covalently attached and can also change the surface properties of a membrane with limited influence on its bulk properties. Grafting can be accomplished by either attaching a grown

polymer from the solution to the membrane ("grafting to", Fig. 1.14(a)) or growing a polymer from the membrane surface ("grafting from", Fig. 1.14(b)) which is more common.

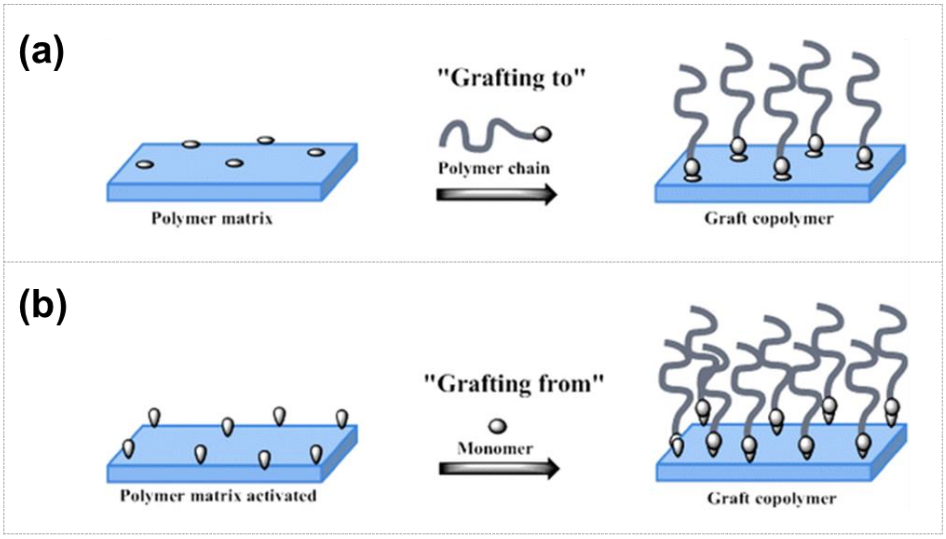

Fig. 1.14. Grafting strategies: (a) "grafting to" and (b) "grafting from" [61].

The most common method for grafting modification of membranes is radical graft polymerization due to its simplicity and versatility. Wide range of vinyl monomers can be polymerized by this method. The basic mechanism of radical grafting is illustrated in Fig. 1.15. The reaction starts with an initiation step - generating of an initial radical (R•). The initial radical is then transferred either to the membrane surface creating a free radical on the trunk polymer, or to the double bond of a vinyl monomer (M•) producing in both cases a primary radical. Such an event is then followed by propagation - the addition of monomers to the growing chain-side reactions of electron transfer, and termination by either disproportion (Fig. 1.15 Termination (i)) or coupling (Fig. 1.15 Termination (ii)) [62]. The primary radical can be formed either directly on the membrane surface using techniques such as ion beam, plasma, γ-irradiation, and ozone

treatment, or by electron transfer from a free radical initiator. The main methods for initiation are discussed below.

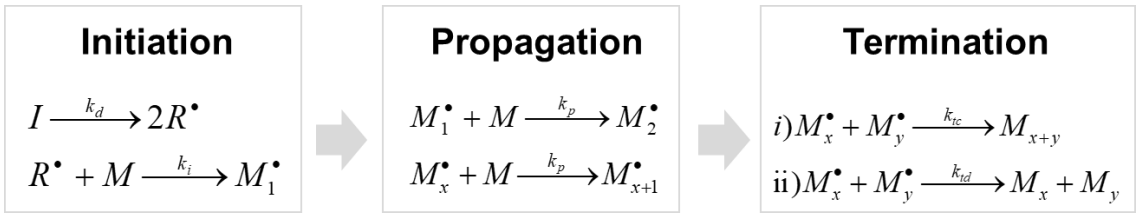

Fig. 1.15. Basic mechanism of radical graft polymerization.

1.6.3.1. Plasma

One simple approach is to oxidize the membrane surface by plasma treatment, which involves electron-induced excitation, ionization and dissociation. The active species generated in the plasma can oxidize the upper molecular layers on the membrane surface, thus improving wettability, antifouling and biocompatibility without affecting the bulk of the polymer [63-66].

1.6.3.2. UV irradiation

UV light is extensively used to carry out surface graft polymerization in most cases in the presence of a photo-initiator or a photo-sensitizer. When polymeric surfaces are exposed to UV irradiation, radicals can be formed. Then, in the presence of monomers and a photo-initiator, the graft photo-polymerization can be initiated (Fig. 1.16). Surface graft polymerization induced by UV irradiation exhibit following advantages:

(i) UV wavelength can be selectively adjusted to the specific reaction or to the photo-initiator wavelength, and, hence, undesired side reactions can be avoided or at least significantly

reduced; for example, in the case of polyethersulfone (PES) membrane, the wavelength should be higher than 300 nm to avid membrane degradation.

(ii) Ability to modify the polymer surface to have distinct properties through the choice of many different monomers which can be grafted using this method.

(iii) Controllable introduction of grafted polymer with a high density and relatively exact surface-selective process, without affecting the bulk properties

(iv) long-term chemical stability, which is assured by covalent attachment of grafted polymers [67].

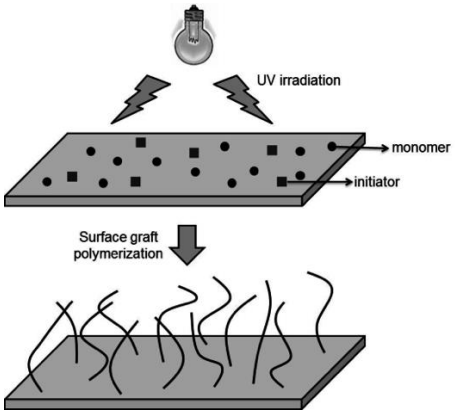

Fig. 1.16. Scheme of surface graft polymerization by UV irradiation. Figure from [68].

Based on these advantages, membrane modification using UV irradiation was studied by many researchers in an attempt to reduce the membrane fouling propensity [69-72]. However, by using UV irradiation, suitable UV irradiation intensity and time should be optimized to membrane modification process because a deterioration of membrane separation performance occurred when excess UV energy is used and over-irradiation could break the monomers that had already been grafted on the membrane surface [73].

1.6.3.3. Redox reaction

Redox reaction, an electron transfers from a reductant to an oxidant (for example the redox reaction of ammonium persulfate (APS) and tetramethylethylenediamine (TEMED) in Fig. 1.17), is an effective indirect way for producing the initial free radical due to the simplicity, low cost, short induction time, and low activation energy. The membrane modification using the redox couple is carried out by simply soaking the membrane in an aqueous solution of monomer and initiators at room temperature for desired period depending on the desired modification degree. However, the free radical graft modification using the redox couple has some major disadvantages such as low surface specificity, slow kinetics, and the polymerization of polymers that grows in the solution, but not attached to the membrane surface.

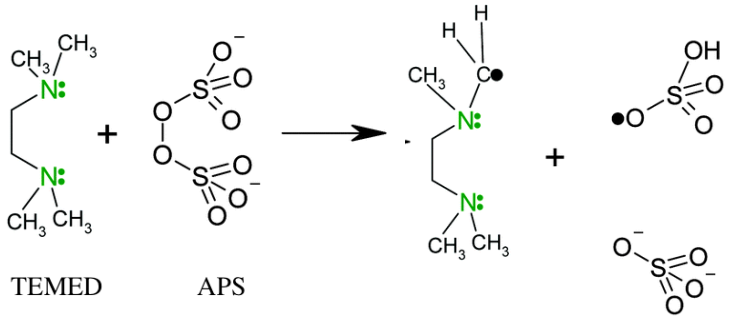

Fig. 1.17. Mechanism of the primary radical formation in redox initiation by ammonium persulfate (APS) and tetramethylethylenediamine (TEMED) [74, 75].

1.6.3.4. Surface-initiated atom transfer radical polymerization

Surface-initiated atom transfer radical polymerization (SI-ATRP) provides a simple route to many well-defined (co)polymers with precisely controlled functionalities, topologies, and compositions [76, 77]. It has been very successfully applied to the preparation of many nanocomposites, hybrids, and bioconjugates [78-82]. The advantages of SI-ATRP include the large range of available monomers and (macro)initiators, the simplicity of reaction setup, and the

ability to conduct the process over a large range of temperatures, solvents, and dispersed media [83-85].

SI-ATRP (Fig. 1.18) is a repetitive atom-transfer process between a macromolecular alkyl halide P_n-X and a redox-active transition-metal complex Cu^I-X/ligand in which $P_n^{\cdot}$ radicals propagate (rate constant of propagation k_p) and are reversibly formed (rate constants k_a and k_{da}). The growing radicals also are terminated by coupling or disproportionation (rate constant k_t). However, a limitation of this conventional SI-ATRP is the presence of a catalyst (a transition-metal complex with various ligands, i.e. Cu^I-X/ligand in Fig. 1.18). Cu^I-X/ligand is oxidized easily in the presence of air. Thus, it highly requires oxygen free environment and high amount of Cu^I for SI-ATRP reaction, which is not applicable in the industries.

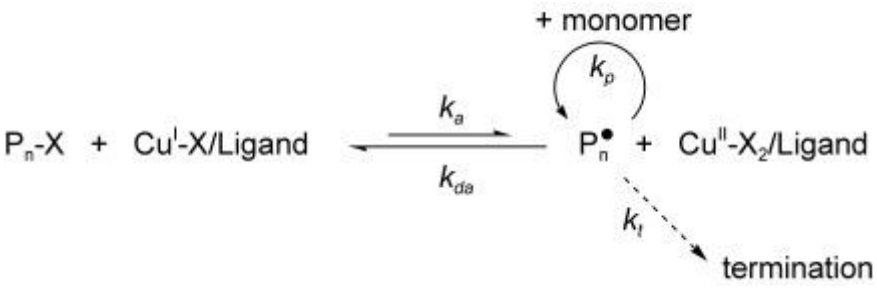

Fig. 1.18. Mechanism of SI-ATRP using Cu^I-X/ligand.

These limitations can be overcome by the addition of an appropriate reducing agent, such as L-ascorbic acid. Such process employs a very small amount of Cu^{II} species that is continuously regenerated to the Cu^I activator state by an excess of an appropriate reducing agent, in a word, the activators are continuously regenerated by electron transfer (Fig. 1.19.). This developed SI-ATRP technique requires a smaller amount of copper catalyst, tolerates a limited amount of oxygen [86-88], and enables to modify large membrane surface areas under ordinary laboratory

and industrial conditions. In this thesis, the improved SI-ATRP (Fig. 1.19.) is used as the membrane surface modification method.

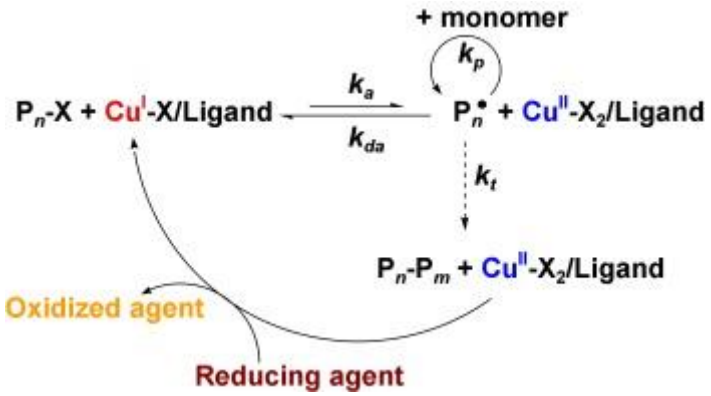

Fig. 1.19. Mechanism of the improved SI-ATRP reaction.

1.7. Anti-biofouling materials

Biofouling is particularly difficult to be addressed in RO processes. Biofouling can be affected by various factors, including feed water characteristics, hydrodynamic conditions, and membrane surface properties. Conventionally, pretreatments of feed water by disinfection, coagulation, filtration and/or adsorption are adopted to remove or inactivate microorganisms and to reduce organic/nutrient loading [89, 90]. In addition, operating at moderate flux level seems to be effective in preventing severe biofouling at the initial fouling stage [91]. However, the biofilm growth and colonization of microorganisms on membranes after initial attachment remains an unsolved issue [89]. It can be seen that the membrane surface properties play a key role in affecting biofilm formation. Therefore, solving membrane biofouling problem of RO processes through surface modification of RO membrane is the main target of this thesis. Besides modification methods mentioned in section 1.6, the investigation of anti-biofouling materials for

surface modification is also important. Several types of common and effective anti-biofouling materials are discussed as below.

1.7.1. Hydrophilic polymers

The first generation of anti-biofouling polymers were hydrophilic polymers such as hydroxyethyl methacrylate (HEMA) and poly(ethylene glycol) (PEG) [92-95]. When hydrophilic polymers are in contact with bulk water, water molecules penetrate into the polymer film to form a hydrogen-bond network in the polymers (called as "hydration layer"). The high surface hydration leads to the increase of resistance to nonspecific protein adsorption. Poly(HEMA) (pHEMA) has been shown to have good stability and biocompatibility [96]. Kochkodan et al. found that the polyethersulfone and poly(vinylidene fluoride) (PVDF) membranes effectively resisted the adhesion of Escherichia coli after the pHEMA coatings [97]. Song et al. showed that the polysulfone membranes coated with pHEMA were able to reduce oil emulsion fouling [98]. Yan et al. claimed that the PVDF membranes with pHEMA brushes simultaneously achieved the higher water permeability and ultralow protein absorption [99].

Poly(PEG) (pPEG) is a promising anti-biofouling polymer that has good hydrophilicity and nontoxicity [100]. The surface modification with surface bounded PEG is effective to prevent the membrane surfaces from the adsorption of hydrophobic or large molecules [101], which already has been applied in MF [102, 103], UF [104, 105], NF [106], and RO [107-109] membranes for anti-biofouling. For example, Belfer and Freger et al. grafted PEG onto polyamide RO membrane surfaces using a redox-initiated method to improve biofouling resistance [107, 108]. However, it was found that PEG decomposes in the presence of transition metal ions and oxygen, which would occur in biochemically relevant solutions and water [95, 110, 111, 112].

1.7.2. Zwiterion

Zwitterion materials, that contain both positively charged and negatively charged units within a single pendant group, and net charge is zero, have recently been shown to have excellent anti-biofouling properties in many diverse environments. Examples of zwiterionic polymers include poly(2-methacryloyloxyethyphosphorylcholines) (pMPC), poly(carboxybetaine methacrylate) (pCBMA), and poly [(2-methacryloyloxy)ethyl]dimethyl-(3-sulfopropyl)ammonium hydroxide (pMEDSAH) (their chemical structures are shown in Fig. 1.18). MPC is based on the composition of the natural phospholipid components of the cell membrane [113, 114]. It has been shown that surfaces coated with pMPC form an excellent antifouling coating on multiple platforms [115-117]. The antifouling properties of pCBMA and pMEDSAH have also been demonstrated by many researchers [94, 118-120].

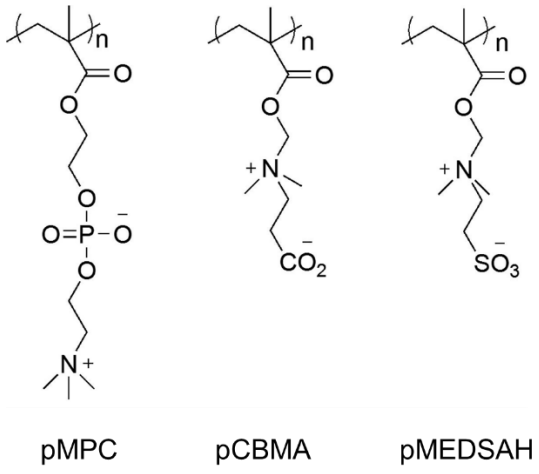

Fig. 1.18. Chemical structures of some commonly used zwitterionic polymers. Figure from [121].

The fundamental principle of the anti-biofouling behavior of zwitterion materials lies in their excellent ability to form a strong hydration layer via electrostatic interaction [122, 123] which is

determined by the balanced charge and the minimized dipole of zwitterions [124]. Two additional important criteria are their low protein interaction rates and low self-association [122]. Specifically, the self-association among zwitterionic moieties originates from the electrostatic attraction between the cationic and anionic groups, which cause the removal of water molecules around the charge groups because of the excluded-volume effect. Thus, the low self-association leads to the strong hydration [125]. These three criteria, and consequently the anti-biofouling properties of zwitterions, are governed by the chemical structure of the charged moieties [126-128].

1.7.3. Polyampholyte

Polyampholytes (Fig.1.19b) are the amphoteric polymers with a homogeneous molecular level mixture of positively and negatively charged regions with a similar structure to zwitterionic polymers (Fig.1.19a). The net charge of polyampholytes depends on pH of solution, unlike zwitterionic polymers. Polyampholytes also have antifouling properties. Recently, the research on polyampholytes as antifouling polymers gained interest [120, 129-131], since polyampholytes offer a broad spectrum of combinations of the acid-co-base simply through changing one of the many available acidic/basic monomers. On the other hand, unlike zwitterionic polymers, polyampholytes might have a net charge (either positive or negative) depending on pH [132] which can result in an increase in the fouling propensity of the coated surface. In addition, the polyampholyte composition might not be identical to the monomer molar ratio in the polymerization solution [133, 134], and thus requires pre-experiments.

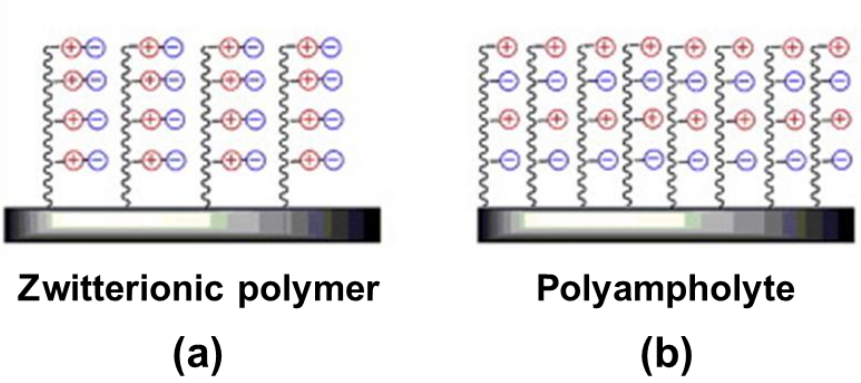

Fig. 1.19. Illustration of the structure of (a) zwitterionic polymer that contain both positive charged and negative charged units within a single monomer, and (b) polyampholyte synthesized by two opposite charged monomers [123].

1.7.4. Multi-mechanism for biofouling mitigation

Besides grafting of hydrophilic materials such PEG and zwitterionic polymers, synthesis of effective materials with multi-mechanism for anti-biofouling is a promising path as well. Two examples were discussed as follow.

i) Constructing amphiphilic surfaces was proposed to fabricate next generation antifouling membranes that would contain both hydrophilic (e.g., pPEG) and low surface energy (e.g., perfluoropolyether segments) segments [135-139]. In addition to providing a simple "fouling resistant" strategy by using hydrophilic segments, amphiphilic surfaces could also take advantage of low surface energy segments to weaken the interfacial bonds, so that the deposited foulants would easily slip from the amphiphilic surfaces with low hydraulic washing [140-142], which is referred to as a ''fouling release'' strategy. Polyacrylonitrile (PAN), PES, and polyvinylidene fluoride (PVDF)-based UF membranes have already been successfully prepared with surfaces consisting of polydimethylsiloxane (PDMS) or perfluoropolyether-based polymer segments to promote fouling release and hydrophilic polyethylene glycol (PEO)-based segments to promote

fouling resistance [137, 143, 144]. These optimal membrane surfaces displayed excellent "fouling resistant" and "fouling release" properties against various foulants.

ii) Other anti-biofouling strategies using surface modification can be classified into two mechanisms: resistance to adhesion of biocontaminants ("fouling resistance") and degradation of the biocontaminants ("fouling attacking"). It is generally accepted that a hydrophilic surface offers biofouling resistance because of the hydrophobic nature of biofoulants such as proteins. A classic "resistance" protocol, therefore, involves modification of membrane surface chemistry to increase hydrophilicity by introducing PEG or zwitterionic polymer. The "attacking" strategy, on the other hand, involves membrane functionalization with releasable bacteria-killing substances, such as silver nanoparticles (AgNPs) [145] and antibiotics [146], or decoration with bactericidal functionalities like quaternary ammonium salts (QAS) [147-149], graphene oxide [150], and photoactive agents [151] for contact killing. Inactivation of bacterial cells on the surface was found to reduce the rate of biofilm formation on biocide-functionalized membranes [152, 153], demonstrating the potential of anti-microbial membrane design for biofouling prevention. In recent years, numerous researchers have attempted to combine these two complementary biofouling mitigation strategies to impart both nonadhesive and bactericidal capabilities on the membrane surfaces.

1.8. Aim and overview of this thesis

Previous sections have generally introduced the development of TFC RO membrane and pointed out the drawback of TFC RO membrane is biofouling. Further, various strategies to solve the biofouling problem have reviewed. In this thesis, the aim is to provide deep understanding on anti-biofouling mechanism and to develop novel materials and methods for membrane surface

modification to improve the anti-biofouling properties of TFC RO membranes. The overview of each chapter is described as follows.

This thesis included 6 chapters.

In **Chapter 1,** the background as well as the objectives of this thesis were generally introduced.

In **Chapter 2**, the objectives of this study are firstly to develop an effective method to immobilize initiators of surface-initiated atom transfer radical polymerization (SI-ATRP) on the less reactive surface of polyamide RO membranes, and secondly to evaluate the effect of the main chain length of a zwitterionic polymer on biofouling prevention systematically. 3-Aminopropyltrimethoxysilane (APTS) was used to aminate the surface of a polyamide RO membrane to improve the BIBB immobilization. After BIBB immobilization, poly[(2-methacryloyloxy)ethyl]dimethyl[3-sulfopropyl]ammonium hydroxide (pMEDSAH) was grafted on the membrane surface via SI-ATRP. The main chain length of the grafted zwitterionic polymer was controlled by changing polymerization time and quantified by gel permeation chromatography (GPC). The surface chemical properties of the modified membranes with various polymer main chain lengths were characterized by attenuated total reflection-Fourier transform infrared (ATR-FTIR) spectroscopy, X-ray photoelectron spectroscopy (XPS), and contact angle measurements. The surface morphology was observed using scanning electron microscopy (FE-SEM) and atomic force microscopy (AFM). The biofouling resistance of the modified membranes was evaluated by static bacterial adhesion and dynamic biofouling filtration experiments.

In **Chapter 3**, the features of various hydrophilic polymers were systematically characterized and the effect of polymer structure on biofouling behavior of polyamide RO membranes was assessed. First, polyamide RO membranes were modified with well structurally controlled hydrophilic polymers including poly (2-Hydroxyethyl methacrylate) (pHEMA),

poly[poly(ethylene glycol)methacrylate] (pPEG), and pMEDSAH via SI-ATRP reaction. To assess the grafted polymer structure, the surface chemical properties of the modified membranes were analyzed by using ATR-FTIR spectroscopy and XPS. Thickness of the active layer and surface roughness were evaluated by FE-SEM and the AFM, respectively. Furthermore, molecular dynamics (MD) simulation was used for determining side chain length and hydrogen number of given polymers with water molecules. To evaluate biofouling behavior of grafted membranes, a static bacterial adhesion test and a dynamic biofouling filtration test were conducted. The membranes modified with a longer main chain of pMEDSAH and a long side chain of pPEG had good resistance against both the bacterial adhesion and dynamic biofouling. Experimental results between the static and dynamic biofouling behavior did not correlate with each other. MD simulation clarified that pPEG had a longer side chain than pHEMA and pMEDSAH, and that pMEDSAH possessed stronger hydration than pPEG and pHEMA. Experimental results and MD simulation indicated that the main chain length, side chain length, and hydration of the modifying polymer should be taken into account for developing anti-biofouling membranes.

In **Chapter 4**, a polyamide RO membrane was modified with a polyampholyte composed of anionic 2-carboxyethyl acrylate (CAA) and cationic [2-(acryloyloxy)ethyl] trimethyl ammonium chloride (TMA) by SI-ATRP, in order to improve its anti-biofouling properties. The anti-biofouling properties of membranes with different CAA/TMA surface ratios were evaluated by protein adsorption, static bacterial attachment, and long-term dynamic biofouling filtration experiments. It was found that an electrostatic attraction resulted in a severe biofouling, even if the water contact angle was 5–20°, and the membrane hydrophilicity was sufficiently high. However, the RO membrane with CAA/TMA surface ratio of 1:1, fabricated from a mixed monomer solution with 3:1 CAA/TMA ratio showed an excellent anti-biofouling performance

even in long-term dynamic biofouling filtration experiments. These good anti-biofouling properties derive from the high hydrophilicity of the membrane surface, resulting from its large content of ionic groups, and the almost complete lack of electrostatic attractions with charged bacteria, because the net surface charge is close to zero.

In **Chapter 5**, a novel amphiphilic polymer architecture for TFC membranes were developed to integrate "resistant" and "release" strategies against membrane fouling. A zwitterionic polymer with strong hydration and a fluorine-based polymer with low surface energy were sequentially grafted on a membrane surface by dual SI-ATRP. Compared with conventional hydrophilic modifications (e.g., a hydrophilic TFC membrane), amphiphilic diblock copolymer modified membranes (e.g., an amphiphilic TFC membrane) possess not only strong hydration energy but also lower surface energy, which yield both fouling resistant and fouling release properties. The superiority of possessing multi-defense properties was further confirmed by the long-term, multi-cycle membrane fouling and cleaning filtration. The experimental data demonstrated that, compared with pristine and hydrophilic TFC membranes, the amphiphilic TFC membranes showed less water flux decline and higher water flux recovery. These results strongly suggest that fabricating an amphiphilic TFC membrane is an effective and novel approach to establishing realistic antifouling properties.

In **Chapter 6,** the conclusion of this thesis was summarized.

References

[1] T.R. Malthus, An Essay on the Principle of Population, 1872.
[2] P. Raskin, P. Gleick, P. Kirshen, G. Pontius, K. Strzepek, Comprehensive assessment of the freshwater resources of the world. Water futures: assessment of long-range patterns and problems, (1997).
[3] M.M. Mekonnen, A.Y. Hoekstra, Four billion people facing severe water scarcity, Science advances, 2 (2016) e1500323.

[4] W.H. Organization, UNICEF, Global water supply and sanitation assessment 2000 report, in, World Health Organization (WHO), 2000.
[5] P.H. Gleick, Global freshwater resources: soft-path solutions for the 21st century, Science, 302 (2003) 1524-1528.
[6] A. Prüss, D. Kay, L. Fewtrell, J. Bartram, Estimating the burden of disease from water, sanitation, and hygiene at a global level, Environmental Health Perspectives, 110 (2002) 537-542.
[7] J. Mallevialle, P.E. Odendaal, M.R. Wiesner, Water treatment membrane processes, American Water Works Association, 1996.
[8] G. Crini, E. Lichtfouse, Advantages and disadvantages of techniques used for wastewater treatment, Environmental Chemistry Letters, 17 (2019) 145-155.
[9] T. Stephenson, K. Brindle, S. Judd, B. Jefferson, Membrane bioreactors for wastewater treatment, IWA publishing, 2000.
[10] J.-M. Laîné, D. Vial, P. Moulart, Status after 10 years of operation—overview of UF technology today, Desalination, 131 (2000) 17-25.
[11] W. Gao, H. Liang, J. Ma, M. Han, Z.-l. Chen, Z.-s. Han, G.-b. Li, Membrane fouling control in ultrafiltration technology for drinking water production: a review, Desalination, 272 (2011) 1-8.
[12] P. Parhi, Supported liquid membrane principle and its practices: A short review, Journal of Chemistry, 2013 (2012).
[13] B. Van der Bruggen, C. Vandecasteele, T. Van Gestel, W. Doyen, R. Leysen, A review of pressure-driven membrane processes in wastewater treatment and drinking water production, Environmental Progress, 22 (2003) 46-56.
[14] R.J. Petersen, Composite reverse osmosis and nanofiltration membranes, Journal of Membrane Science, 83 (1993) 81-150.
[15] M. Elimelech, W.A. Phillip, The future of seawater desalination: energy, technology, and the environment, Science, 333 (2011) 712-717.
[16] J.A. López-Ramírez, M.C. Oviedo, J.Q. Alonso, Comparative studies of reverse osmosis membranes for wastewater reclamation, Desalination, 191 (2006) 137-147.
[17] S. Loeb, Sea water demineralization by means of an osmotic membrane, Advances in Chemistry Series, 38 (1962) 117-132.
[18] J. Cadotte, R. Petersen, R. Larson, E. Erickson, A new thin-film composite seawater reverse osmosis membrane, Desalination, 32 (1980) 25-31.
[19] S. Avlonitis, K. Kouroumbas, N. Vlachakis, Energy consumption and membrane replacement cost for seawater RO desalination plants, Desalination, 157 (2003) 151-158.

[20] K.P. Lee, T.C. Arnot, D. Mattia, A review of reverse osmosis membrane materials for desalination—development to date and future potential, Journal of Membrane Science, 370 (2011) 1-22.
[21] D. Li, H. Wang, Recent developments in reverse osmosis desalination membranes, Journal of Materials Chemistry, 20 (2010) 4551-4566.
[22] S.H. Maruf, D.U. Ahn, A.R. Greenberg, Y. Ding, Glass transition behaviors of interfacially polymerized polyamide barrier layers on thin film composite membranes via nano-thermal analysis, Polymer, 52 (2011) 2643-2649.
[23] A. Subramani, E.M. Hoek, Biofilm formation, cleaning, re-formation on polyamide composite membranes, Desalination, 257 (2010) 73-79.
[24] W.S. Ang, S. Lee, M. Elimelech, Chemical and physical aspects of cleaning of organic-fouled reverse osmosis membranes, Journal of Membrane Science, 272 (2006) 198-210.
[25] S. Creber, J. Vrouwenvelder, M. Van Loosdrecht, M. Johns, Chemical cleaning of biofouling in reverse osmosis membranes evaluated using magnetic resonance imaging, Journal of Membrane Science, 362 (2010) 202-210.
[26] M. Goosen, S. Sablani, H. Al-Hinai, S. Al-Obeidani, R. Al-Belushi, a. Jackson, Fouling of reverse osmosis and ultrafiltration membranes: a critical review, Separation Science and Technology, 39 (2005) 2261-2297.
[27] R.R. Choudhury, J.M. Gohil, S. Mohanty, S.K. Nayak, Antifouling, fouling release and antimicrobial materials for surface modification of reverse osmosis and nanofiltration membranes, Journal of Materials Chemistry A, 6 (2018) 313-333.
[28] A. Matin, Z. Khan, S. Zaidi, M. Boyce, Biofouling in reverse osmosis membranes for seawater desalination: phenomena and prevention, Desalination, 281 (2011) 1-16.
[29] H.-C. Flemming, Reverse osmosis membrane biofouling, Experimental Thermal and Fluid Science, 14 (1997) 382-391.
[30] F. Fiessinger, Y. Richard, A. Montiel, P. Musquere, Advantages and disadvantages of chemical oxidation and disinfection by ozone and chlorine dioxide, Science of the Total Environment, 18 (1981) 245-261.
[31] S. Jiang, Y. Li, B.P. Ladewig, A review of reverse osmosis membrane fouling and control strategies, Science of the Total Environment, 595 (2017) 567-583.
[32] Z. Hu, A. Antony, G. Leslie, P. Le-Clech, Real-time monitoring of scale formation in reverse osmosis using electrical impedance spectroscopy, Journal of Membrane Science, 453 (2014) 320-327.
[33] K.D. Cobry, Z. Yuan, J. Gilron, V.M. Bright, W.B. Krantz, A.R. Greenberg, Comprehensive experimental studies of early-stage membrane scaling during nanofiltration, Desalination, 283 (2011) 40-51.

[34] J.J. Sadhwani, J.M. Veza, Cleaning tests for seawater reverse osmosis membranes, Desalination, 139 (2001) 177-182.
[35] J.-Y. Yang, Y.-S. Li, B. Huang, Research on refurbishing of the used RO membrane through chemical cleaning and repairing with a new system, Desalination, 320 (2013) 49-55.
[36] T. Koo, Y. Lee, R. Sheikholeslami, Silica fouling and cleaning of reverse osmosis membranes, Desalination, 139 (2001) 43-56.
[37] S. Madaeni, S. Samieirad, Chemical cleaning of reverse osmosis membrane fouled by wastewater, Desalination, 257 (2010) 80-86.
[38] M. Sohrabi, S. Madaeni, M. Khosravi, A. Ghaedi, Chemical cleaning of reverse osmosis and nanofiltration membranes fouled by licorice aqueous solutions, Desalination, 267 (2011) 93-100.
[39] K.J. Varin, N.H. Lin, Y. Cohen, Biofouling and cleaning effectiveness of surface nanostructured reverse osmosis membranes, Journal of Membrane Science, 446 (2013) 472-481.
[40] Q. Gan, J. Howell, R. Field, R. England, M. Bird, M. McKechinie, Synergetic cleaning procedure for a ceramic membrane fouled by beer microfiltration, Journal of Membrane Science, 155 (1999) 277-289.
[41] A. Al-Amoudi, R.W. Lovitt, Fouling strategies and the cleaning system of NF membranes and factors affecting cleaning efficiency, Journal of Membrane Science, 303 (2007) 4-28.
[42] E. Filloux, J. Wang, M. Pidou, W. Gernjak, Z. Yuan, Biofouling and scaling control of reverse osmosis membrane using one-step cleaning-potential of acidified nitrite solution as an agent, Journal of Membrane Science, 495 (2015) 276-283.
[43] G.Z. Ramon, T.-V. Nguyen, E.M. Hoek, Osmosis-assisted cleaning of organic-fouled seawater RO membranes, Chemical Engineering Journal, 218 (2013) 173-182.
[44] I.C. Escobar, E.M. Hoek, C.J. Gabelich, F.A. DiGiano, Committee report: recent advances and research needs in membrane fouling, American Water Works Association. Journal, 97 (2005) 79.
[45] D. Rana, T. Matsuura, Surface modifications for antifouling membranes, Chemical Reviews, 110 (2010) 2448-2471.
[46] E.M. Vrijenhoek, S. Hong, M. Elimelech, Influence of membrane surface properties on initial rate of colloidal fouling of reverse osmosis and nanofiltration membranes, Journal of Membrane Science, 188 (2001) 115-128.
[47] A. Weis, M.R. Bird, M. Nyström, C. Wright, The influence of morphology, hydrophobicity and charge upon the long-term performance of ultrafiltration membranes fouled with spent sulphite liquor, Desalination, 175 (2005) 73-85.
[48] N. Hilal, O.O. Ogunbiyi, N.J. Miles, R. Nigmatullin, Methods employed for control of fouling in MF and UF membranes: a comprehensive review, Separation Science and Technology, 40 (2005) 1957-2005.

[49] A. Fane, C. Fell, A review of fouling and fouling control in ultrafiltration, Desalination, 62 (1987) 117-136.
[50] A. Nabe, E. Staude, G. Belfort, Surface modification of polysulfone ultrafiltration membranes and fouling by BSA solutions, Journal of Membrane Science, 133 (1997) 57-72.
[51] B. Van der Bruggen, M. Mänttäri, M. Nyström, Drawbacks of applying nanofiltration and how to avoid them: a review, Separation and Purification Technology, 63 (2008) 251-263.
[52] V. Kochkodan, D.J. Johnson, N. Hilal, Polymeric membranes: Surface modification for minimizing (bio) colloidal fouling, Advances in Colloid and Interface Science, 206 (2014) 116-140.
[53] Y. Kouwonou, R. Malaisamy, K.L. Jones, Modification of PES membrane: reduction of biofouling and improved flux recovery, Separation Science and Technology, 43 (2008) 4099-4112.
[54] Y.-H. Zhao, B.-K. Zhu, L. Kong, Y.-Y. Xu, Improving hydrophilicity and protein resistance of poly (vinylidene fluoride) membranes by blending with amphiphilic hyperbranched-star polymer, Langmuir, 23 (2007) 5779-5786.
[55] A. Venault, Y.-H. Liu, J.-R. Wu, H.-S. Yang, Y. Chang, J.-Y. Lai, P. Aimar, Low-biofouling membranes prepared by liquid-induced phase separation of the PVDF/polystyrene-b-poly (ethylene glycol) methacrylate blend, Journal of Membrane Science, 450 (2014) 340-350.
[56] R. Kumar, A.M. Isloor, A. Ismail, T. Matsuura, Synthesis and characterization of novel water soluble derivative of chitosan as an additive for polysulfone ultrafiltration membrane, Journal of Membrane Science, 440 (2013) 140-147.
[57] D. Song, J. Xu, Y. Fu, L. Xu, B. Shan, Polysulfone/sulfonated polysulfone alloy membranes with an improved performance in processing mariculture wastewater, Chemical Engineering Journal, 304 (2016) 882-889.
[58] Y.P. Tang, J.X. Chan, T.S. Chung, M. Weber, C. Staudt, C. Maletzko, Simultaneously covalent and ionic bridging towards antifouling of GO-imbedded nanocomposite hollow fiber membranes, Journal of Materials Chemistry A, 3 (2015) 10573-10584.
[59] Q. GenáZhang, G. LuáHan, A. MeiáZhu, Q. LináLiu, Ultrathin self-assembled anionic polymer membranes for superfast size-selective separation, Nanoscale, 5 (2013) 11028-11034.
[60] S. Liang, K. Xiao, Y. Mo, X. Huang, A novel ZnO nanoparticle blended polyvinylidene fluoride membrane for anti-irreversible fouling, Journal of Membrane Science, 394 (2012) 184-192.
[61] V.H. Pino-Ramos, A. Ramos-Ballesteros, F. López-Saucedo, J.E. López-Barriguete, G.H. Varca, E. Bucio, Radiation grafting for the functionalization and development of smart polymeric materials, in: Applications of Radiation Chemistry in the Fields of Industry, Biotechnology and Environment, Springer, 2017, pp. 67-94.

[62] D.W. Jenkins, S.M. Hudson, Review of vinyl graft copolymerization featuring recent advances toward controlled radical-based reactions and illustrated with chitin/chitosan trunk polymers, Chemical Reviews, 101 (2001) 3245-3274.
[63] K. Kim, K. Lee, K. Cho, C. Park, Surface modification of polysulfone ultrafiltration membrane by oxygen plasma treatment, Journal of Membrane Science, 199 (2002) 135-145.
[64] H.-Y. Yu, Y.-J. Xie, M.-X. Hu, J.-L. Wang, S.-Y. Wang, Z.-K. Xu, Surface modification of polypropylene microporous membrane to improve its antifouling property in MBR: CO2 plasma treatment, Journal of Membrane Science, 254 (2005) 219-227.
[65] H.-Y. Yu, L.-Q. Liu, Z.-Q. Tang, M.-G. Yan, J.-S. Gu, X.-W. Wei, Surface modification of polypropylene microporous membrane to improve its antifouling characteristics in an SMBR: Air plasma treatment, Journal of Membrane Science, 311 (2008) 216-224.
[66] H.-Y. Yu, X.-C. He, L.-Q. Liu, J.-S. Gu, X.-W. Wei, Surface modification of polypropylene microporous membrane to improve its antifouling characteristics in an SMBR: N2 plasma treatment, Water Research, 41 (2007) 4703-4709.
[67] S. Minko, Grafting on solid surfaces:"Grafting to" and "grafting from" methods, in: Polymer surfaces and interfaces, Springer, 2008, pp. 215-234.
[68] P. Alves, P. Ferreira, M. Gil, Biomedical polyurethane-based materials, Polyurethane: Properties, Structure and Applications. New York: Nova Publishers, (2012) 1-25.
[69] A. Rahimpour, UV photo-grafting of hydrophilic monomers onto the surface of nano-porous PES membranes for improving surface properties, Desalination, 265 (2011) 93-101.
[70] Y. Mansourpanah, E.M. Habili, Preparation and modification of thin film PA membranes with improved antifouling property using acrylic acid and UV irradiation, Journal of Membrane Science, 430 (2013) 158-166.
[71] T. Hong Anh Ngo, S. Mori, D. Thi Tran, Photo-induced grafting of poly (ethylene glycol) onto polyamide thin film composite membranes, Journal of Applied Polymer Science, 134 (2017) 45454.
[72] N. Liu, G. Sun, S. Gaan, P. Rupper, Controllable surface modifications of polyamide by photo-induced graft polymerization using immobilized photo-initiators, Journal of Applied Polymer Science, 116 (2010) 3629-3637.
[73] L.Y. Ng, A. Ahmad, A.W. Mohammad, Alteration of polyethersulphone membranes through UV-induced modification using various materials: A brief review, Arabian Journal of Chemistry, 10 (2017) S1821-S1834.
[74] X.D. Feng, X.Q. Guo, K.Y. Qiu, Study of the initiation mechanism of the vinyl polymerization with the system persulfate/N, N, N′ , N′ -tetramethylethylenediamine, Die Makromolekulare Chemie: Macromolecular Chemistry and Physics, 189 (1988) 77-83.

[75] B. Strachota, L. Matějka, A. Zhigunov, R. Konefał, J. Spěváček, J. Dybal, R. Puffr, Poly (N-isopropylacrylamide)–clay based hydrogels controlled by the initiating conditions: evolution of structure and gel formation, Soft Matter, 11 (2015) 9291-9306.
[76] T.E. Patten, K. Matyjaszewski, Atom transfer radical polymerization and the synthesis of polymeric materials, Advanced Materials, 10 (1998) 901-915.
[77] V. Coessens, T. Pintauer, K. Matyjaszewski, Functional polymers by atom transfer radical polymerization, Progress in Polymer Science, 26 (2001) 337-377.
[78] D. Bontempo, H.D. Maynard, Streptavidin as a macroinitiator for polymerization: in situ protein− polymer conjugate formation, Journal of the American Chemical Society, 127 (2005) 6508-6509.
[79] K. Matyjaszewski, Macromolecular engineering: From rational design through precise macromolecular synthesis and processing to targeted macroscopic material properties, Progress in Polymer Science, 30 (2005) 858-875.
[80] M.L. Becker, J. Liu, K.L. Wooley, Peptide-polymer bioconjugates: hybrid block copolymers generated via living radical polymerizations from resin-supported peptides, Chemical Communications, (2003) 180-181.
[81] K. Koh, K. Ohno, Y. Tsujii, T. Fukuda, Precision synthesis of organic/inorganic hybrid nanocapsules with a silanol-functionalized micelle template, Angewandte Chemie International Edition, 42 (2003) 4194-4197.
[82] T. von Werne, T.E. Patten, Atom transfer radical polymerization from nanoparticles: a tool for the preparation of well-defined hybrid nanostructures and for understanding the chemistry of controlled/“living” radical polymerizations from surfaces, Journal of the American Chemical Society, 123 (2001) 7497-7505.
[83] K. Matyjaszewski, J. Xia, Atom transfer radical polymerization, Chemical Reviews, 101 (2001) 2921-2990.
[84] M. Kamigaito, T. Ando, M. Sawamoto, Metal-catalyzed living radical polymerization, Chemical Reviews, 101 (2001) 3689-3746.
[85] J. Qiu, B. Charleux, K. Matyjaszewski, Controlled/living radical polymerization in aqueous media: homogeneous and heterogeneous systems, Progress in Polymer Science, 26 (2001) 2083-2134.
[86] K. Matyjaszewski, Atom transfer radical polymerization (ATRP): current status and future perspectives, Macromolecules, 45 (2012) 4015-4039.
[87] K. Matyjaszewski, H. Dong, W. Jakubowski, J. Pietrasik, A. Kusumo, Grafting from surfaces for “everyone”: ARGET ATRP in the presence of air, Langmuir, 23 (2007) 4528-4531.
[88] W. Jakubowski, K. Min, K. Matyjaszewski, Activators regenerated by electron transfer for atom transfer radical polymerization of styrene, Macromolecules, 39 (2006) 39-45.

[89] V. Chen, J. Mansouri, T. Charlton, Biofouling in membrane systems, Membrane Technology: Volume 4: Membranes for Water Treatment, 4 (2010) 25-51.
[90] T. Nguyen, F.A. Roddick, L. Fan, Biofouling of water treatment membranes: a review of the underlying causes, monitoring techniques and control measures, Membranes, 2 (2012) 804-840.
[91] R. Field, Fundamentals of fouling, Membranes for water treatment, 4 (2010) 1-23.
[92] K. Feldman, G. Hähner, N. Spencer, P. Harder, M. Grunze, Probing resistance to protein adsorption of oligo (ethylene glycol)-terminated self-assembled monolayers by scanning force microscopy, Journal of the American Chemical Society, 121 (1999) 10134-10141.
[93] A.S. Hoffman, Non-fouling surface technologies, Journal of Biomaterials Science, Polymer Edition, 10 (1999) 1011-1014.
[94] H. Ma, J. Hyun, P. Stiller, A. Chilkoti, "Non-fouling" oligo (ethylene glycol)-functionalized polymer brushes synthesized by surface-initiated atom transfer radical polymerization, Advanced Materials, 16 (2004) 338-341.
[95] L. Li, S. Chen, S. Jiang, Protein interactions with oligo (ethylene glycol)(OEG) self-assembled monolayers: OEG stability, surface packing density and protein adsorption, Journal of Biomaterials Science, Polymer Edition, 18 (2007) 1415-1427.
[96] J.-P. Montheard, M. Chatzopoulos, D. Chappard, 2-hydroxyethyl methacrylate (HEMA): chemical properties and applications in biomedical fields, Journal of Macromolecular Science, Part C: Polymer Reviews, 32 (1992) 1-34.
[97] V. Kochkodan, N. Hilal, V. Goncharuk, L. Al-Khatib, T. Levadna, Effect of the surface modification of polymer membranes on their microbiological fouling, Colloid Journal, 68 (2006) 267-273.
[98] K.-H. Song, K.-H. Kim, S.-H. Cho, K.-R. Lee, J.-H. Lim, S.-S. Bae, Permeation flux of surface-modified hydrophilic polysulfone membrane, Korean Chemical Engineering Research, 42 (2004) 59-64.
[99] Y. Sui, Z. Wang, X. Gao, C. Gao, Antifouling PVDF ultrafiltration membranes incorporating PVDF-g-PHEMA additive via atom transfer radical graft polymerizations, Journal of Membrane Science, 413 (2012) 38-47.
[100] H. Zhang, M. Chiao, Anti-fouling coatings of poly (dimethylsiloxane) devices for biological and biomedical applications, Journal of Medical and Biological Engineering, 35 (2015) 143-155.
[101] T. McPherson, A. Kidane, I. Szleifer, K. Park, Prevention of protein adsorption by tethered poly (ethylene oxide) layers: experiments and single-chain mean-field analysis, Langmuir, 14 (1998) 176-186.
[102] Y. Chang, Y.-J. Shih, R.-C. Ruaan, A. Higuchi, W.-Y. Chen, J.-Y. Lai, Preparation of poly (vinylidene fluoride) microfiltration membrane with uniform surface-copolymerized poly

(ethylene glycol) methacrylate and improvement of blood compatibility, Journal of Membrane Science, 309 (2008) 165-174.
[103] Y. Chang, T.-Y. Cheng, Y.-J. Shih, K.-R. Lee, J.-Y. Lai, Biofouling-resistance expanded poly (tetrafluoroethylene) membrane with a hydrogel-like layer of surface-immobilized poly (ethylene glycol) methacrylate for human plasma protein repulsions, Journal of Membrane Science, 323 (2008) 77-84.
[104] M. Ulbricht, H. Matuschewski, A. Oechel, H.-G. Hicke, Photo-induced graft polymerization surface modifications for the preparation of hydrophilic and low-proten-adsorbing ultrafiltration membranes, Journal of Membrane Science, 115 (1996) 31-47.
[105] S. Wang, T. Li, C. Chen, B. Liu, J.C. Crittenden, PVDF ultrafiltration membranes of controlled performance via blending PVDF-g-PEGMA copolymer synthesized under different reaction times, Frontiers of Environmental Science & Engineering, 12 (2018) 3.
[106] S. Belfer, R. Fainshtain, Y. Purinson, J. Gilron, M. Nyström, M. Mänttäri, Modification of NF membrane properties by in situ redox initiated graft polymerization with hydrophilic monomers, Journal of Membrane Science, 239 (2004) 55-64.
[107] S. Belfer, Y. Purinson, R. Fainshtein, Y. Radchenko, O. Kedem, Surface modification of commercial composite polyamide reverse osmosis membranes, Journal of Membrane Science, 139 (1998) 175-181.
[108] V. Freger, J. Gilron, S. Belfer, TFC polyamide membranes modified by grafting of hydrophilic polymers: an FT-IR/AFM/TEM study, Journal of Membrane Science, 209 (2002) 283-292.
[109] G. Kang, M. Liu, B. Lin, Y. Cao, Q. Yuan, A novel method of surface modification on thin-film composite reverse osmosis membrane by grafting poly (ethylene glycol), Polymer, 48 (2007) 1165-1170.
[110] D.A. Herold, K. Keil, D.E. Bruns, Oxidation of polyethylene glycols by alcohol dehydrogenase, Biochemical Pharmacology, 38 (1989) 73-76.
[111] L. Li, S. Chen, J. Zheng, B.D. Ratner, S. Jiang, Protein adsorption on oligo (ethylene glycol)-terminated alkanethiolate self-assembled monolayers: the molecular basis for nonfouling behavior, The Journal of Physical Chemistry B, 109 (2005) 2934-2941.
[112] V. Gaberc-Porekar, I. Zore, B. Podobnik, V. Menart, Obstacles and pitfalls in the PEGylation of therapeutic proteins, Current Opinion in Drug Discovery and Development, 11 (2008) 242.
[113] A.L. Lewis, Phosphorylcholine-based polymers and their use in the prevention of biofouling, Colloids and Surfaces B: Biointerfaces, 18 (2000) 261-275.
[114] K. Ishihara, H. Nomura, T. Mihara, K. Kurita, Y. Iwasaki, N. Nakabayashi, Why do phospholipid polymers reduce protein adsorption?, Journal of Biomedical Materials Research:

An Official Journal of The Society for Biomaterials, The Japanese Society for Biomaterials, and the Australian Society for Biomaterials, 39 (1998) 323-330.
[115] W. Feng, J. Brash, S. Zhu, Atom-transfer radical grafting polymerization of 2-methacryloyloxyethyl phosphorylcholine from silicon wafer surfaces, Journal of Polymer Science Part A: Polymer Chemistry, 42 (2004) 2931-2942.
[116] W. Feng, S. Zhu, K. Ishihara, J.L. Brash, Adsorption of fibrinogen and lysozyme on silicon grafted with poly (2-methacryloyloxyethyl phosphorylcholine) via surface-initiated atom transfer radical polymerization, Langmuir, 21 (2005) 5980-5987.
[117] W. Feng, J.L. Brash, S. Zhu, Non-biofouling materials prepared by atom transfer radical polymerization grafting of 2-methacryloloxyethyl phosphorylcholine: separate effects of graft density and chain length on protein repulsion, Biomaterials, 27 (2006) 847-855.
[118] Y. Chang, S. Chen, Z. Zhang, S. Jiang, Highly protein-resistant coatings from well-defined diblock copolymers containing sulfobetaines, Langmuir, 22 (2006) 2222-2226.
[119] Q. Zhou, X.-P. Lei, J.-H. Li, B.-F. Yan, Q.-Q. Zhang, Antifouling, adsorption and reversible flux properties of zwitterionic grafted PVDF membrane prepared via physisorbed free radical polymerization, Desalination, 337 (2014) 6-15.
[120] G. Li, H. Xue, C. Gao, F. Zhang, S. Jiang, Nonfouling polyampholytes from an ion-pair comonomer with biomimetic adhesive groups, Macromolecules, 43 (2009) 14-16.
[121] P. Singha, J. Locklin, H. Handa, A review of the recent advances in antimicrobial coatings for urinary catheters, Acta biomaterialia, 50 (2017) 20-40.
[122] Q. Shao, S. Jiang, Molecular understanding and design of zwitterionic materials, Advanced Materials, 27 (2015) 15-26.
[123] S. Chen, L. Li, C. Zhao, J. Zheng, Surface hydration: Principles and applications toward low-fouling/nonfouling biomaterials, Polymer, 51 (2010) 5283-5293.
[124] S. Chen, J. Zheng, L. Li, S. Jiang, Strong resistance of phosphorylcholine self-assembled monolayers to protein adsorption: insights into nonfouling properties of zwitterionic materials, Journal of the American Chemical Society, 127 (2005) 14473-14478.
[125] O. Azzaroni, A.A. Brown, W.T. Huck, UCST wetting transitions of polyzwitterionic brushes driven by self-association, Angewandte Chemie International Edition, 45 (2006) 1770-1774.
[126] Q. Shao, Y. He, A.D. White, S. Jiang, Difference in hydration between carboxybetaine and sulfobetaine, The Journal of Physical Chemistry B, 114 (2010) 16625-16631.
[127] Q. Shao, S. Jiang, Influence of charged groups on the properties of zwitterionic moieties: a molecular simulation study, The Journal of Physical Chemistry B, 118 (2014) 7630-7637.
[128] A. Laschewsky, Structures and synthesis of zwitterionic polymers, Polymers, 6 (2014) 1544-1601.

[129] S.C. Dobbins, D.E. McGrath, M.T. Bernards, Nonfouling hydrogels formed from charged monomer subunits, The Journal of Physical Chemistry B, 116 (2012) 14346-14352.
[130] S. Chen, S. Jiang, An new avenue to nonfouling materials, Advanced Materials, 20 (2008) 335-338.
[131] S. Sakata, Y. Inoue, K. Ishihara, Precise control of surface electrostatic forces on polymer brush layers with opposite charges for resistance to protein adsorption, Biomaterials, 105 (2016) 102-108.
[132] M. Gao, K. Gawel, B.T. Stokke, Polyelectrolyte and antipolyelectrolyte effects in swelling of polyampholyte and polyzwitterionic charge balanced and charge offset hydrogels, European Polymer Journal, 53 (2014) 65-74.
[133] C.L. McCormick, J. Middleton, D. Cummins, Water-soluble copolymers. 37. Synthesis and characterization of responsive hydrophobically modified polyelectrolytes, Macromolecules, 25 (1992) 1201-1206.
[134] T. Yamaguchi, F. Miyata, S.-i. Nakao, Pore-filling type polymer electrolyte membranes for a direct methanol fuel cell, Journal of Membrane Science, 214 (2003) 283-292.
[135] W. Chen, Y. Su, J. Peng, X. Zhao, Z. Jiang, Y. Dong, Y. Zhang, Y. Liang, J. Liu, Efficient wastewater treatment by membranes through constructing tunable antifouling membrane surfaces, Environmental Science & Technology, 45 (2011) 6545-6552.
[136] W. Chen, Y. Su, J. Peng, Y. Dong, X. Zhao, Z. Jiang, Engineering a robust, versatile amphiphilic membrane surface through forced surface segregation for ultralow flux-decline, Advanced Functional Materials, 21 (2011) 191-198.
[137] A. Asatekin, S. Kang, M. Elimelech, A.M. Mayes, Anti-fouling ultrafiltration membranes containing polyacrylonitrile-graft-poly (ethylene oxide) comb copolymer additives, Journal of Membrane Science, 298 (2007) 136-146.
[138] S. Kang, A. Asatekin, A.M. Mayes, M. Elimelech, Protein antifouling mechanisms of PAN UF membranes incorporating PAN-g-PEO additive, Journal of Membrane Science, 296 (2007) 42-50.
[139] W. Ma, S. Rajabzadeh, A.R. Shaikh, Y. Kakihana, Y. Sun, H. Matsuyama, Effect of type of poly (ethylene glycol)(PEG) based amphiphilic copolymer on antifouling properties of copolymer/poly (vinylidene fluoride)(PVDF) blend membranes, Journal of Membrane Science, 514 (2016) 429-439.
[140] R.F. Brady Jr, I.L. Singer, Mechanical factors favoring release from fouling release coatings, Biofouling, 15 (2000) 73-81.
[141] R.B. Pernites, C.M. Santos, M. Maldonado, R.R. Ponnapati, D.F. Rodrigues, R.C. Advincula, Tunable protein and bacterial cell adsorption on colloidally templated superhydrophobic polythiophene films, Chemistry of Materials, 24 (2011) 870-880.

[142] M.P. Sousa, J.o.F. Mano, Superhydrophobic paper in the development of disposable labware and lab-on-paper devices, ACS Applied Materials & Interfaces, 5 (2013) 3731-3737.
[143] X. Zhao, Y. Su, Y. Li, R. Zhang, J. Zhao, Z. Jiang, Engineering amphiphilic membrane surfaces based on PEO and PDMS segments for improved antifouling performances, Journal of Membrane Science, 450 (2014) 111-123.
[144] R. Revanur, B. McCloskey, K. Breitenkamp, B.D. Freeman, T. Emrick, Reactive amphiphilic graft copolymer coatings applied to poly (vinylidene fluoride) ultrafiltration membranes, Macromolecules, 40 (2007) 3624-3630.
[145] M.S. Rahaman, H. Thérien-Aubin, M. Ben-Sasson, C.K. Ober, M. Nielsen, M. Elimelech, Control of biofouling on reverse osmosis polyamide membranes modified with biocidal nanoparticles and antifouling polymer brushes, Journal of Materials Chemistry B, 2 (2014) 1724-1732.
[146] I. Banerjee, D. Mondal, J. Martin, R.S. Kane, Photoactivated antimicrobial activity of carbon nanotube− porphyrin conjugates, Langmuir, 26 (2010) 17369-17374.
[147] Y. Liu, C. Leng, B. Chisholm, S. Stafslien, P. Majumdar, Z. Chen, Surface structures of PDMS incorporated with quaternary ammonium salts designed for antibiofouling and fouling release applications, Langmuir, 29 (2013) 2897-2905.
[148] A.J. Blok, R. Chhasatia, J. Dilag, A.V. Ellis, Surface initiated polydopamine grafted poly ([2-(methacryoyloxy) ethyl] trimethylammonium chloride) coatings to produce reverse osmosis desalination membranes with anti-biofouling properties, Journal of Membrane Science, 468 (2014) 216-223.
[149] L. Ni, J. Meng, X. Li, Y. Zhang, Surface coating on the polyamide TFC RO membrane for chlorine resistance and antifouling performance improvement, Journal of Membrane Science, 451 (2014) 205-215.
[150] F. Perreault, M.E. Tousley, M. Elimelech, Thin-film composite polyamide membranes functionalized with biocidal graphene oxide nanosheets, Environmental Science & Technology Letters, 1 (2013) 71-76.
[151] A. Mollahosseini, A. Rahimpour, Interfacially polymerized thin film nanofiltration membranes on TiO2 coated polysulfone substrate, Journal of Industrial and Engineering Chemistry, 20 (2014) 1261-1268.
[152] T. Vercellino, A. Morse, P. Tran, A. Hamood, T. Reid, L. Song, T. Moseley, The use of covalently attached organo-selenium to inhibit S. aureus and E. coli biofilms on RO membranes and feed spacers, Desalination, 317 (2013) 142-151.
[153] M. Ben-Sasson, X. Lu, E. Bar-Zeev, K.R. Zodrow, S. Nejati, G. Qi, E.P. Giannelis, M. Elimelech, In situ formation of silver nanoparticles on thin-film composite reverse osmosis membranes for biofouling mitigation, Water Research, 62 (2014) 260-27.

Chapter 2

Zwitterionic polymer modification of polyamide reverse osmosis membranes via surface amination and atom transfer radical polymerization for anti-biofouling

2.1. Introduction

Polyamide reverse osmosis (RO) membranes are on the cutting edge of membrane technology, being widely applied for seawater and brackish water desalination, as well as water reuse, owing to their compactness, modularity, reliability, and energy- and space-saving [1]. These membranes exhibit excellent performance to purify water containing organic foulants such as bacteria, proteins, and polysaccharides [2-5]. One of the major drawbacks of most polyamide RO membranes is biofouling, which causes the water flux decline, shortens the membrane lifetime, and increases the energy consumption [6, 7]. Therefore, many strategies have been devised to achieve ultra-low biofouling [8].

Increasing the hydrophilicity of membrane surfaces is regarded to be an effective method to reduce biofouling because the hydration layer forms an energetic barrier to prevent foulant adsorption [9-11]. Thus, extensive efforts have been devoted to investigating surface modifications of polyamide RO membranes with hydrophilic materials. Poly(ethylene glycol)

(PEG) has been proposed as an anti-biofouling material because neutrally charged PEG grafting results in high surface hydrophilicity and excluded volume effects, improving the resistance toward nonspecific adsorption of organic foulants [12]. However, PEG tends to auto-oxidize in the presence of oxygen, losing its antifouling capacity [13].

Over recent years, zwitterionic polymers such as polyphosphobetaine, polysulfobetaine, and polycarboxybetaine have been considered as excellent anti-biofouling materials [14-17]. Zwitterionic species containing both positively and negatively charged groups are able to bind water molecules even more strongly and stably than other hydrophilic materials via electrostatically induced hydration [18]. On zwitterionic polymer-grafted surfaces, the high water content prevents the irreversible adsorption of organic foulants without significant conformational changes [19]. Therefore, many researches about the surface modification of RO membranes using zwitterionic polymers were conducted for anti-biofouling. Wang et al. modified the RO membrane surface with polycarboxybetaine via redox-initiated reaction, and reported that the permselectivity, anti-biofouling and cleaning properties of RO membranes were significantly improved [20]. Gleason et al. reported the RO membranes modified with polycarboxybetaine [21] or polysulfobetaine [22] via initiated chemical vapor deposition technique effectively prevented the bacterial adhesion. Azari et al. incorporated a redox functional amino acid 3-(3,4-dihydroxyphenyl)-L-alanine onto commercial RO membranes to create a zwitterionic surface that resisted membrane fouling [23]. As above, the surface modification using zwitterionic polymer is a promising way to prevent the bacterial adhesion. However, the effect of the polymer grafting and polymer main chain length on the dynamic biofouling behavior for water filtration applications has still not been clarified. The difficulty to evaluate the anti-biofouling properties is time-dependent, slow and complicated behavior of biofouling [24]. Biofouling is sequential phenomenon corresponding to bacterial adhesion, growth, biofilm formation, and pore blocking.

In the previous studies, the protein-containing water [20, 23], bacterial suspended water [25-28] or actual waste water like as membrane bioreactor-treated water [29, 30] were used as the feed water. These systems wouldn't reflect the biofouling behavior including bacterial adhesion, bacterial growth, and biofilm formation on the membrane surface.

There are several preparation approaches for commercial polyamide RO membrane with zwitterionic polymers, including redox reactions [20, 31], electrostatic coating [32], UV-initiated radical grafting [33, 34], and initiated chemical vapor deposition [21, 22, 35]. However, these modification methods have some major disadvantages, such as low surface density, low stability, and degradation of the separation performance. Notably, all these approaches are limited to increase the grafted-polymer density and control the polymer main chain length precisely. In contrast, surface-initiated atom transfer radical polymerization (SI-ATRP) is a promising method to accurately and efficiently control the main chain length of grafted polymers on material surfaces [36]. Recently, SI-ATRP has been applied for the surface modification of water purification membranes for specific applications, such as antifouling, stimulus-responsiveness, adsorption functionalities, and pervaporation [37]. Initiator immobilization on the membrane surface is a crucial step of SI-ATRP reactions. The acyl halide-type initiator α-bromoisobutyryl bromide (BIBB) is generally used because acyl halide groups react readily with the hydroxyl and amino groups of membrane surfaces. However, commercial polyamide RO membranes have a small number of these terminal groups on their surface and are less reactive, limiting the reaction with such initiators. To apply SI-ATRP to polyamide RO membranes, the modification of the membrane fabrication process is feasible [25, 38, 39] but it is less acceptable to the commercialization. Thus, additional efforts are needed to improve the immobilization of SI-ATRP initiators for easy application on the polyamide RO membrane.

Objectives in this work are firstly to develop an effective method to immobilize SI-ATRP initiators on the less reactive surface of polyamide RO membranes, and secondly to evaluate the effect of the main chain length of a zwitterionic polymer on biofouling prevention systematically. 3-Aminopropyltrimethoxysilane (APTS) was used to aminate the surface of a polyamide RO membrane to improve the BIBB immobilization. Then, after BIBB immobilization, poly[2-(methacryloyloxy)ethyl]dimethyl(3-sulfopropyl)ammonium hydroxide (pMEDSAH) was grafted on the membrane surface via SI-ATRP. The main chain length of the grafted zwitterionic polymer was controlled by changing polymerization time and quantified by gel permeation chromatography (GPC). The surface chemical properties of the modified membranes with various polymer main chain lengths were characterized by attenuated total reflection-Fourier transform infrared (ATR-FTIR) spectroscopy, X-ray photoelectron spectroscopy (XPS), and contact angle measurements. The surface morphology was observed using scanning electron microscopy (FE-SEM) and atomic force microscopy (AFM). The biofouling resistance of the modified membranes was evaluated by static bacterial adhesion and dynamic biofouling filtration experiments.

2.2. Experimental

2.2.1. Materials

Commercial polyamide RO membranes (ES20) were purchased from Nitto Denko (Osaka, Japan). 3-Aminopropyltrimethoxysilane (APTS) was used to modify the surface of the RO membranes. α-Bromoisobutyryl bromide (BIBB; Sigma-Aldrich, St. Louis, MO, USA) was used as the initiator for SI-ATRP. L-Ascorbic acid (Tokyo Chemical Industry, Tokyo, Japan), copper (II) bromide ($CuBr_2$), and tris(2-pyridylmethyl)amine (TPMA) were used for the SI-ATRP reaction. MEDSAH (Sigma-Aldrich) was used as the zwitterionic monomer. Ethyl-2-bromoisobutyrate (EBIB; Tokyo Chemical Industry) was used as the SI-ATRP initiator for

polymerization in solution. Sphingomonas paucimobilis NBRC 13935 was obtained from the NITE Biological Resource Center (Chiba, Japan) and used as the model bacteria strain. Tryptic soy broth (TSB; Becton, Dickinson and Company, Franklin Lakes, NJ, USA) was used to culture the bacteria and SYTO9 (Life Technologies, Carlsbad, CA, USA) to stain them. All other chemicals were purchased from Wako Pure Chemical Industry, Osaka, Japan. Milli-Q water was obtained from a Milli-Q water purification system (Merck Millipore, Darmstadt, Germany) and used in all the experiments.

2.2.2. Membrane modification

A scheme of the membrane modification process is presented in Fig. 2.1. First, a pretreatment was performed to facilitate the BIBB immobilization. A circular polyamide RO membrane with 36-mm diameter was immersed in an aqueous solution of APTS and then subjected to vacuum at room temperature for 10 min. Then, the membrane was immersed in a hexane solution of BIBB at room temperature for 1 min and rinsed thoroughly with hexane and Milli-Q water.

For the SI-ATRP reaction, the BIBB-immobilized membrane was placed in a glass bottle. A mixture of 14.0 mL Milli-Q water and methanol (1:1, v/v) containing 10 mmol of MEDSAH and 0.8 mmol of ascorbic acid were added to the bottle. After 10 min of nitrogen bubbling, 4 mL of Milli-Q water/methanol (1:1, v/v) containing 0.02 mmol of $CuBr_2$ and 0.04 mmol of TPMA was added to initiate the SI-ATRP reaction. The mixed solution was then stirred for a given polymerization time, after which RO membrane grafted with pMEDSAH was obtained. The membrane was washed with Milli-Q water in a shaker overnight at 40 °C and kept in Milli-Q water for further use.

The BIBB-immobilized membranes are denoted by *x*S*y*B, in which *x* and *y* indicate the concentration of APTS (vol%) and BIBB (wt%) during membrane fabrication, respectively.

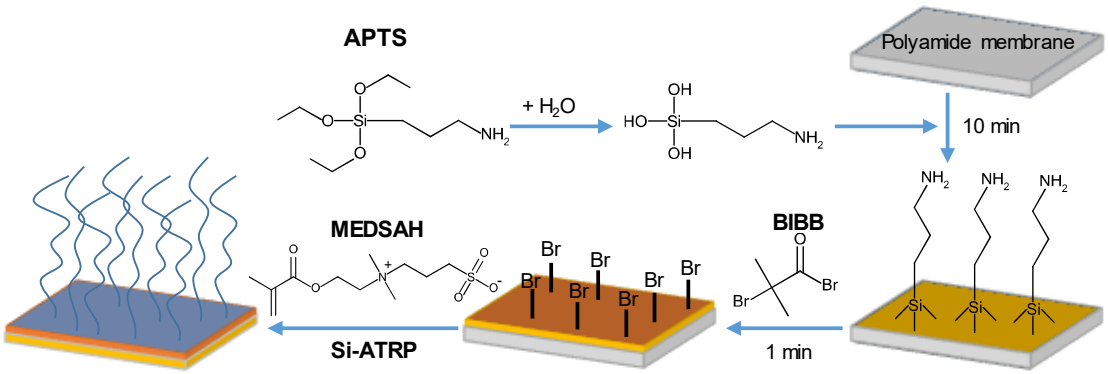

Fig. 2.1. Scheme of the SI-ATRP reaction of MEDSAH on a polyamide RO membrane after APTS pretreatment.

2.2.3. Surface characterization

2.2.3.1. Surface morphology

The surface morphology of the fabricated membranes was observed by both field emission scanning electron microscopy (FE-SEM; JSF-7500, JEOL, Tokyo, Japan) and atomic force microscopy (AFM; SPA-400, Hitachi High-Technologies, Tokyo, Japan). The surface roughness R_a was determined by AFM using the dynamic force mode and a SI-DF40 cantilever. For FE-SEM and AFM observation, the membrane samples were freeze-dried under vacuum using a freeze-dryer (FDU-1200, Tokyo Rikakikai, Tokyo, Japan).

2.2.3.2. Chemical and physical properties

The surface chemistry of the pristine and modified membranes was evaluated by ATR-FTIR spectroscopy (Nicolet iS5, Thermo Fisher Scientific, MA, USA). The surface elemental content of the membranes was evaluated by XPS (JPS-9010MC, JEOL). Before the measurements, the

membranes were completely dried. The surface hydrophilicity of the membranes was determined by the water droplet method in a contact angle meter (DM-300, Kyowa Interface Science, Saitama, Japan). The reported contact angle values are the average of at least two different membrane samples after ten measurements of each sample.

2.2.4. Quantification of grafted pMEDSAH

The main chain length of the pMEDSAH grafted on the membrane surface was evaluated from SI-ATRP in solution using EBIB as the SI-ATRP initiator. The average molecular weight of the synthesized pMEDSAH was determined by a GPC apparatus (Viscotek TDAmax, Malvern Instruments, Worcestershire, UK) and a Shodex GF-510HQ column (Showa Denko, Tokyo, Japan).

2.2.5. Membrane performance

2.2.5.1. Water permeability and salt rejection

The water permeability and salt rejection properties of the fabricated membranes were evaluated using a laboratory scale cross-flow membrane test unit (Fig. 2.2), as described in a previous study [40]. The effective surface area of the membrane was 8.0 cm^2. Milli-Q water and aqueous 0.05 wt% NaCl were used as the feed water to measure the water permeability and salt rejection, respectively. The feed water was introduced at 2.0 mL/min using a plunger pump (NPL-120, Nihon Seimitsu Kagaku, Tokyo, Japan). The applied pressure on the membrane was controlled using a back-pressure valve at 0.75 MPa. The feed water side of the membrane surface was magnetically stirred at 500 rpm. The water permeability (L; L/(m^2 h MPa); LMH/MPa) was calculated by:

$$L = \frac{Q}{A \times t \times P} \quad (1)$$

where Q is the volume of accumulated permeate, A is the effective surface area of the membrane, t is the time, and P is the applied pressure on the membrane surface. In the case of salt rejection measurements, the electric conductivity of the feed (C_f) and permeate (C_p) water was monitored with a conductivity meter (B-771, Horiba, Kyoto, Japan) and the salt rejection (R) was calculated as follows:

$$R\ (\%) = \frac{C_f - C_p}{C_f} \times 100 \quad (2)$$

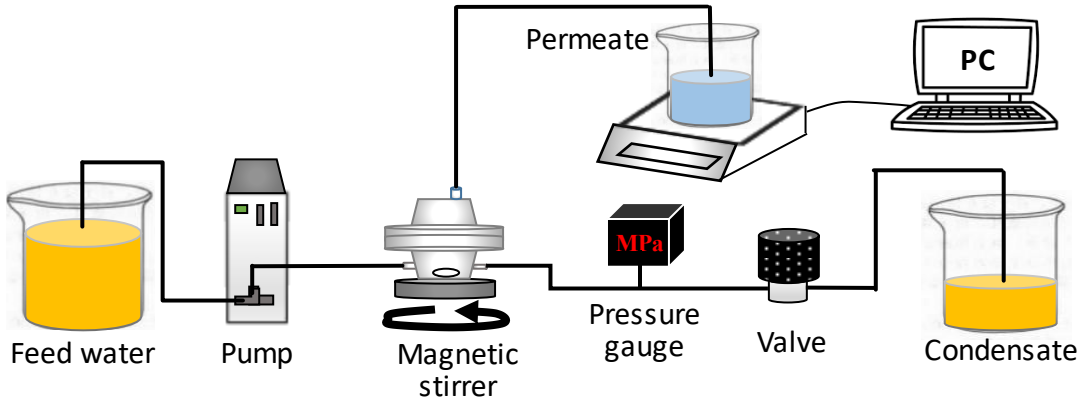

Fig. 2.2. Scheme of the laboratory-scale cross-flow membrane test unit to evaluate the membrane performance.

2.2.5.2. Protein adsorption test

Bovine serum albumin labelled with fluorescein isothiocyanate (FITC-BSA, Sigma-Aldrich) was selected as a model of proteins. First, 100 ppm of FTIC-BSA was dissolved in buffer solution (pH=7.4) containing 10 mM 4-(2-hydroxyethyl)-1-piperazineethanesulfonic acid (HEPES) and 150 mM NaCl. The pristine and pMEDSAH-grafted membranes were immersed into the prepared FTIC-BSA solution at 120 rpm and 30 °C for 1 hour, and washed with the HEPES buffer solution three times at 120 rpm and 30 °C for 10 min. The membranes were observed using a confocal laser scanning microscopy (CLSM; FV1000D, Olympus, Tokyo, Japan), and the fluorescence

intensity on the membrane surfaces was quantified using ImageJ software (National Institutes of Health, Bethesda, MD, USA). The relative fluorescence intensity was calculated by the following equation.

$$Relative\ \ fluorescence\ \ intensity\ \ (\%) = \frac{I_m}{I_{RO}} \times\ 100 \qquad (3)$$

where I_m and I_{RO} are the fluorescence intensity of the modified membrane and pristine RO membrane, respectively.

2.2.5.3. Static bacteria adhesion tests

The bacterial adhesion propensity of the fabricated membranes was evaluated by static bacteria adhesion tests, as described in a previous study [32]. Bacteria were precultured in TSB medium for 12 h at 30 ℃. Then, the precultured bacterial suspension was diluted 50 times with fresh TSB medium and cultured again for 4 h at 30 ℃. The bacterial suspension was diluted with fresh TSB medium to a final optical density of 0.05 at 450 nm for each of the experiments. The optical density was measured using a spectrophotometer (V-650, Jasco, Tokyo, Japan). The membranes were immersed in a bacteria suspension at 120 rpm at 30 ℃ for 24 h. The membranes were gently rinsed twice with aqueous 0.85 wt% NaCl and immersed in aqueous 0.85 wt% NaCl containing SYTO9 for 20 min to stain the bacteria adhered to the membrane surface. To fix the stained bacteria on the membrane surface, the membranes were immersed in aqueous 2.5% glutaraldehyde for 3 min, and rinsed and kept in aqueous 0.85 wt% NaCl. The stained membranes were observed using CLSM and the coverage of adhered bacteria was calculated with the ImageJ software.

2.2.5.4. Dynamic biofouling filtration tests

The biofouling propensity of pristine and modified membranes was assessed by dynamic biofouling tests, as described in a previous study [41]. This evaluation system can simulate the biofouling behavior of bacterial growth, biofilm formation, and water flux decline. A bacterial suspension was prepared similarly to that for the static bacterial adhesion tests. First, 2 mL bacterial solution was poured on the surface of the fabricated membrane and incubated at 30 ℃ for 1 h for adhesion of bacteria on the membrane surface. The membrane was briefly washed with aqueous 0.85 wt% NaCl and set in a cross-flow membrane test unit (Fig. 2.2). TSB medium, diluted five times with aqueous 0.85 wt% NaCl, was fed to the membrane cell at 2.0 mL/min and 1.5 MPa for 20 h. The organic concentration of this feed water is higher than that of actual waste water to accelerate the biofouling [42, 43]. The feed water side of the membrane surface was magnetically stirred at 200 rpm and the whole membrane cell was incubated at 30 ℃. The accumulated permeate weight was recorded to calculate the changes in the permeability. After the filtration experiment, the tested membrane was washed with aqueous 0.85 wt% NaCl and the adhered bacteria were stained with SYTO9, as described for the static bacterial adhesion tests. The stained membrane surfaces were observed using CLSM and FE-SEM. The bacterial coverage was calculated with the ImageJ software.

2.3. Results and discussion

2.3.1. Effect of APTS treatment on BIBB immobilization

In order to improve the initiator immobilization on the polyamide RO membrane, different pretreatments were studied. Table 2.1 shows the effect of the pretreatments on the membrane performance and Br ratio (Br_{3d}, measured by XPS) on the membrane surface after BIBB immobilization. The BIBB-modified membrane without any pretreatment exhibited a similar

membrane performance and Br ratio than the pristine membrane. BIBB is easily decomposed by water and loses reactivity; therefore, BIBB was barely immobilized on the surface of the membrane covered with water molecules. Drying the membrane before BIBB immobilization was also attempted as a pretreatment. Although the BIBB content increased compared to that of the membrane without any pretreatments, both the water permeability and salt rejection decreased, indicating that the membrane structure collapsed upon drying. When the APTS-treated membrane was reacted with BIBB, the Br ratio increased while the membrane performance was maintained. The APTS treatment affords a polysiloxane layer on the membrane surface via a sol–gel reaction that improves the salt rejection [44], while simultaneously introducing amino groups able to react easily with BIBB. Therefore, the APTS treatment was applied as a SI-ATRP pretreatment throughout the work described here.

Table 2.1. Effect of pretreatments before BIBB immobilization on the water permeability, salt rejection, and Br ratio of the fabricated membranes

Pretreatment	Water permeability (LMH/MPa)	NaCl rejection (%)	Br_{3d} (atomic %)**
Pristine membrane*	67.48	97.3	0
No pretreatment	49.37	98.3	0.04
Drying	36.82	83.0	2.04
1 % (v/v) APTS treatment	50.48	96.9	1.98

All the results are the average of three measurements with less than 5% variation. The BIBB concentration was 3 wt%.

* Without BIBB immobilization.

** Elemental ratio measured by XPS.

2.3.2. Effect of APTS and BIBB concentration on BIBB immobilization

In order to optimize the conditions for BIBB immobilization, the effect of the concentration of APTS and BIBB on the water permeability, salt rejection, and surface elemental ratio was investigated. The water permeability and salt rejection properties of BIBB-immobilized membranes at different APTS concentrations are presented in Fig. 2.3. With the increasing APTS concentration, the water permeability decreased, while there were no significant changes in the salt rejection. High APTS concentrations reduce the surface hydrophilicity due to the larger number of carbon groups, affording a reduction of the water permeability and an increase of the salt rejection [44]. Table 2.2 shows the elemental ratios of BIBB-immobilized membranes at different APTS concentrations. The Si and Br ratios increased with the APTS concentration, corresponding to the introduction of APTS and BIBB on the membrane surface, respectively.

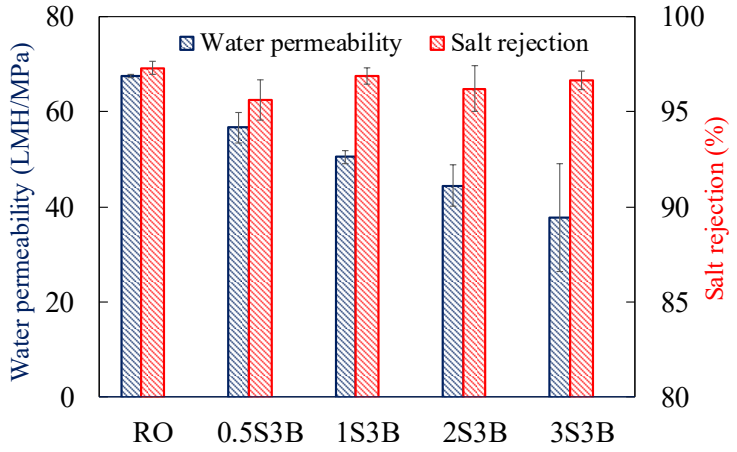

Fig. 2.3. Effect of the APTS concentration on the water permeability and salt rejection of pristine and BIBB-immobilized membranes. The BIBB concentration was fixed at 3.0 wt%.

Table 2.2. Effect of the APTS concentration on the surface elemental ratios of pristine and BIBB-immobilized membranes

	Elemental ratio (atomic %)				
Membrane	C_{1s}	O_{1s}	N_{1s}	Si_{2p}	Br_{3d}
Pristine RO	70.74	16.42	12.84	0.00	0.00
0.5S3B	69.79	15.97	10.95	2.17	0.98
1S3B	67.67	17.01	10.57	2.77	1.98
2S3B	64.72	17.75	11.16	3.68	2.70
3S3B	65.64	16.95	10.17	4.09	3.15

Next, the effect of the BIBB concentration on the BIBB immobilization was investigated. Fig. 2.4 shows the performance of membranes fabricated at different BIBB concentrations. The salt rejection barely changed with the increasing BIBB concentration, although the water permeability of the BIBB-immobilized membranes slightly decreased compared to that of the pristine membrane. The BIBB layer hinders the permeation of water molecules [25]. The elemental ratios of the membrane surfaces are presented in Table 2.3, which shows the Br ratio increased with the increasing BIBB concentration, indicating that the APTS treatment promotes the introduction of amino groups, thus facilitating the immobilization of BIBB on the surface of the polyamide RO membranes.

In the following, BIBB immobilization was carried out with 1 vol% of APTS and 3 wt% of BIBB, as these conditions resulted in the optimal immobilization of BIBB on the surface of the commercial polyamide RO membrane while maintaining its performance at satisfactory levels.

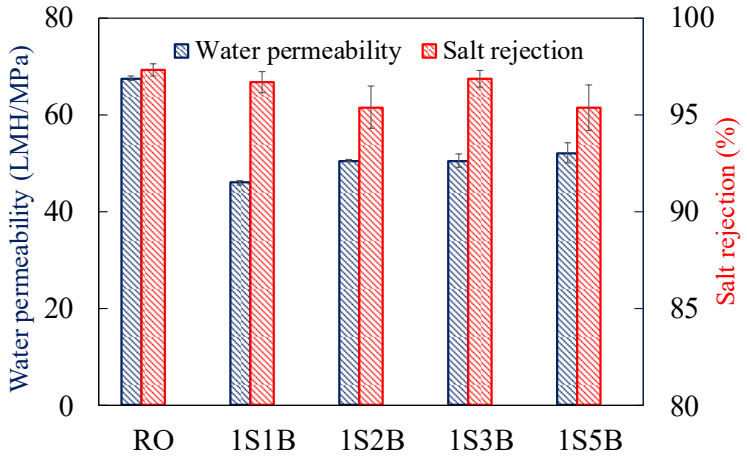

Fig. 2.4. Effect of the BIBB concentration on the water permeability and salt rejection of pristine and BIBB-immobilized membranes. The APTS concentration was fixed at 1.0 vol%.

Table 2.3. Effect of the BIBB concentration on the elemental ratios of pristine and BIBB-immobilized membranes

Membrane	Elemental ratio (atomic %)				
	C_{1s}	O_{1s}	N_{1s}	Si_{2p}	Br_{3d}
Pristine RO	70.74	16.42	12.84	0.00	0.00
1S1B	63.97	19.05	11.24	2.12	1.01
1S2B	69.87	15.57	11.02	2.54	1.49
1S3B	67.67	17.01	10.57	2.77	1.98
1S5B	68.22	16.81	10.23	2.22	2.52

2.3.3. Effect of the polymerization time on the SI-ATRP of the RO membrane surface

Effect of the polymerization time of SI-ATRP on the structure of the RO membranes was investigated. Figures 2.5 and 2.6 show the surface morphology and average roughness of the membrane surfaces, respectively. The pristine and BIBB-immobilized membranes presented ridge-and-valley structures. The surface roughness increased significantly upon BIBB immobilization probably due to the aggregation of APTS during the immobilization process. With

the increasing polymerization time, the surface structure became smoother and the surface roughness decreased. It seems that pMEDSAH with longer main chain lengths is able to fill the ridges and valleys of the polyamide layer [45].

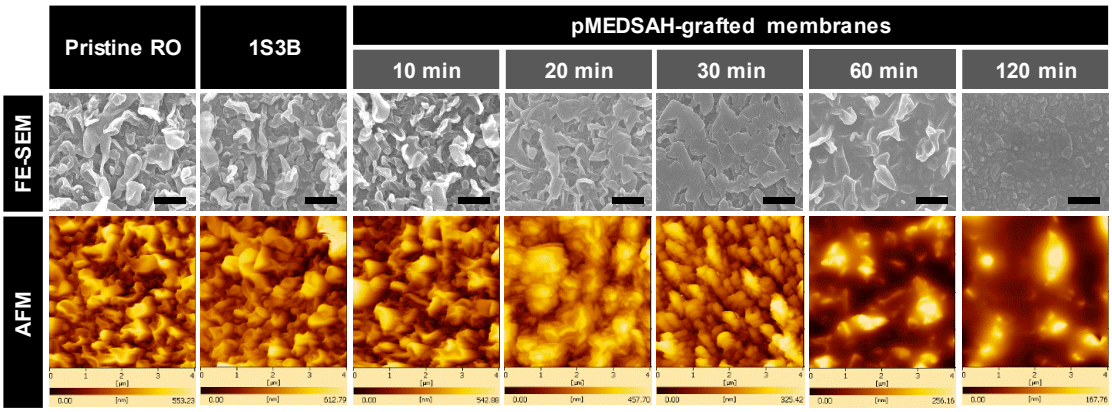

Fig. 2.5. FE-SEM and AFM images of the pristine (RO), BIBB-immobilized (1S3B), and pMEDSAH-grafted membranes fabricated at different polymerization times. The scale bar in the SEM images indicates 500 nm.

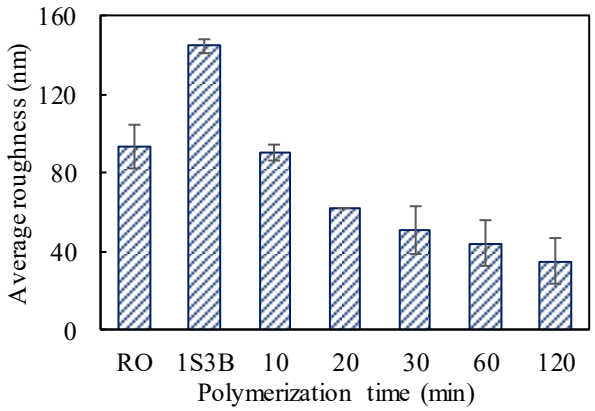

Fig. 2.6. Surface roughness of the fabricated membranes determined by AFM.

Figure 2.7(a) shows the ATR-FTIR spectra of the membranes subjected to different polymerization times. The chemical composition of the membrane surface was not significantly

changed upon BIBB immobilization, as reported in a previous study [25]. The characteristic bands of the main functional groups of MEDSAH (Fig. 2.7(b)) are observed in the spectrum of the membrane after 10 min of SI-ATRP at 1720, 1039, and 953 cm^{-1}, attributed to carbonyl, sulfonate, and quaternary amine groups, respectively [46, 47]. The absorbance changes in these peaks are presented in Fig. 2.7(c). The intensity of all these bands increased with the polymerization time. In particular, the absorbance of the sulfonate group at 1039 cm^{-1} increased more dramatically than that of the other functional groups. Furthermore, the element sulfur was only detected by XPS in the pMEDSAH-grafted membranes (Fig. 2.8), whose ratio increased with the polymerization time. These results indicate that the main chain length of pMEDSAH on the membrane surface increases with the polymerization time. The weight-average molecular weight of pMEDSAH on the membrane surface was estimated by GPC. The SI-ATRP reaction was carried out in solution using EIBB as the SI-ATRP initiator. The weight-average molecular weight of pMEDSAH gradually increased from 22054 to 60811 kDa upon elongating the polymerization time from 30 to 120 min, indicating that the main chain length of pMEDSAH also increased with the polymerization time.

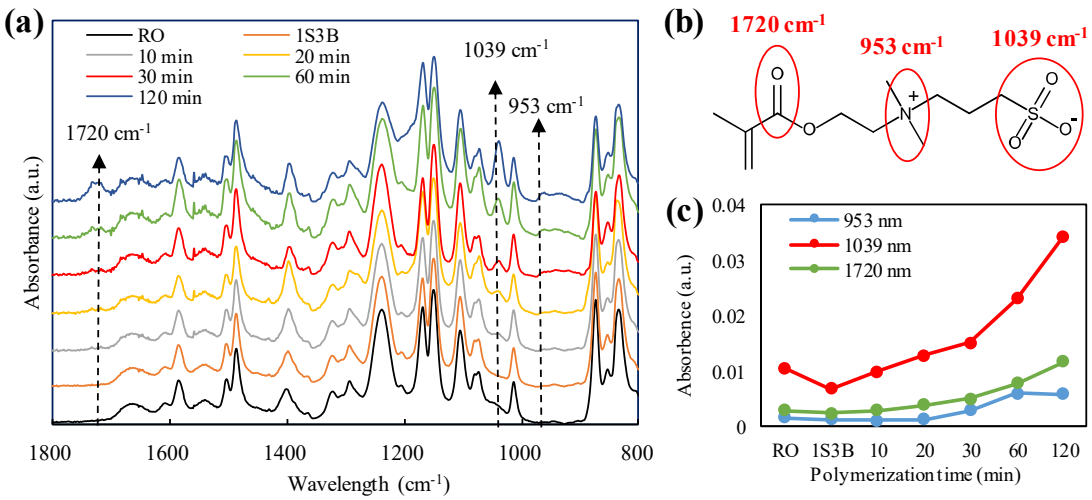

Fig. 2.7. (a) ATR-FTIR spectra of pristine (RO), BIBB-immobilized (1S3B), and pMEDSAH-grafted membranes fabricated at different polymerization times; (b) chemical structure of pMEDSAH and the absorbance wavelengths of its functional groups; and (c) variation in the absorbance of the different functional groups with the polymerization time.

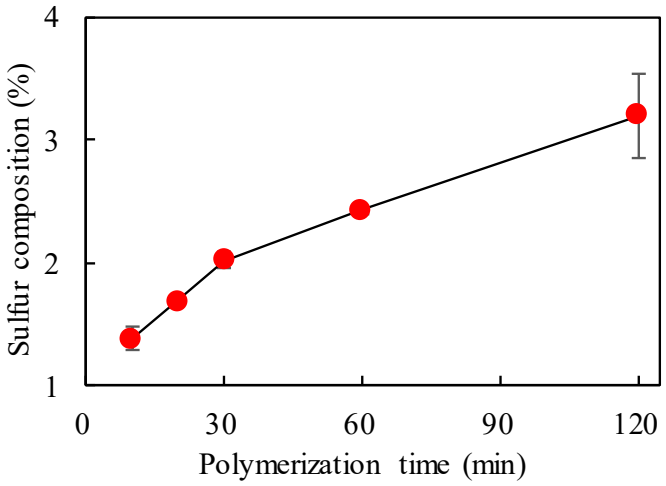

Fig. 2.8. Sulfur content in pMEDSAH-grafted membranes at different polymerization times.

Water contact angle measurements were carried out to investigate the surface hydrophilicity of the fabricated membranes. Fig. 2.9 shows the water contact angle of the fabricated membranes. The water contact angle significantly decreased after BIBB immobilization (1S3B) and SI-ATRP treatment. The short hydrocarbon chain of APTS reduced the surface hydrophobicity [44]. Upon pMEDSAH grafting, the water contact angle was further reduced and the membrane surface became hydrophilic due to the strong hydration capacity of the zwitterionic polymer [48]. The hydrophilicity of the membrane surface slightly increased with the increasing polymerization time. These results further confirm the introduction of the zwitterionic pMEDSAH on the surface of polyamine RO membranes is very useful to make the membrane surface more hydrophilic.

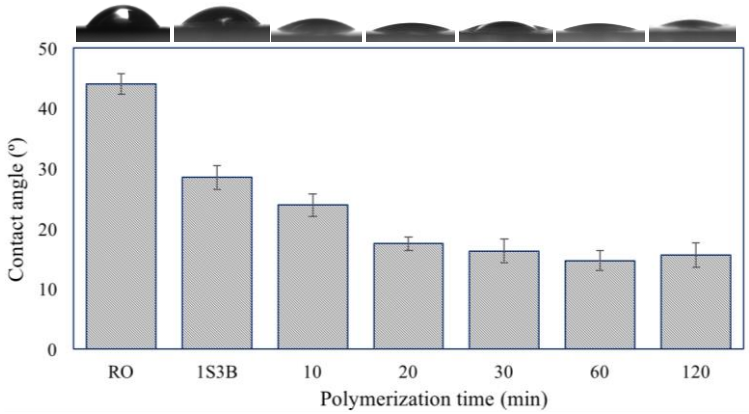

Fig. 2.9. Contact angle of pristine RO and pMEDSAH-grafted membranes at increasing polymerization times.

The water permeability and salt rejection properties of the fabricated membranes are presented in Fig. 2.10. With the increasing polymerization time, the water permeability decreased gradually owing to a thick layer of pMEDSAH formed on the membrane surface, resulting in hindered water permeation. On the other hand, the salt rejection barely changed upon pMEDSAH grafting.

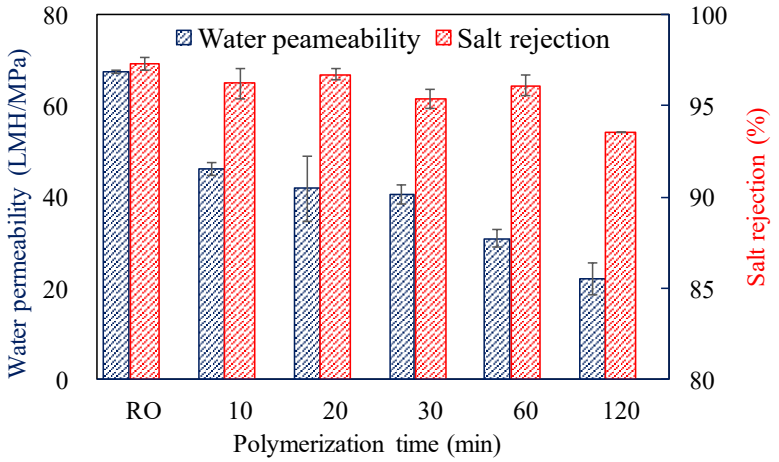

Fig. 2.10. Water permeability and salt rejection properties of pMEDSAH-grafted membranes at different polymerization times.

2.3.4. Static bacterial adhesion on pMEDSAH-modified membranes

Resistance to bacterial adhesion is critical for biofouling mitigation since the adhesion of bacteria typically leads to subsequent colonization and formation of biofilms [49]. The bacterial adhesion data for the pristine and pMEDSAH-grafted membranes at different polymerization times from static adhesion tests are shown in Fig. 2.11. The degree of bacterial adhesion was clearly prevented by pMEDSAH-grafting, which decreased with the increasing polymerization time, similarly to the case of the surface hydrophilicity. The pMEDSAH-grafted membranes also effectively prevented the protein adsorption (Fig. 2.12) as same as previously reported [38, 50]. The tendency of the prevention of the protein adsorption showed a same manner as that of the bacterial adhesion, suggesting that the bacterial adhesion is partially caused by the proteins on their surface [51]. As the membrane surface becomes more hydrophilic, a hydration layer is easily formed on the membrane surface, which prevents the adsorption and deposition of hydrophobic bacteria on the membrane surface, thus reducing fouling [52].

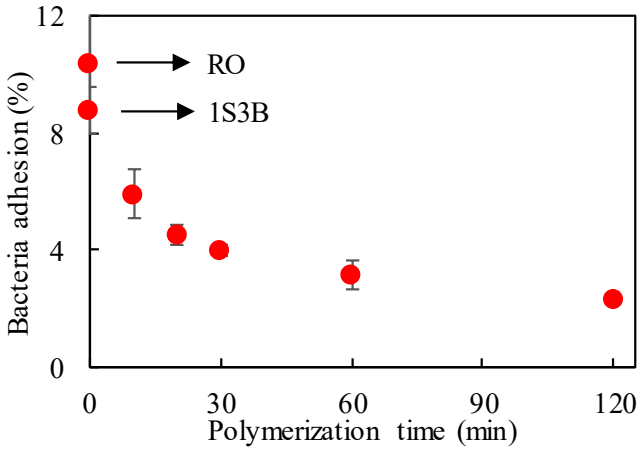

Fig. 2.11. Bacterial adhesion on pristine and pMEDSAH-grafted membranes at different polymerization times.

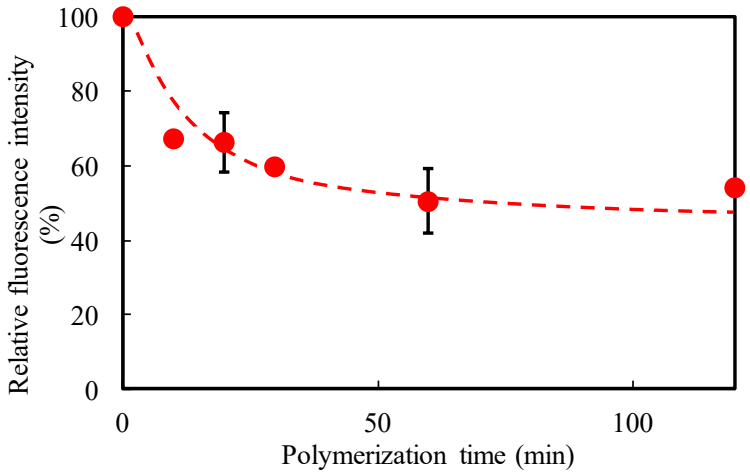

Fig. 2.12. The relative fluorescence intensity of the pMEDSAH-grafted membranes with various polymerization time.

2.3.5. Dynamic biofouling

Finally, the effect of the main chain length of the grafted pMEDSAH on the biofouling behavior of RO membranes was investigated. Fig. 2.13 shows the changes in the water permeability from cross-flow bacterial filtration tests. The permeability of the pristine membrane remarkably decreased after 10 h, suggesting the biofilm formation and pore blocking. On the other hand, that of the pMEDSAH-grafted membranes, especially with over 60-min polymerization, didn't show the permeability decline at 10 h. After 20-h filtration experiments, the water permeability of the pMEDSAH-grafted membranes was higher than that of the pristine membrane, which decreased to values below 40% of the initial value. Such a permeability reduction was inhibited upon pMEDSAH grafting, and the suppression degree increased with the increasing polymerization time. At polymerization times of 10, 30, and 40 min, the water permeability decreased slightly after 20 h of filtration. On the other hand, when the polymerization time was over 60 min, the pMEDSAH-grafted membranes maintained the initial water permeability

throughout the filtration test. Although the membranes modified by polymerization for 60 min presented a lower initial permeability than the pristine membrane due to the surface modification, it exhibited the highest water permeability after 20 h of filtration because of the complete biofouling prevention.

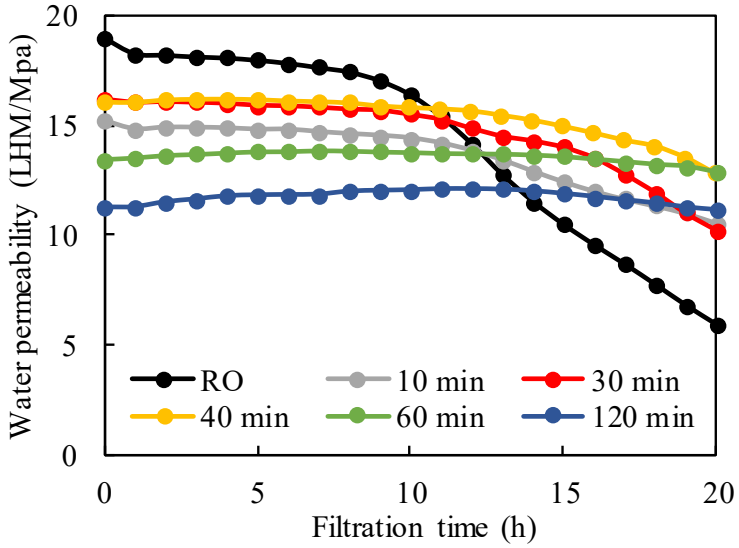

Fig. 2.13. Time course for the water permeability of pristine and pMEDSAH-grafted membranes from biofouling filtration tests using a cross-flow membrane test unit.

Figure 2.14 shows the biofilm structure on the tested membrane surfaces obtained by CLSM and SEM. The surface of the pristine membrane appears significantly covered with bacteria, indicating that bacteria easily adhere to the pristine membrane surface and form a biofilm. With the increasing polymerization time, the biofilm became smaller and thinner, as well as less dense. Fig. 2.15 compiles the bacterial adhesion data obtained from static adhesion tests and dynamic biofouling tests. The bacterial coverage from both static bacterial adhesion and dynamic biofouling tests decreased with the increasing polymerization time. However, the relationship between two correlated data was not a linear correlation. Regarding the pMEDSAH-grafted

membrane after 1 h of polymerization, the bacterial adhesion in the dynamic biofouling test was prevented more significantly than that in the static adhesion test. The main chain length of the grafted polymer is one of the important factors influencing the biofouling behavior. pMEDSAH with short main chain length reduces the adhesion force of bacteria on the polyamide RO membrane surface and prevents the bacterial adhesion, although it barely reduced the biofilm growth in the dynamic tests, while pMEDSAH with longer main chain length is able to prevent both bacterial adhesion and biofilm growth.

The poly-zwitterionic materials used in this study have both positively and negatively charged moieties on the same monomer unit, resulting in uniform charge distribution and neutrality on the membrane surface. Through electrostatically induced hydration, zwitterionic materials are able to bind water molecules even more strongly and stably than other hydrophilic materials such as PEG and polyvinyl alcohol. In this way, poly-zwitterionic materials with suitable main chain length are able to maximize the surface hydration and reduce the electrostatic interactions with the foulant [18]. Moreover, the dense and smooth surface obtained with the zwitterionic polymer with longer main chain length also leads to excellent biofouling resistance owing to the lower surface roughness, which reduces the surface area for membrane–foulant interactions [53, 54]. In addition, the movement of pMEDSAH chain will be easier and larger in the case of longer chain [55], which is another reason for the prevention of biofouling. Thus, control of the architecture of the grafted polymer is crucial to develop anti-biofouling membranes.

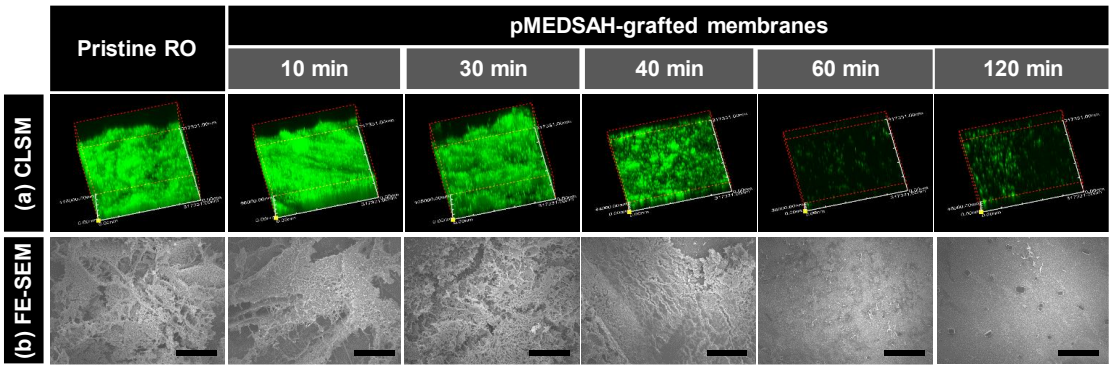

Fig. 2.14. Bacteria adhesion on the surface of pMEDSAH-grafted membranes at different polymerization times after dynamic biofouling filtration tests. 3D images obtained by (a) CLSM and (b) FE-SEM. The scale bar in the FE-SEM images indicates 50 μm.

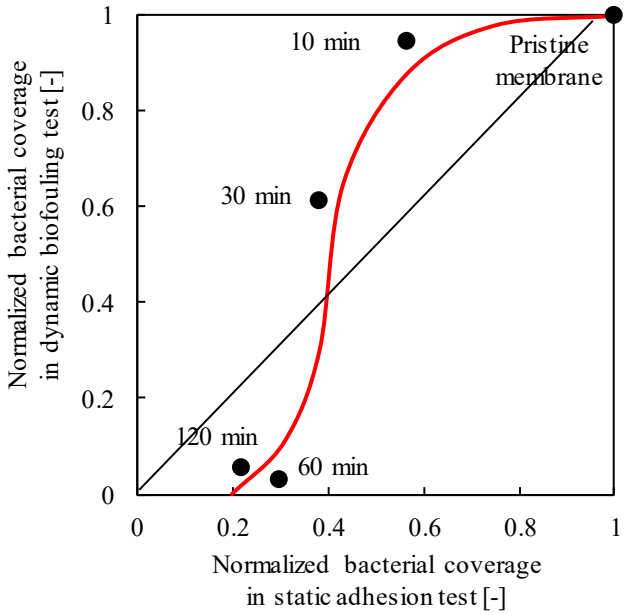

Fig. 2.15. Relationship between the bacterial adhesion from static bacterial adhesion tests and dynamic biofouling filtration tests. The bacterial coverage on the pMEDSAH-grafted membranes was normalized to that on the pristine membrane. The bacterial coverage in the dynamic biofouling tests was obtained by analyzing the CLSM images with the ImageJ software.

2.4. Conclusions

In this work, a surface modification method for polyamide RO membranes with a zwitterionic polymer via aminosilane treatment and SI-ATRP was proposed for surface amination and anti-biofouling purposes. The APTS treatment effectively introduced amino groups on the polyamide layer of the RO membrane and facilitated the immobilization of an SI-ATRP initiator (BIBB), while maintaining the water permeability and salt rejection properties of the original membrane. A zwitterionic polymer, pMEDSAH, was grafted on the surface of BIBB-immobilized membranes and its main chain length was found to increase with the polymerization time. The hydrophilicity and static bacterial adhesion of the membranes was improved by increasing the polymerization time. The dynamic biofouling tests showed that biofilm formation and biofouling were effectively prevented by the pMEDSAH grafting and the increase of polymerization time.

The strategy using APTS treatment is applicable for facilitating the SI-ATRP initiator immobilization on less reactive surfaces of commercial RO membranes, maintaining the permeation properties. Furthermore, this study not only demonstrated the great potential of the zwitterionic polymer modification of RO membranes for the biofouling prevention, but also clarified that the control of the pMEDSAH main chain length is necessary to obtain the best performance for the improvement of the anti-biofouling property.

References

[1] M. Elimelech, W.A. Phillip, The future of seawater desalination: energy, technology, and the environment, Science, 333 (2011) 712-717.
[2] C. Leroy, C. Delbarre, F. Ghillebaert, C. Compere, D. Combes, Influence of subtilisin on the adhesion of a marine bacterium which produces mainly proteins as extracellular polymers, Journal of Applied Microbiology, 105 (2008) 791-799.

[3] S. Lee, M. Elimelech, Relating organic fouling of reverse osmosis membranes to intermolecular adhesion forces, Environmental Science & Technology, 40 (2006) 980-987.
[4] M. Herzberg, M. Elimelech, Biofouling of reverse osmosis membranes: role of biofilm-enhanced osmotic pressure, Journal of Membrane Science, 295 (2007) 11-20.
[5] W.S. Ang, A. Tiraferri, K.L. Chen, M. Elimelech, Fouling and cleaning of RO membranes fouled by mixtures of organic foulants simulating wastewater effluent, Journal of Membrane Science, 376 (2011) 196-206.
[6] Y. Mo, A. Tiraferri, N.Y. Yip, A. Adout, X. Huang, M. Elimelech, Improved antifouling properties of polyamide nanofiltration membranes by reducing the density of surface carboxyl groups, Environmental Science & Technology, 46 (2012) 13253-13261.
[7] W. Guo, H.-H. Ngo, J. Li, A mini-review on membrane fouling, Bioresource Technology, 122 (2012) 27-34.
[8] G.-R. Xu, J.-N. Wang, C.-J. Li, Strategies for improving the performance of the polyamide thin film composite (PA-TFC) reverse osmosis (RO) membranes: Surface modifications and nanoparticles incorporations, Desalination, 328 (2013) 83-100.
[9] E. Ostuni, R.G. Chapman, R.E. Holmlin, S. Takayama, G.M. Whitesides, A survey of structure− property relationships of surfaces that resist the adsorption of protein, Langmuir, 17 (2001) 5605-5620.
[10] M. He, K. Gao, L. Zhou, Z. Jiao, M. Wu, J. Cao, X. You, Z. Cai, Y. Su, Z. Jiang, Zwitterionic materials for antifouling membrane surface construction, Acta Biomaterialia, 40 (2016) 142-152.
[11] W. Chen, Y. Su, J. Peng, X. Zhao, Z. Jiang, Y. Dong, Y. Zhang, Y. Liang, J. Liu, Efficient wastewater treatment by membranes through constructing tunable antifouling membrane surfaces, Environmental Science & Technology, 45 (2011) 6545-6552.
[12] G. Kang, M. Liu, B. Lin, Y. Cao, Q. Yuan, A novel method of surface modification on thin-film composite reverse osmosis membrane by grafting poly (ethylene glycol), Polymer, 48 (2007) 1165-1170.
[13] I. Banerjee, R.C. Pangule, R.S. Kane, Antifouling coatings: recent developments in the design of surfaces that prevent fouling by proteins, bacteria, and marine organisms, Advanced Materials, 23 (2011) 690-718.
[14] Y. Chang, S. Chen, Q. Yu, Z. Zhang, M. Bernards, S. Jiang, Development of biocompatible interpenetrating polymer networks containing a sulfobetaine-based polymer and a segmented polyurethane for protein resistance, Biomacromolecules, 8 (2007) 122-127.
[15] S. Chen, F. Yu, Q. Yu, Y. He, S. Jiang, Strong resistance of a thin crystalline layer of balanced charged groups to protein adsorption, Langmuir, 22 (2006) 8186-8191.
[16] R.E. Holmlin, X. Chen, R.G. Chapman, S. Takayama, G.M. Whitesides, Zwitterionic SAMs that resist nonspecific adsorption of protein from aqueous buffer, Langmuir, 17 (2001) 2841-2850.

[17] Z. Zhang, S. Chen, Y. Chang, S. Jiang, Surface grafted sulfobetaine polymers via atom transfer radical polymerization as superlow fouling coatings, The Journal of Physical Chemistry B, 110 (2006) 10799-10804.
[18] S. Chen, L. Li, C. Zhao, J. Zheng, Surface hydration: principles and applications toward low-fouling/nonfouling biomaterials, Polymer, 51 (2010) 5283-5293.
[19] K. Ishihara, H. Nomura, T. Mihara, K. Kurita, Y. Iwasaki, N. Nakabayashi, Why do phospholipid polymers reduce protein adsorption?, Journal of Biomedical Materials Research, 39 (1998) 323-330.
[20] J. Wang, Z. Wang, J. Wang, S. Wang, Improving the water flux and bio-fouling resistance of reverse osmosis (RO) membrane through surface modification by zwitterionic polymer, Journal of Membrane Science, 493 (2015) 188-199.
[21] H.Z. Shafi, A. Matin, Z. Khan, A. Khalil, K.K. Gleason, Surface modification of reverse osmosis membranes with zwitterionic coatings: A potential strategy for control of biofouling, Surface and Coating Technology, 279 (2015) 171-179.
[22] R. Yang, J. Xu, G. Ozaydin-Ince, S.Y. Wong, K.K. Gleason, Surface-tethered zwitterionic ultrathin antifouling coatings on reverse osmosis membranes by initiated chemical vapor deposition, Chemistry of Materials, 23 (2011) 1263-1272.
[23] S. Azari, L. Zou, Fouling resistant zwitterionic surface modification of reverse osmosis membranes using amino acid l-cysteine, Desalination, 324 (2013) 79-86.
[24] H.-C. Flemming, Reverse osmosis membrane biofouling, Experimental Thermal Fluid Science, 14 (1997) 382-391.
[25] D. Saeki, T. Tanimoto, H. Matsuyama, Anti-biofouling of polyamide reverse osmosis membranes using phosphorylcholine polymer grafted by surface-initiated atom transfer radical polymerization, Desalination, 350 (2014) 21-27.
[26] Y. Baek, J. Yu, S.-H. Kim, S. Lee, J. Yoon, Effect of surface properties of reverse osmosis membranes on biofouling occurrence under filtration conditions, Journal of Membrane Science, 382 (2011) 91-99.
[27] X. Zhu, H.-E. Loo, R. Bai, A novel membrane showing both hydrophilic and oleophobic surface properties and its non-fouling performances for potential water treatment applications, Journal of Membrane Science, 436 (2013) 47-56.
[28] F. Razi, I. Sawada, Y. Ohmukai, T. Maruyama, H. Matsuyama, The improvement of antibiofouling efficiency of polyethersulfone membrane by functionalization with zwitterionic monomers, Journal of Membrane Science, 401 (2012) 292-299.
[29] J. Lee, H.-R. Chae, Y.J. Won, K. Lee, C.-H. Lee, H.H. Lee, I.-C. Kim, J.-m. Lee, Graphene oxide nanoplatelets composite membrane with hydrophilic and antifouling properties for wastewater treatment, Journal of Membrane Science, 448 (2013) 223-230.

[30] R. Yang, H. Jang, R. Stocker, K.K. Gleason, Synergistic Prevention of Biofouling in Seawater Desalination by Zwitterionic Surfaces and Low-Level Chlorination, Advance Materials, 26 (2014) 1711-1718.
[31] J. Meng, Z. Cao, L. Ni, Y. Zhang, X. Wang, X. Zhang, E. Liu, A novel salt-responsive TFC RO membrane having superior antifouling and easy-cleaning properties, Journal of Membrane Science, 461 (2014) 123-129.
[32] D. Saeki, T. Tanimoto, H. Matsuyama, Prevention of bacterial adhesion on polyamide reverse osmosis membranes via electrostatic interactions using a cationic phosphorylcholine polymer coating, Colloids and Surfaces A: Physicochemical and Engineering Aspects, 443 (2014) 171-176.
[33] Y.-F. Yang, Y. Li, Q.-L. Li, L.-S. Wan, Z.-K. Xu, Surface hydrophilization of microporous polypropylene membrane by grafting zwitterionic polymer for anti-biofouling, Journal of Membrane Science, 362 (2010) 255-264.
[34] M.L.M. Tirado, M. Bass, M. Piatkovsky, M. Ulbricht, M. Herzberg, V. Freger, Assessing biofouling resistance of a polyamide reverse osmosis membrane surface-modified with a zwitterionic polymer, Journal of Membrane Science, 520 (2016) 490-498.
[35] H.Z. Shafi, Z. Khan, R. Yang, K.K. Gleason, Surface modification of reverse osmosis membranes with zwitterionic coating for improved resistance to fouling, Desalination, 362 (2015) 93-103.
[36] P. Król, P. Chmielarz, Recent advances in ATRP methods in relation to the synthesis of copolymer coating materials, Progress in Organic Coatings, 77 (2014) 913-948.
[37] J. Ran, L. Wu, Z. Zhang, T. Xu, Atom transfer radical polymerization (ATRP): a versatile and forceful tool for functional membranes, Progress Polymer Science, 39 (2014) 124-144.
[38] Y. Zhang, Z. Wang, W. Lin, H. Sun, L. Wu, S. Chen, A facile method for polyamide membrane modification by poly (sulfobetaine methacrylate) to improve fouling resistance, Journal of Membrane Science, 446 (2013) 164-170.
[39] C. Liu, J. Lee, J. Ma, M. Elimelech, Antifouling thin-film composite membranes by controlled architecture of zwitterionic polymer brush layer, Environmental Science & Technology, 51 (2017) 2161-2169.
[40] D. Saeki, S. Nagao, I. Sawada, Y. Ohmukai, T. Maruyama, H. Matsuyama, Development of antibacterial polyamide reverse osmosis membrane modified with a covalently immobilized enzyme, Journal of Membrane Science, 428 (2013) 403-409.
[41] D. Saeki, H. Karkhanechi, H. Matsuura, H. Matsuyama, Effect of operating conditions on biofouling in reverse osmosis membrane processes: Bacterial adhesion, biofilm formation, and permeate flux decrease, Desalination, 378 (2016) 74-79.

[42] S. Rosenberger, U. Krüger, R. Witzig, W. Manz, U. Szewzyk, M. Kraume, Performance of a bioreactor with submerged membranes for aerobic treatment of municipal waste water, Water Research, 36 (2002) 413-420.
[43] M.-h. Huang, Y.-m. Li, G.-w. Gu, Chemical composition of organic matters in domestic wastewater, Desalination, 262 (2010) 36-42.
[44] N. Kim, D.H. Shin, Y.T. Lee, Effect of silane coupling agents on the performance of RO membranes, Journal of Membrane Science, 300 (2007) 224-231.
[45] V. Freger, J. Gilron, S. Belfer, TFC polyamide membranes modified by grafting of hydrophilic polymers: an FT-IR/AFM/TEM study, Journal of Membrane Science, 209 (2002) 283-292.
[46] J. Huang, W. Xu, Zwitterionic monomer graft copolymerization onto polyurethane surface through a PEG spacer, Applied Surface Science, 256 (2010) 3921-3927.
[47] J. Zhang, J. Yuan, Y. Yuan, J. Shen, S. Lin, Chemical modification of cellulose membranes with sulfo ammonium zwitterionic vinyl monomer to improve hemocompatibility, Colloids and Surfaces B: Biointerfaces, 30 (2003) 249-257.
[48] J.B. Schlenoff, Zwitteration: coating surfaces with zwitterionic functionality to reduce nonspecific adsorption, Langmuir, 30 (2014) 9625-9636.
[49] D. Pavithra, M. Doble, Biofilm formation, bacterial adhesion and host response on polymeric implants—issues and prevention, Biomedical Materials, 3 (2008) 034003.
[50] Q. Li, B. Zhou, Q.Y. Bi, X.L. Wang, Surface modification of PVDF membranes with sulfobetaine polymers for a stably anti-protein-fouling performance, Journal of Applied Polymer Science, 125 (2012) 4015-4027.
[51] M. Herzberg, S. Kang, M. Elimelech, Role of extracellular polymeric substances (EPS) in biofouling of reverse osmosis membranes, Environmental Science & Technology, 43 (2009) 4393-4398.
[52] R. Kumar, A. Ismail, Fouling control on microfiltration/ultrafiltration membranes: Effects of morphology, hydrophilicity, and charge, Journal of Applied Polymer Science, 132 (2015).
[53] G.-d. Kang, Y.-m. Cao, Development of antifouling reverse osmosis membranes for water treatment: a review, Water Research, 46 (2012) 584-600.
[54] E.M. Vrijenhoek, S. Hong, M. Elimelech, Influence of membrane surface properties on initial rate of colloidal fouling of reverse osmosis and nanofiltration membranes, Journal of Membrane Science, 188 (2001) 115-128.
[55] D.J. Irvine, A.-V.G. Ruzette, A.M. Mayes, L.G. Griffith, Nanoscale clustering of RGD peptides at surfaces using comb polymers. 2. Surface segregation of comb polymers in polylactide, Biomacromolecules, 2 (2001) 545-556.

Chapter 3

Effect of polymer structure modified on RO membrane surfaces via surface-initiated ATRP on dynamic biofouling behavior

3.1. Introduction

For nearly 30 years, polyamide membranes are the predominance of the commercial reverse osmosis (RO) membrane market [1]. The major concern of RO membranes in desalination systems is membrane fouling [2-6]. The fouling of RO membranes has four classifications: colloidal fouling, crystalline fouling, organic fouling, and biofouling. In general, simply decreasing the foulant contents in feed water enables to control the first three types of fouling effectively but not works for biofouling [7-10], which makes the biofouling become the most severe problem for RO membrane processes.

Biofouling on water purification membranes is a complicated phenomenon that bacteria adhere on the membrane surface initially, and then secret extracellular polymeric substances where they inset and form biofilms by weak chemical interactions including van der Waal's, hydrogen-bonding, electrostatic, hydrophobic interactions [11]. Biofilm development is based on the induction, logarithmical growth and plateau phase [8]. The overall hydraulic resistance and the fluid friction resistance of the membrane will be augmented once the plateau phase occurs

[12], which causes a severe permeability decline, demanding increased energy usage to reach the higher pressures required to maintain flux. Therefore, extensive researches focus on exploring the anti-biofouling materials applicable to polyamide RO membranes.

2-Hydroxyethyl methacrylate (HEMA), poly(ethylene glycol)methacrylate (PEG) and zwitterionic polymers that have been widely used for antifouling materials. PolyHEMA (pHEMA) has been shown to have good stability and biocompatibility [13]. Kochkodan et al. [3] found that the polyethersulfone and poly(vinylidene fluoride) (PVDF) membranes effectively resisted the adhesion of *Escherichia coli* after the pHEMA coatings [14]. Song et al. showed that the polysulfone membranes coated with pHEMA were able to reduce oil emulsion fouling [15]. Yan et al. claimed that the PVDF membranes with pHEMA brushes simultaneously achieved the higher water permeability and ultralow protein absorption [16].

PEG is a promising antifouling polymer that has good hydrophilicity and nontoxicity [17]. It is effective using surface-bounded PEG molecules for surface modification to prevent the membrane surfaces from the hydrophobic or large molecules [18], which already has been applied in microfiltration [19, 20], ultrafiltration [21, 22], nanofiltration [23], and RO [24-26] membranes for antifouling. For example, Belfer and Freger et al. grafted PEG onto polyamide RO membrane surfaces using a redox-initiated method to improve fouling resistance [24, 25].

A zwitterionic monomer exhibits overall electrical neutrality resulting from an identical amount of cationic and anionic groups [27]. A previous study already reviewed and proposed the great anti-biofouling potential of the poly[2-(methacryloyloxy)ethyl]dimethyl(3-sulfopropyl)ammonium hydroxide (pMEDSAH) which is one of the most presentative zwitterionic polymers [28].

Based on the review above, the pHEMA, polyPEG (pPEG), and pMEDSAH enable to improve the anti-biofouling properties of membranes. This good anti-biofouling property is

related to hydrophilic groups of each polymer. However, the systematically comparative study of each polymer on anti-biofouling has not been reported. Therefore, more understanding is needed on how the polymer structure, including the hydration and polymer chain length, influences the membrane biofouling behavior, which will provide more guidance for choosing the anti-biofouling polymers and offer more insight on how to furthest enhance the anti-biofouling property of membranes by using these anti-biofouling polymers.

In this research, HEMA, PEG (average M_n = 360), and MEDSAH monomers were selected to investigate the influence of the polymer structure grafted on the membrane surface, because they have a different, typical structure correlated with the non-biofouling ability. First, the formation of a hydration layer, which adsorbs water molecules tightly, is critical for anti-biofouling, as the hydration layer is an effective barrier to resist the adsorption of foulants [29, 30]. One unit of HEMA and PEG is able to integrate with one and six water molecules, respectively, because each unit of -CH_2CH_2O- includes an oxygen atom integrated with one water molecule via the hydrogen bonding. In contrast, one MEDSAH monomer consists of a cationic quaternary ammonium group and an anionic sulfonate, which is integrated with eight water molecules via the electrostatic interaction [29]. The order of hydration is: MEDSAH > PEG > HEMA. Secondly, chain flexibility also plays an important role in anti-biofouling, because it can result in a steric repulsion to resist the adsorption of foulants. The high chain flexibility results from the long chain length including side chain length and main chain length. The side chain length was defined as the length of offshoot extending from backbone of the monomer [31]. Based on the chemical structure, HEMA, PEG, and MEDSAH monomers have the different side chain length, and the theoretical order of the side chain length is: PEG > MEDSAH > HEMA. The main chain length was defined as the number of monomer unit in a polymer [32]. And the main chain length can be controlled by the polymerization time. A comprehensive study that meticulously

explores the characterizations of these polymer structures, thoroughly analyzes their effect on dynamic biofouling behavior, and carefully assesses the anti-biofouling mechanism could significantly facilitate the fabrication of desirable anti-biofouling membranes.

In order to precisely control the main chain length of the polymers on the membrane surface, surface-initiated atom transfer radical polymerization (SI-ATRP) was applied in this research. Although at present there are several surface modification approaches such as UV-initiated radical grafting, redox reactions, electrostatic coating, and initiated chemical vapor deposition, these modification methods have some major disadvantages, such as low surface density, low stability, and degradation of the separation performance. More importantly, all these approaches are limited to control the main chain length of the polymer accurately. In contrast, SI-ATRP has an excellent ability of controlling the polymer main chain length because of the narrow polydispersity and relatively slow polymerization [33, 34]. Therefore, SI-ATRP is a desirable modification method for systematically exploring the characterization of polymer structure on the membrane surface.

Additionally, previous studies have mainly focused on developing surface modification methods with HEMA, PEG, and zwitterionic polymers for preventing protein fouling or bacterial adhesion. However, biofouling is a sequential phenomenon associated with initial bacterial adhesion, growth, and biofilm formation. Particularly, biofilm formation is a time-dependent, tardy, and complicated behavior that cannot accurately be reflected by simple membrane evaluation systems using bacterial suspended water, protein-containing water, or actual wastewater as feed water [9, 10, 35, 36]. A dynamic biofouling filtration test established in a previous study can simulate these sequential phenomenon [28].

In this research, the features of various hydrophilic polymers were systematically characterized and the effect of polymer structure on biofouling behavior of polyamide RO membranes was assessed. First, pHEMA, polyPEG (pPEG), and pMEDSAH were grafted on

polyamide RO membranes surface via surface-initiated atom transfer radical polymerization (SI-ATRP). In order to isolate the effect of the main chain length, the grafting density was fixed by using the same concentration of initiators, and different SI-ATRP polymerization time was applied for merely controlling the main chain length of the grafted polymer on the membrane surfaces. To assess the grafted polymer structure, the surface chemical properties of the modified membranes were analyzed by using attenuated total reflection-Fourier transform infrared (ATR-FTIR) spectroscopy and X-ray photoelectron spectroscopy (XPS). The thickness of the active layer and surface roughness were evaluated by field emission scanning electron microscopy (FE-SEM) and the atomic force microscopy (AFM), respectively. Furthermore, the molecular dynamics (MD) simulation was used for determining side chain length and hydrogen number of given polymers with water molecules. To evaluate biofouling behavior of grafted membranes, static bacterial adhesion tests and dynamic biofouling filtration tests were conducted.

3.2. Material and methods

3.2.1. Materials

Polyamide RO membranes (ES20, Osaka, Japan) were used as a model of commercial RO membranes. HEMA (Tokyo Chemical Industry) and PEG (average M_n = 360; Sigma-Aldrich, St. Louis, MO, USA) and MEDSAH (Sigma-Aldrich) were used as hydrophilic monomers. 3-Aminopropyltrimethoxysilane (APTS; Wako Pure Chemical Industry, Osaka, Japan), Ethyl α-bromoisobutyrate (EBIB, Tokyo Chemical Industry), α-Bromoisobutyryl bromide (BIBB; Sigma-Aldrich), copper (II) bromine (Wako Pure Chemical Industry), tris(2-pyridylmethyl)amine (Wako Pure Chemical Industry) and L-ascorbic acid (Tokyo Chemical Industry, Tokyo, Japan) were used for SI-ATRP reaction. *Sphingomonas paucimobilis* NBRC 13935 (NITE Biological Resource Center, Chiba, Japan), SYTO9 (Life Technologies, Carlsbad, CA, USA), tryptic soy broth (TSB;

Becton, Dickinson and Company, Franklin Lakes, NJ, USA) were used for bacterial experiments. Milli-Q water was used for all the experiments.

3.2.2. Synthesis and characterizations of bulk polymers

To synthesize the bulk polymer of pHEMA, pPEG, and pMEDSAH, 1:1(v/v) methanol/Milli-Q water was selected as a solvent for polymerization solution. First, 6.2 mL of monomer aqueous solution containing 5 mmol monomer was put into a 50-mL glass bottle. Then, 0.8 mL of 0.5 M ascorbic acid as a reducer, and 1 mL of 88 mM EBIB as an initiator were added to the bottle. After 10 min of nitrogen bubbling, 2 mL aqueous solution containing 0.02 mmol of $CuBr_2$ (catalyst) and 0.04 mmol of TPMA (ligand) were added by a syringe to initiate the SI-ATRP reaction. The reaction was conducted at 25 °C for giving polymerization time. Then, the polymerization solution was diluted five times by Milli-Q water for reaction termination and then dialyzed in the Fisherbrand dialysis tubing (MWCO 3500) against Milli-Q water for 1 week, followed by freeze drying. The synthesize bulk polymers, pHEMA, pPEG, and pMEDSAH are represented as H*x*, P*x*, and M*x*, respectively, where *x* indicates the polymerization time (min).

Chemical composition of synthesized bulk polymers was analyzed by ^{1}H-NMR spectrometer (JEOL RESONANCE, Tokyo, Japan). 0.02 g collected powder of synthesized bulk polymers was dissolved in 0.5 mL D_2O for ^{1}H-NMR measurement.

The weights and polymerized monomer amount of the synthesized bulk polymers was characterized to estimate the main chain length of pHEMA, pPEG, and pMEDSAH. The weights were obtained from the dried polymers after SI-ATRP, and the polymerized monomer amount (mmol) was calculated as follows.

$$n\ (mmol) = \frac{\mathrm{m\ (g)}}{\mathrm{M\ (g/mol)}} \times 1000 \qquad (1)$$

where n is the polymerized monomer amount of the synthesized bulk polymers, m is the weight

of the synthesized bulk polymers, M is the molecular weight of each monomer. Specifically, M value of HEMA, PEG, and MEDSAH are 130.1 g/mol, 360 g/mol, and 279.4 g/mol, respectively. Since an initial monomer amount is the same and grafting density is fixed by using the fixed concentration of initiator EBIB, the polymerized monomer amount reflects the main chain length of the synthesized polymers.

3.2.3. Membrane surface modification

The pHEMA-, pPEG-, and pMEDSAH-grafted membranes are fabricated by SI-ATRP, as described in a previous study [28]. Briefly, a polyamide RO membrane was immersed in 1 vol% APTS aqueous solution for 10 min to aminate the surface and 3 wt% BIBB hexane solution for 1 min to immobilize SI-ATRP initiator, and applied to the SI-ATRP reaction as descripted in a previous study [28]. pHEMA-, pPEG-, and pMEDSAH-grafted membranes are represented as H*x*, P*x*, and M*x*, respectively, where *x* indicates the polymerization time (min).

3.2.4. Surface characterizations

3.2.4.1. Chemical composition

The analysis of surface chemical composition was handled by both ATR-FTIR spectroscopy (Nicolet iS5, Thermo Fisher Scientific, MA, USA) and XPS (JPS-9010MC, JEOL). The degree of grafting (DG), which is an index of a chemical composition of a specific functional group [37], was used to estimate the main chain length of the grafted polymer, because it is difficult to accurately measure the main chain length on the membrane surface. pHEMA, pPEG, and pMEDSAH have C=O groups which is represented at 1720 cm^{-1} in the ATR-FTIR spectra, thus the DG values attributed to C=O groups enable to estimate the monomer units of the grafted polymer on the membrane surface. The same DG value leads to the same main chain length of

grafted polymers under the same grafting density. The DG value was calculated via ATR-FTIR spectra of the modified membranes using the following formula:

$$\mathrm{DG} = \frac{I_{modify}}{I_{mem}} \quad (2)$$

where I_{modify} and I_{mem} are the intensity value of the C=O peak at 1720 cm^{-1} from the surface of pHEMA, pPEG, and pMEDSAH-grafted membranes [20] and the intensity value of the N-C peak at 1540 cm^{-1} band from polyamide RO membrane surface [38], respectively.

3.2.4.2. Membrane morphologies

The morphology of the surface and cross section of the modified membranes was observed via the FE-SEM (JSF-7500, JEOL, Tokyo, Japan). The cross-section images were also applied to quantify the modification layer thickness of the grafted polymers. Additionally, the surface roughness was evaluated by AFM (SPA-400, Hitachi High-Technologies, Tokyo, Japan) using a dynamic force mode and a SI-DF40 cantilever. All the membrane samples were freeze-dried before FE-SEM and AFM observations.

3.2.4.3. Surface hydrophilicity

Surface hydrophilicity was estimated through the captive air bubble technique by using a contact angle meter (DM-300, Kyowa Interface Science, Saitama, Japan). An air bubble was injected to contact with the membrane surface inverted in Milli-Q water, and determined the air contact angle from the average value of 10 measurements. A larger air contact angle correlates with a more hydrophilic surface.

3.2.4.4. MD simulation

A hydrogen-bond network was formed within the polymer when water molecules penetrate

into the polymer. The polymer that is highly hydrated exhibits a non-biofouling property, and, thus, hydration plays an important role in anti-biofouling propensity [39]. Based on molecular dynamics (MD) simulation procedures, three molecular models, pHEMA, pPEG, and pMEDSAH were established via BIOVIA Materials Studio® commercial software for analyzing the hydration feature. The model construction and simulation parameters are shown in the supplementary data. Relative hydrogen bond number (*Rh*) was used to characterize hydration and calculated as follows:

$$Rh = \frac{\mathrm{h}}{\mathrm{H}} \times 100\% \quad (3)$$

where h is the number of hydrogen bond in the simulation module formed between water molecules and polymer molecules; H is the number of hydrogen bond in the simulation module of pHEMA, pPEG, or pMEDSAH, which are 700, 500, and 500, respectively.

In addition, the side chain length of HEMA, PEG, and MEDSAH monomers was determined by MD as well.

3.2.5. Membrane performances

3.2.5.1. Membrane transfer parameters

The membrane transfer parameters including water permeability and salt rejection properties were estimated as described in previous studies [28, 40]. The water permeability (LMH/MPa) and salt rejection (%) against a 0.05 % NaCl solution (implies 0.05 g NaCl fill to 100 mL Milli-Q water) were calculated using the accumulated permeate weight and electric conductivity, respectively.

3.2.5.2. Static bacteria adhesion and dynamic biofouling filtration

Membrane biofouling refers to the undesirable accumulation of microorganisms, which

attach and grow on a membrane surface [41]. Specifically, bacterial attachment is an early stage of RO membrane biofouling, which was determined by a static bacterial adhesion test; biofilm growth follows as the bacterial adheres to the membrane surface, whose procedure was evaluate by a dynamic biofouling filtration test. *Sphingomonas paucimobilis* NBRC 13935 was selected as the module bacteria. And the experimental protocols were described in previous studies [28, 42].

Briefly, for the static bacterial adhesion test, the pristine RO membrane and modified membranes were immersed in bacterial suspension and then shaken at 120 rpm at 30 ℃ for 24 hours. For the dynamic biofouling filtration test, in order to determine the role of biofilm growth on biofouling behavior, first, 2 mL bacterial suspension was added on the membrane surface and incubated at 30 °C for 1 h for initial bacterial adhesion of bacteria. Afterwards, the membrane was briefly washed with aqueous 0.85 wt% NaCl and set in a cross-flow membrane test unit (effective membrane area: 8.07 cm^2). An aqueous medium containing 3 g/L TSB medium and 7.65 g/L NaCl was fed to the membrane cell at 2.0 mL/min and 1.5 MPa for 20 hours. The weight of accumulate permeate was recorded.

After the static bacterial adhesion and dynamic biofouling tests, all the tested membranes were stained with SYTO9 and observed the status of bacterial attachment and biofilm formation using confocal laser scanning microscopy (CLSM; FV1000D, Olympus, Tokyo, Japan). The normalized bacterial coverage was calculated as follows:

$$\text{Normalized bacterial coverage} = \frac{c_{modified}}{C_{RO}} \times 100\% \quad (4)$$

where C_{RO} and $c_{modified}$ are bacterial coverage of pristine and modified membranes, respectively, analyzed by ImageJ software (National Institutes of Health, Bethesda, MD, USA) from CLSM images.

3.3. Results and discussion

3.3.1. Characterizations of synthesized bulk polymers

^{1}H-NMR spectra of synthesized bulk polymers were shown in Fig. 3.1. The peak area of pHEMA and pMEDSAH became larger with the increase of polymerization time (Fig. 3.1 (a) and (b)), suggesting that the main chain length grew. However, ^{1}H-NMR spectra of the bulk pPEG can not be obtained because the molecular weight of bulk pPEG is very high, which made it difficult to be dissolve in any solvent.

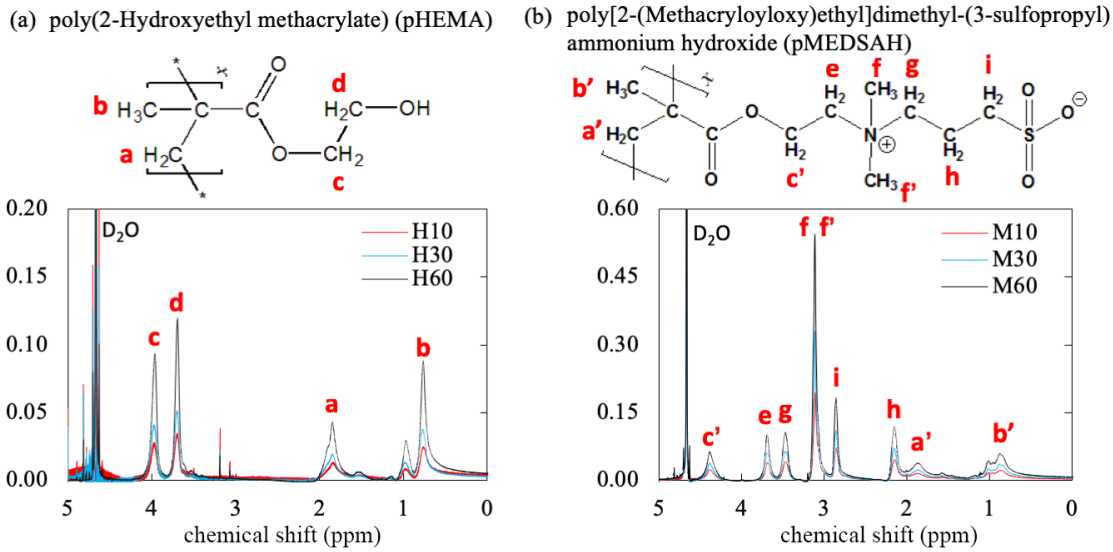

Fig. 3.1. ^{1}H-NMR spectra of the synthesized bulk polymers with various polymerization time: (a) pHEMA; (b) pMEDSAH. ^{1}H-NMR spectra of pPEG is unable to obtain because the molecular weight is too high to dissolved in any solvent.

Table 1 shows the weights and polymerized monomer amounts of the synthesized bulk polymers. The weights and polymerized monomer amounts of pHEMA, pPEG, and pMEDSAH increased with increasing the polymerization time, meaning the growth of the main chain length. Besides, the polymerized monomer amounts of pHEMA, pPEG, and pMEDSAH at the same

polymerization time presented the similar values, indicating the main chain length of each polymer was almost same. These results demonstrated that the main chain length of pHEMA, pPEG and pMEDSAH is controllable by using the SI-ATRP method.

Table 3.1. Weights and polymerized monomer amounts of the synthesized bulk polymers

Polymer code	Synthesized bulk polymer	
	Weight (g)	Amount (mmol)
H10	0.07	0.54
H30	0.18	1.38
H60	0.29	2.23
P10	0.21	0.58
P30	0.57	1.58
P60	0.93	2.58
M10	0.11	0.39
M30	0.32	1.15
M60	0.60	2.15

3.3.2. Membrane characterizations

The ATR-FTIR spectra of pHEMA- and pPEG-grafted membranes with various SI-ATRP polymerization time are presented in Fig. 3.2 (a) and (b), respectively. In comparison to the spectra of the pristine RO membrane, a C=O peak at 1720 cm^{-1} appears in those of the grafted RO membranes, proving the existence of pHEMA and pPEG chains on the grafted RO membranes. Additionally, the intensity of the C=O peak in the spectra of the pHEMA- and pPEG- grafted membranes clearly increased with polymerization time, indicating main chain length growth of pHEMA and pPEG on the surface. The DG values calculated by equation (2) are shown in Fig. 3.2(c). The DG value increased with polymerization time, further indicating the main chain length successfully increased during the SI-ATRP reaction. Moreover, with the same polymerization

time, the DG values of pHEMA-, pPEG-, and pMEDSAH- grafted membranes were similar, reflecting main chain length growth behavior of pHEMA, pPEG, and pMEDSAH is almost the same when using the same SI-ATRP polymerization time. These results show highly agreement on the result of synthesized polymer characterizations in section 3.3.1.

Table 3.3 displays the modification layer thickness measured by SEM (the SEM images and detail calculation are presented in Fig. 3.3 and Table 3.3, respectively.) and elemental ratio measured by XPS on the membrane surface after the modification with each hydrophilic polymer. On all the pHEMA-, pPEG-, and pMEDSAH- grafted membrane, the modification layer thickness increased with polymerization time. With the same polymerization time, the modification layer thickness of pHEMA- and pMEDSAH-grafted membranes are similar but much lower than that of pPEG-grafted membranes, this is probably because of the higher molecular weight of PEG monomer.

About the elemental ratio presented in Table 3.2, on the surface of pHEMA- and pPEG-grafted membranes, the nitrogen ratio, N_{1s}, decreased with polymerization time. As nitrogen exists in the molecular structure of polyamide but not in that of HEMA and PEG, the decreased N_{1s} signal results from the thicker modification layer. As for the pMEDSAH-grafted membrane, the higher S_{2p} composition confirms the thickness of pMEDSAH increased with polymerization time, but N_{1s} of pMEDSAH is not comparable with pHEMA and pPEG because nitrogen exists in the molecular structure of pMEDSAH.

These results suggest that the main chain length of pHEMA-, pPEG-, and pMEDSAH-grafted on the membrane surface at the same polymerization time is similar because of the similar DG values. However, the modification layer thickness of pPEG-grafted membranes was larger than that of pHEMA- and pMEDSAH- grafted membranes.

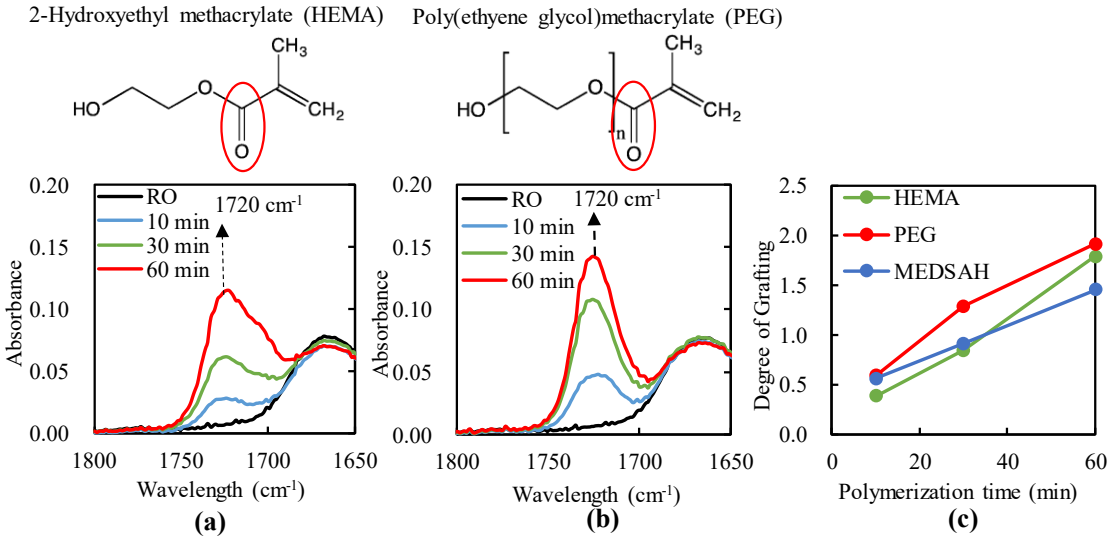

Fig. 3.2. ATR-FTIR spectra of (a) pHEMA- and (b) pPEG- grafted membranes as a function of polymerization time. (c) degree of grafting (DG) for the modified membranes. The data of pMEDSAH was replotted from [28].

Table 3.2. Modification layer thickness and elemental ratio on the surface of the pHEMA-, pPEG- and pMEDSAH-grafted membranes with various polymerization times.

Membrane	Modification layer thickness (nm)	Element composition (atomic %)			
		C_{1s}	O_{1s}	N_{1s}	S_{2p}
RO	0	73.22	17.05	9.73	0
H10	71	68.03	30.81	1.17	0
H30	324	67.25	32.66	0.09	0
H60	491	68.61	31.31	0.00	0
P10	263	69.05	30.38	0.57	0
P30	550	65.84	34.11	0.04	0
P60	849	66.12	33.88	0.00	0
M10*	46	69.28	19.31	10.09	1.31
M30*	317	68.86	20.64	8.54	1.97
M60*	532	68.55	22.11	6.89	2.45

* The element composition data of MEDSAH (M10, M30 and M60) was replotted from [28].

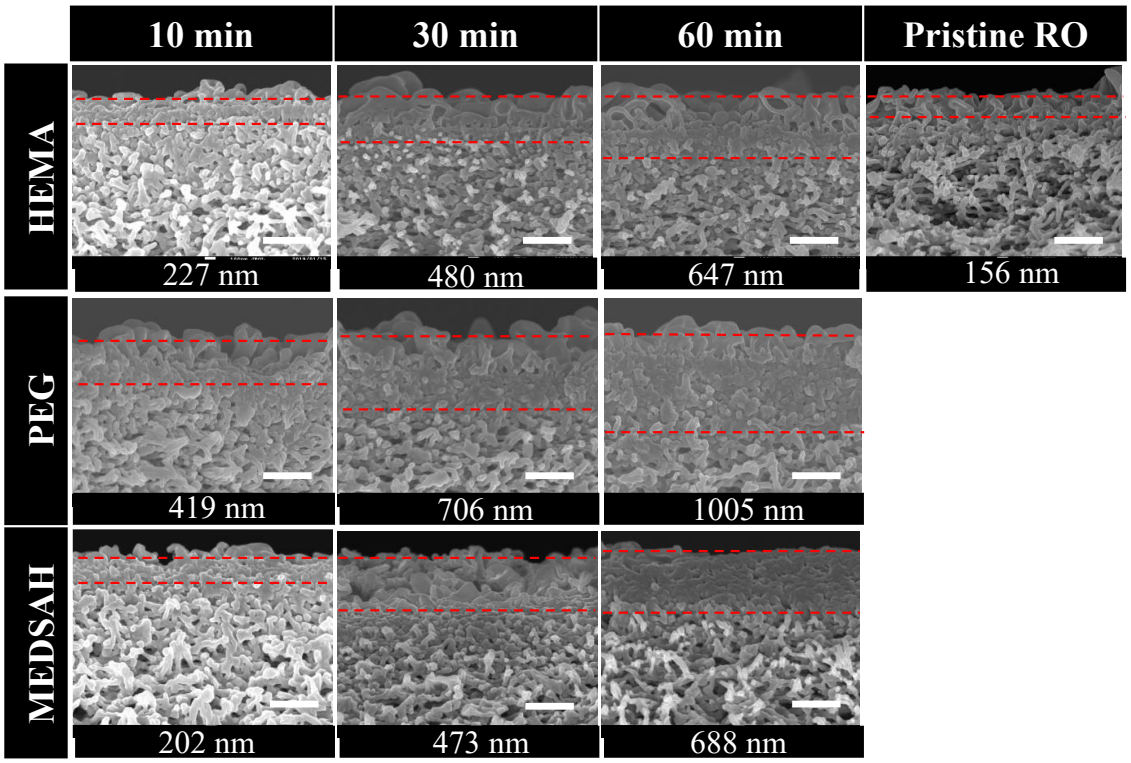

Fig. 3.3. Cross-sectional SEM images of the pristine RO membrane and pHEMA-, pPEG-, and pMEDSAH-grafted membranes. The area between two dotted lines is a denser layer containing the polyamide layer and modification layer and its total thickness (T_{total}) is presented below the SEM images. The scale bar represents 500 nm.

The surface morphology was observed by SEM (Fig. 3.4), and the surface roughness (R_a) analyzed through AFM was shown in Fig. 3.5. From Fig. 3.4, the membrane surfaces after the pHEMA and pPEG grafting were denser and smoother than that of the pristine membrane. With the increase of polymerization time in the range of 10 to 60 min, the aggregation of the grafted polymer was observed in the surface morphology because the polymers with a higher molecular weight formed on the membrane surface.

Table 3.3. Modification layer thickness of the grafted polymers on the pHEMA-, pPEG-, and pMEDSAH-grafted membranes.

Samples	T_{total} (nm)	T_g (nm)
RO	156	-
H10	227	71
H30	480	324
H60	647	491
P10	419	263
P30	706	550
P60	1005	849
M10	202	46
M30	473	317
M60	688	532

*$T_g = T_{total} - T_{PA}$

where the T_g is the modification layer thickness of grafted polymer; T_{total} is the total thickness containing the polyamide layer and modification layer as shown in Fig. 3.3; T_{PA} is the thickness of polyamide layer (156 nm) as shown in Fig. 3.3.

According to the result of surface roughness in Fig. 3.5, the surface of the pristine RO membrane became smoother after the surface modification. On the pHEMA- and pPEG- grafted membranes, with 10 to 60 min polymerization time, the difference of the surface roughness is less than 10 nm, which can be regarded as an experimental error range. It suggested that with the increase of main chain length and modification layer thickness, there is no significant effect on the surface roughness of the pHEMA- and pPEG- grafted membranes. But overall, the pPEG-grafted membrane surface was less rough than that of the pHEMA-grafted membrane. In contrast, with the increase of the main chain length and modification layer thickness, the surface roughness of the pMEDSAH-grafted membrane decreased significantly when the polymerization time over

10 min, probably because the modification layer thickness of M10 membrane is too thin to affect the surface roughness.

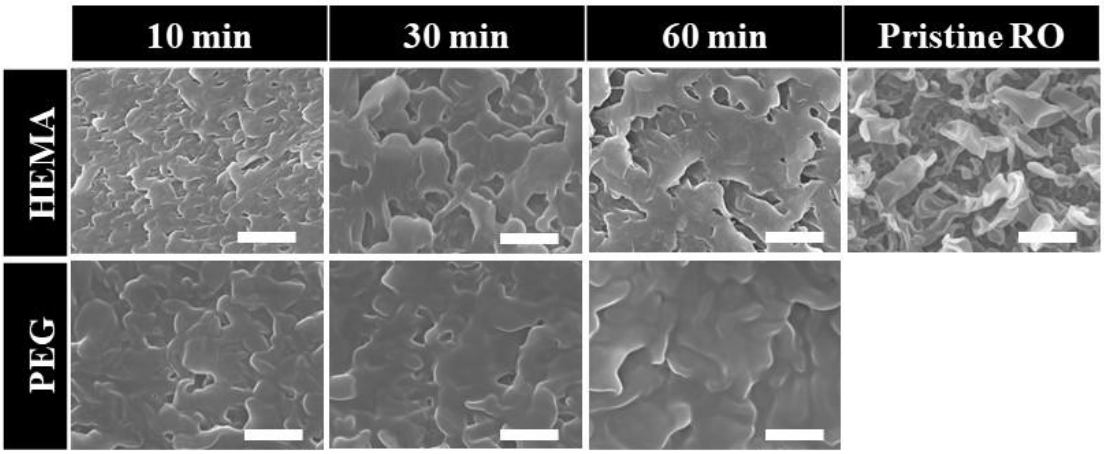

Fig. 3.4. SEM images of pristine RO, pHEMA- and pPEG-grafted membranes with various polymerization times. The scale bar represents 500 nm.

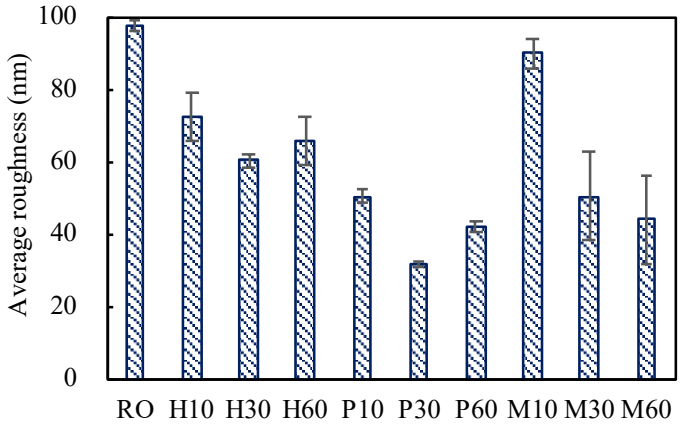

Fig. 3.5. Average roughness of the pristine RO, pHEMA-, pPEG-, and pMEDSAH- grafted membranes with various polymerization times. The data of pMEDSAH was replotted from [28].

The air contact angle of the pristine and modified membranes was shown in Fig. 3.6. The air contact angle of all modified membranes was larger than that of the pristine RO membrane,

indicating the pHEMA, pPEG, and pMEDSAH grafting made the polyamide RO membrane surface more hydrophilic. The surface hydrophilicity of pHEMA- and pMEDSAH- grafted membranes increased with increasing the polymerization time, while that of the pPEG-grafted membrane had no obvious change after 30 min because its hydrophilicity reached to an equilibrium state. Notably, with a polymerization time of 60 min, the pMEDSAH-grafted membrane displayed similar surface hydrophilicity to the pPEG-grafted membrane, but the surface of the pHEMA-grafted membrane was less hydrophilic than the other modified membranes.

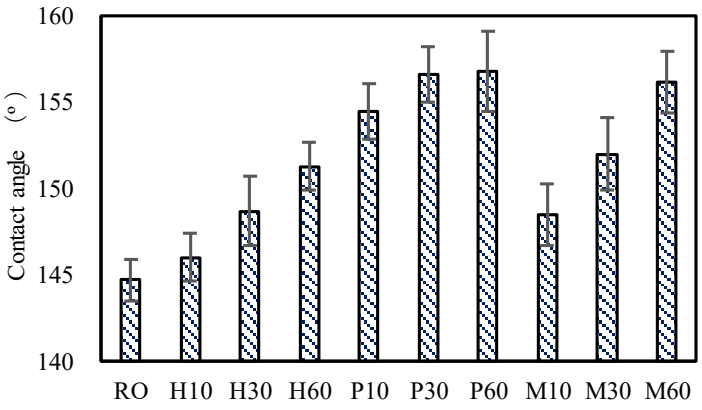

Fig. 3.6. Air contact angle of the modified membranes.

Figure 3.7 presents the membrane transfer parameters including the water permeability and salt rejection. Water permeability obviously decreased with increasing the polymerization time, which displayed a trend similar to pMEDSAH grafting in a previous study [28], due to a thick layer of pHEMA and pPEG. Specially, compared to the pristine RO membrane, P10 membrane showed ~50 % decline of water permeability. Besides, even if the P10 membrane has similar main chain length to H10 and M10 membranes, it still showed lower water permeability than that of H10 and M10 membrane. Because the modification layer thickness of P10 is 3.7 ~ 5.7 times

higher than that of H10 and M10. Further, there was no permeate in the case of using PEG as a monomer when over 10 min of the polymerization time was used, indicating P30 and P60 membranes are too thick (over 500 nm) to permeate water.

In Fig. 3.7, it can be seen that the surface modification has no significant effect on salt rejection compared with the pristine RO membrane, remaining ~ 97 % salt rejection. This result suggests that the SI-ATRP method doesn't affect the structure and separation performance of the active separation layer of the pristine RO membrane.

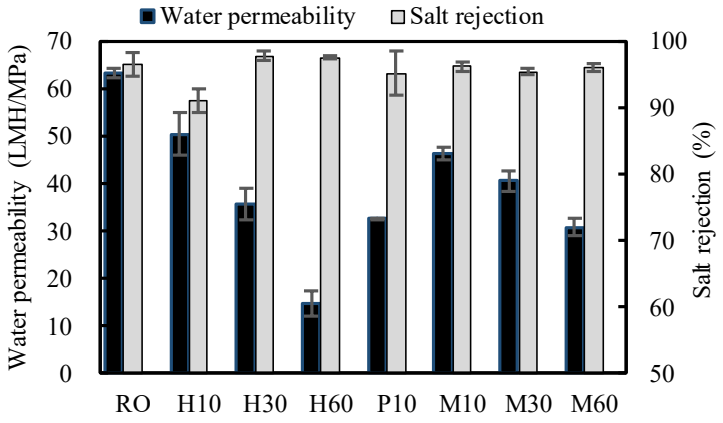

Fig. 3.7. Water permeability and salt rejection of the pHEMA-, pPEG-, and pMEDSAH- grafted membranes with various polymerization times. The data of pMEDSAH was replotted from [28].

3.3.3. Anti-biofouling performance

The bacterial coverage data for the static bacterial adhesion test are presented in Fig. 3.8, and the CLSM images of the static bacterial adhesion test are shown in Fig. 3.9. Compared to the pristine RO membrane, there was less bacterial amount adhered on the membranes modified with pHEMA, pPEG, and pMEDSAH. The bacterial adhesion of pHEMA-grafted membranes gradually decreased with the polymerization time from 4.3% (10 min) to 2.8% (60 min).

pMEDSAH-grafted membranes also displayed a tendency similar to pHEMA, although the bacterial adhesion decreased to a lesser 0.5 % (60 min). These results suggest that pHEMA or pMEDSAH require the longer main chain length to express the anti-biofouling property. In contrary, the pPEG-grafted membranes showed few (only 0.1 %) bacterial adhesion even with the short main chain grafted within a short time.

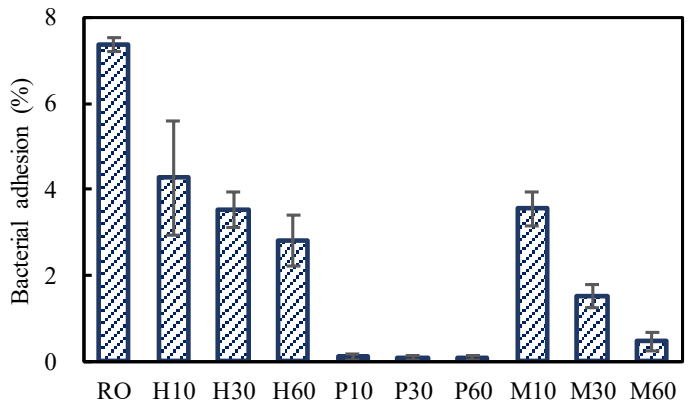

Fig. 3.8. Static bacterial adhesion of the modified membranes.

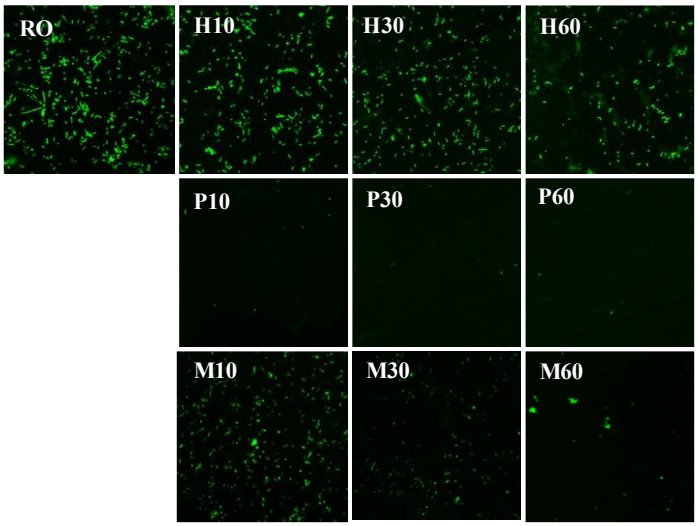

Fig. 3.9. CLSM images of the pristine RO and modified membranes after the static bacterial adhesion test.

Figure 3.10 demonstrates the variation of water permeability during the dynamic biofouling filtration test and the detailed data on water permeability is displayed in Table 3.4. All the modified membranes showed a smaller decline in water permeability and a larger final permeability after 20 hours of filtration compared with the pristine RO membrane, indicating the grafting of pHEMA, pPEG, and pMEDSAH is able to prevent the biofouling effectively and remain of high efficiency. When the polymerization time increased, especially over 60 min, the pHEMA- and pMEDSAH- grafted membranes effectively prevented biofilm formation and the decline of water permeability, which kept at ~80 % and 96 % of initial values, respectively. The pPEG-grafted membrane, with only 10 min of polymerization, not only had a high biofilm resistance but also maintained 90 % of the initial water permeability. The pHEMA- and pPEG-grafted membrane showed the different behavior, although their chemical structure is similar. The longer side chain of pPEG probably resulted in the high anti-biofouling property. The water permeability of P30 and P60 membrane was too low to test the dynamic biofouling filtration. As the surface of P30 and P60 membranes is more hydrophilic than P10 membrane and showed the similar surface roughness and bacterial adhesion to P10 membrane, it can be hypothesized that the P30 and P60 might have similar anti-biofouling performance to the P10 membrane. These results were corresponding to the CLSM images in Fig.3.11 which demonstrated that P10 and M60 membrane showed the tiny bacterial coverage after 20 hours dynamic biofouling filtration.

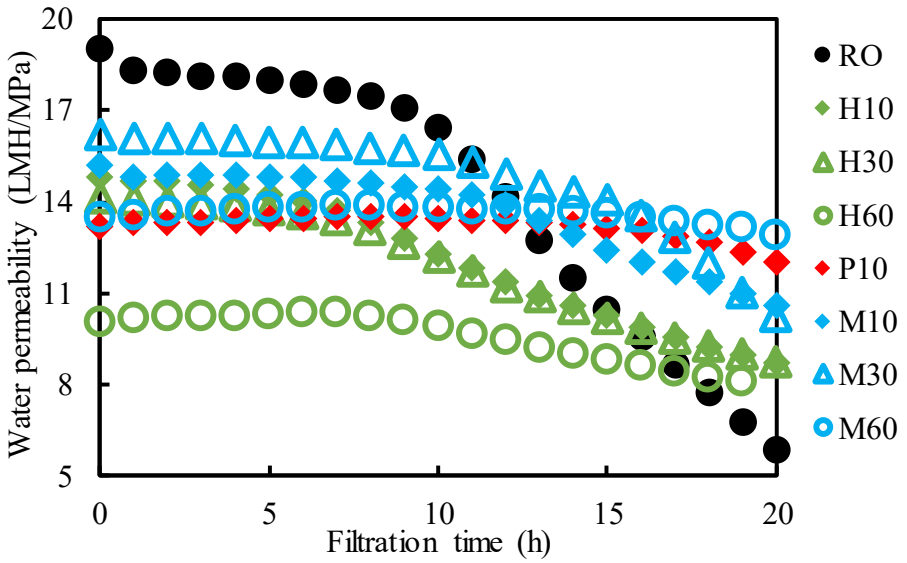

Fig. 3.10. Time course of water permeability during the dynamic biofouling filtration test. The data of MEDSAH (M10, M30 and M60) was replotted from [28].

Table 3.4. Initial permeability, final permeability, and permeability decline of pristine RO and modified membranes in dynamic biofouling filtration tests.

Membranes	Initial permeability (LMH/Mpa)	Final permeability (LMH/Mpa)	Permeability reduction (%)
RO	19.0	5.9	68.9
H10	14.8	8.7	41.2
H30	14.2	8.8	38.0
H60	10.4	8.1	21.9
P10	13.5	12.0	10.8
M10*	15.2	10.6	30.3
M30*	16.2	10.2	37.0
M60*	13.5	12.9	4.4

* The data of MEDSAH (M10, M30 and M60) was from [28].

Higher amount of biofilm formed on the membrane surface causes the decrease of the water permeability. In order to evaluate the biofilm formation and quantify the bacterial coverage on the membrane surface after the dynamic biofouling filtration test, all the tested membranes were observed using the CLSM. The CLSM images are displayed in Fig. 3.11 and the formed biofilm is presented as the green area. In Fig. 3.11, there was a thicker and denser biofilm on the surface of the pristine RO membrane compared to that of the pHEMA-, pPEG, and pMEDSAH- grafted membranes, resulting in the higher decline of the water permeability. Moreover, pHEMA- and pMEDSAH- grafted membranes with the longer polymerization time showed the less biofilm formation, while there was few biofilm forming on the surface of pPEG-grafted membrane. These results have an agreement on the result of the water permeability in the dynamic biofouling filtration test.

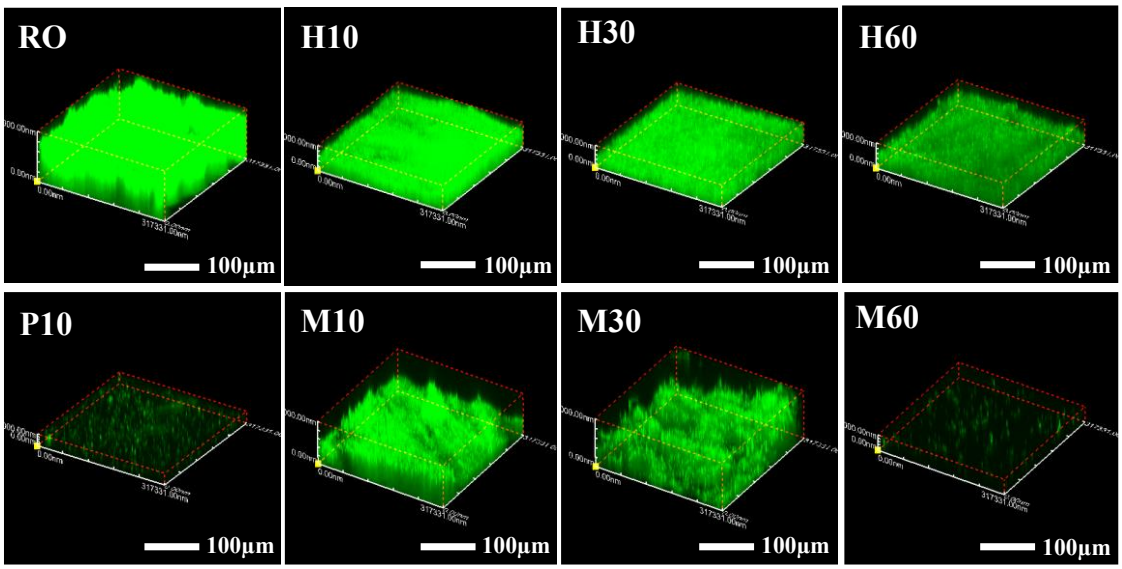

Fig. 3.11. CLSM images of fouled membranes after 20-hour dynamic biofouling filtration. The image of MEDSAH (M10, M30 and M60) was replotted from [28].

Figure 3.12 summarizes the relationship among polymerization time, normalized bacterial coverage in the static and dynamic tests. The detailed data are listed in Table 3.5. Compared with the pristine RO membrane surface, all pHEMA-, pPEG-, and pMEDSAH- grafted membrane surfaces had lower bacterial coverage. Specifically, in the range from 10 to 60 min of the polymerization time, the normalized bacterial coverage of pHEMA- and pMEDSAH- grafted membranes in the static bacterial adhesion test reduced from 58 % to 38 % and 48 % to 6 %, respectively. In the dynamic biofouling filtration test, pHEMA- and pMEDSAH- grafted membranes decreased from 84 % to 72 % and 95 % to 3 %, respectively. While the normalized bacterial coverage of pPEG-grafted membranes, with 10 min polymerization time, was only ~1 % in both the static and dynamic biofouling tests. These results indicate that the main chain length of pHEMA and pMEDSAH plays a crucial role in fabricating anti-biofouling membranes because their anti-biofouling performance changed significantly with changes in polymerization time. Notably, the bacterial coverage between the dynamic biofouling filtration and the static bacterial adhesion is not equivalent to each other. The former evaluation exhibits the whole biofouling behavior composed of the initial adhesion, bacterial growth, and biofilm formation, while the latter only represents the phase of the initial bacterial adhesion. Additionally, the hydrodynamic shear force resulting from the cross-flow in the dynamic biofouling filtration test might prevent the membrane surface from bacteria attachment and biofouling formation [42]. However, further efforts are required to explain the different biofouling behavior between each polymer.

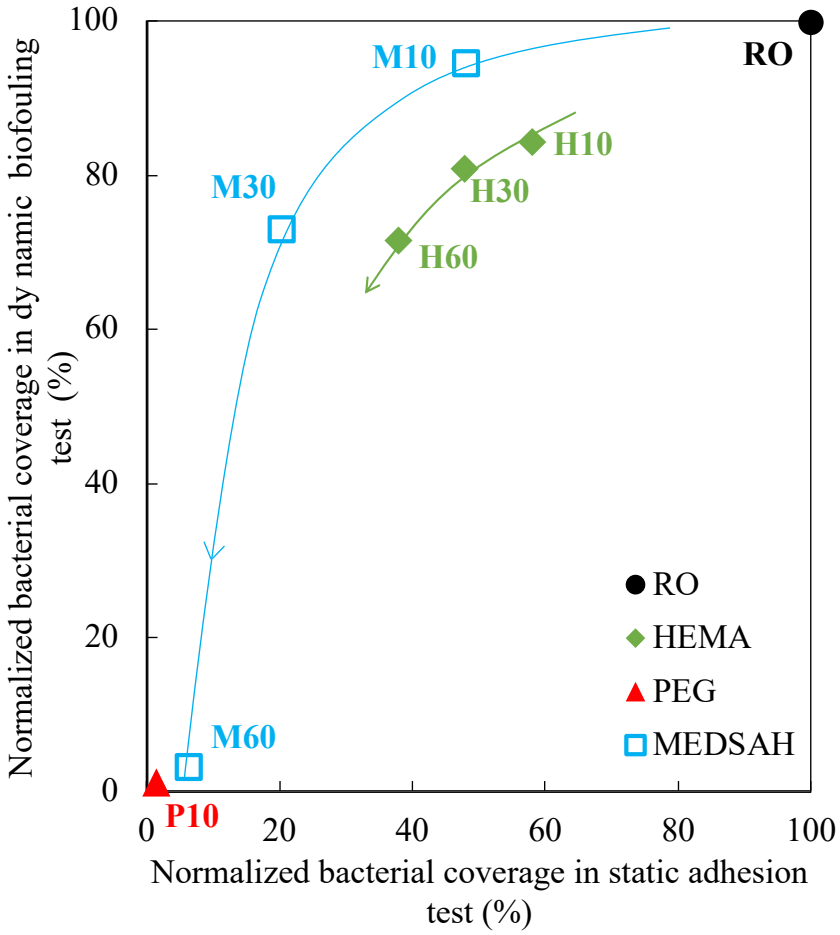

Fig. 3.12. Relationship between normalized bacterial coverage in static bacterial adhesion and normalized bacterial coverage in dynamic biofouling filtration. The dynamic biofouling filtration data of MEDSAH was replotted from [28]. The direction of arrows means the increase of polymerization time.

Table 3.5. Normalized bacterial coverage data of the pristine and modified membranes after the static bacterial adhesion and dynamic biofouling filtration tests.

Membrane	Polymerization time (min)	Static bacterial adhesion test		Dynamic biofouling test	
		Bacterial coverage (%)	Normalized coverage (%)	Bacterial coverage (%)	Normalized coverage (%)
RO	0	7.37	100	96.99	100
H10	10	4.28	58.03	81.90	84.44
H30	30	3.54	47.97	78.59	81.03
H60	60	2.80	38.04	69.58	71.73
P10	10	0.10	1.42	1.09	1.12
P30	30	0.09	1.22	/	/
P60	60	0.09	1.22	/	/
M10	10	3.56	48.25	91.69	94.54
M30	30	1.52	20.62	70.84	73.04
M60	60	0.47	6.32	2.91	3.01

In order to have a comprehensive understanding of how polymer structures of pHEMA, pPEG, and pMEDSAH affect biofouling behavior, the MD simulation method was applied to characterize the side chain length of each polymer and the relative hydrogen bond number (Rh) with water molecules, which are presented in Fig. 3.13(a) and (b), respectively.

From the result of the polymer side chain length obtained from MD simulation in Fig. 3.13(a), the side chain length of pPEG is 2~3 times longer than that of pHEMA and pMEDSAH. It demonstrates that the higher molecule weight ($M_w \approx M_n = 360$) and longer side chain length (19.685 Å) of PEG monomer might lead to the thicker modification layer of pPEG-grafted membranes compared to that of pHEMA- and pMEDSAH- grafted membranes with the same polymerization time as shown in Table 3.2. Besides, there is no significant difference on the side chain length between MEDSAH (9.515 Å**)** and HEMA (6.59 Å), that is, there might be no

significant difference on dimensional size. Therefore, as discussed in section 3.3.2, pMEDSAH-grafted membranes have similar modification layer thickness to pHEMA-grafted membranes even if the molecule weight of MEDSAH monomer (M_w = 279.35) is two times higher than that of HEMA monomer (M_w = 130.14 g/mol).

Combining the experimental and MD simulation results, it can be seen that different polymer structures may lead to different level of anti-biofouling properties, even the polymer is hydrophilic and has been proposed as a good anti-biofouling material. For pPEG, as described in Fig. 3.13(a), the longer side chain probably improves the mobility and flexibility of grafted polymer. When the foulant closes to the surface, the compressed polymer chain produces steric repulsion and resists the foulant due to an unfavorable entropy decrease [43, 44]. Besides, in Fig. 3.13(b), 17 % of relative hydrogen bond number means that the pPEG-grafting on the membrane surface has abundant surface-bound water molecules via hydrogen bonds. This prevents bacterial adhesion via a thermodynamically unfavorable dehydration entropic effect [45]. Thus, long side chains with a hydration layer might be the reasons that the RO membrane grafted with even short main chain of pPEG showed remarkable anti-biofouling property (Fig. 3.12). However, pPEG-grafted membrane with over 500 nm modification layer thickness showed high resistance of water permeate (Fig. 3.7).

The zwitterionic polymer, pMEDSAH, had a higher relative hydrogen bond number (25 %) than pPEG (17 %) in Fig. 3.13(b), indicating that the pMEDSAH can strongly bind water molecules and induce hydration near the surface [17, 46-48]. This tight water bounding layer on the surface constructs a robust and physical barrier to prevent bacterial adhesion. However, in this case, pMEDSAH with short main chain was unable to show the superior anti-biofouling performance because the short main chain of pMEDSAH made the surface less hydrophilic compared with that of long main chain of pMEDSAH (Fig. 3.6). A previous study demonstrated

that increasing the main chain length of pMEDSAH was a feasible method to improve the bacterial resistance, although water flux decreased due to the increasing polymer thickness. Therefore, controlling the main chain length, in combination with strong hydration are important factors of zwitterionic polymers for achieving the best anti-biofouling capability.

Regarding pHEMA, the shorter side chain length and weaker hydration limits its anti-biofouling capacity. A longer main chain can improve the anti-biofouling property of pHEMA-grafted membranes (Fig. 3.12), but they are still not comparable to pPEG and pMEDSAH.

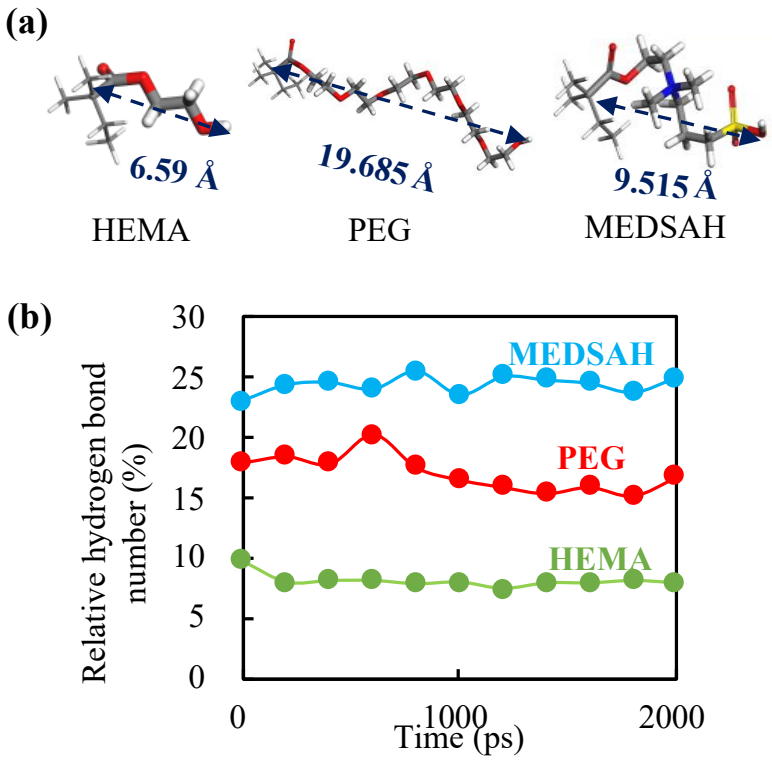

Fig. 3.13. Estimated polymer structures on the membrane surface by MD simulation: (a) side chain length and (b) relative hydrogen bond number of each polymer.

3.4. Conclusion

The polyamide RO membrane was modified by grafting pHEMA, pPEG, or pMEDSAH via

SI-ATRP for the investigation of the influence of the polymer structure modified the membrane surface on biofouling behavior. The pHEMA-grafted membrane was relatively ineffective at preventing biofouling, due to the relatively weaker hydration and lower flexibility, while the combined feature of pPEG with long side chains and a hydration layer effectively prevented biofouling even with short main chain length. The combination of strong hydration and proper main chain length is the main contribution to the anti-biofouling propensity of a zwitterionic polymer, pMEDSAH. This research provides useful information on biofouling behavior on the surface of various polymers, that is, not only the main chain length but also the side chain and hydration state should be taken into account for developing anti-biofouling membranes. However, it also demonstrated that static bacterial adhesion is not equivalent to dynamic biofouling property. Further research is needed to clarify the correlation between the static bacterial adhesion and the dynamic biofouling property.

Appendix 1

A1.1. Simulation molecular model

Simulation models were constructed in order to understand the hydration property of given polymers, pHEMA, pPEG and pMEDSAH. A polymer consisting of 20 repeat monomers was set within a simulation model which filled with water molecules. Each simulation box was constructed and kept under similar atom numbers through the Amorphous Cell module, in which the density values were set as 1 g/cm^3. The interaction between the polymer and water molecules was analyzed via hydrogen bond number.

In this study, the Condensed-phase Optimized Molecular Potential for Atomistic Simulation Studies (COMPASS) force field [49-51] was adopted to perform the simulation models. Force field is used to calculate the potential for given formation atoms. The COMPASS force field

provides a higher accuracy in predicting the polymer properties [50]. To simulate the polymer structure, the Geometry Optimization step was introduced to optimize the energy of the model structure, which utilizes energy calculation and changes in the structures of 5,000 iterations to establish each sensible (lowest energy) initial molecular structure. Afterwards, an MD duration with an NVT ensemble (fixed atom number, system volume and temperature) at 298 K for 100-ps was applied to reach molecular structures under an equilibrium state. Finally, the equilibrium structure was adopted into the hydration property study through a period of 2000 ps calculation using NVT ensemble. The various functional forms *E* in COMPASS are illustrated as follows:

$$E = \sum_{b}\left[K_2(b-b_0)^2 + K_3(b-b_0)^3 + K_4(b-b_0)^4\right]$$

(a)

$$+\sum_{\theta}\left[H_2(\theta-\theta_0)^2 + H_3(\theta-\theta_0)^3 + H_4(\theta-\theta_0)^4\right]$$

(b)

$$+\sum_{\phi}\left\{V_1\left[1-\cos\left(\phi-\phi_1^0\right)\right]+V_2\left[1-\cos\left(2\phi-\phi_2^0\right)\right]+V_3\left[1-\cos\left(3\phi-\phi_3^0\right)\right]\right\}$$

(c)

$$+\sum_{x}K_x x^2 + \sum_{b}\sum_{b'}F_{bb'}(b-b_0)(b'-b'_0) + \sum_{\theta}\sum_{\theta'}F_{\theta\theta'}(\theta-\theta_0)(\theta'-\theta'_0)$$

(d) **(e)** **(f)**

$$+\sum_{b}\sum_{\theta}F_{b\theta}(b-b_0)(\theta-\theta_0) + \sum_{b}\sum_{\phi}(b-b_0)\left[V_1\cos\phi + V_2\cos 2\phi + V_3\cos 3\phi\right]$$

(g) **(h)**

$$+\sum_{b'}\sum_{\phi}(b'-b'_0)\left[V_1\cos\phi + V_2\cos 2\phi + V_3\cos 3\phi\right]$$

(i)

$$+\sum_{\phi}\sum_{\theta}\sum_{\theta'}K_{\phi\theta\theta'}\cos\phi(\theta-\theta_0)(\theta'-\theta'_0) + \sum_{i>j}\frac{q_i q_j}{\varepsilon r_{ij}} + \sum_{i>j}\left[\frac{A_{ij}}{r_{ij}^9} - \frac{B_{ij}}{r_{ij}^6}\right] \qquad \text{(A2)}$$

(j) **(k)** **(l)**

Where, b, θ, ϕ, and x are bond length, bond angle, torsion angle, and out-of-plane angle, respectively. Super- and sub-script of '0' indicate the equilibrated value. q is Coulombic charge, and r is distance of an atom pair. Besides, the energy terms are composed of three categories:

bonded energy terms, cross-interaction terms, and non-bonded energy terms. The bonded energy terms include (a) the covalent bond-stretching energy terms, (b) the bond-angle bending energy terms, and (c) the torsion-angle rotation energy terms. The designation (d) is either the out-of-plane energy or an improper term. The terms for cross-interaction consist of the dynamic variations among bond stretching, bending, and torsion angle rotation interactions ((e)–(j)). The non-bonded energy terms, (k) and (l), represent the Coulombic electrostatic interaction force and the van der Waals (vdW) potential force, respectively.

References

[1] J. Cadotte, R. Petersen, R. Larson, E. Erickson, A new thin-film composite seawater reverse osmosis membrane, Desalination, 32 (1980) 25-31.
[2] S. Belfer, J. Gilron, N. Daltrophe, Y. Oren, Comparative study of biofouling of NF modified membrane at SHAFDAN, Desalination, 184 (2005) 13-21.
[3] K.L. Chen, L. Song, S.L. Ong, W.J. Ng, The development of membrane fouling in full-scale RO processes, Journal of Membrane Science, 232 (2004) 63-72.
[4] C. Jarusutthirak, G. Amy, Role of soluble microbial products (SMP) in membrane fouling and flux decline, Environmental Science & Technology, 40 (2006) 969-974.
[5] C.M. Pang, P. Hong, H. Guo, W.-T. Liu, Biofilm formation characteristics of bacterial isolates retrieved from a reverse osmosis membrane, Environmental Science & Technology, 39 (2005) 7541-7550.
[6] P. Xu, J.E. Drewes, T.-U. Kim, C. Bellona, G. Amy, Effect of membrane fouling on transport of organic contaminants in NF/RO membrane applications, Journal of Membrane Science, 279 (2006) 165-175.
[7] J. Baker, L. Dudley, Biofouling in membrane systems—a review, Desalination, 118 (1998) 81-89.
[8] H.-C. Flemming, Reverse osmosis membrane biofouling, Experimental Thermal and Fluid Science, 14 (1997) 382-391.
[9] M. Herzberg, M. Elimelech, Biofouling of reverse osmosis membranes: role of biofilm-enhanced osmotic pressure, Journal of Membrane Science, 295 (2007) 11-20.
[10] A. Matin, Z. Khan, S. Zaidi, M. Boyce, Biofouling in reverse osmosis membranes for

seawater desalination: phenomena and prevention, Desalination, 281 (2011) 1-16.
[11] M. Pasmore, P. Todd, S. Smith, D. Baker, J. Silverstein, D. Coons, C.N. Bowman, Effects of ultrafiltration membrane surface properties on Pseudomonas aeruginosa biofilm initiation for the purpose of reducing biofouling, Journal of Membrane Science, 194 (2001) 15-32.
[12] H.-C. Flemming, G. Schaule, T. Griebe, J. Schmitt, A. Tamachkiarowa, Biofouling-the Achilles heel of membrane processes, Desalination, 113 (1997) 215-225.
[13] J.-P. Montheard, M. Chatzopoulos, D. Chappard, 2-hydroxyethyl methacrylate (HEMA): chemical properties and applications in biomedical fields, Journal of Macromolecular Science, Part C: Polymer Reviews, 32 (1992) 1-34.
[14] V. Kochkodan, N. Hilal, V. Goncharuk, L. Al-Khatib, T. Levadna, Effect of the surface modification of polymer membranes on their microbiological fouling, Colloid Journal, 68 (2006) 267-273.
[15] K.-H. Song, K.-H. Kim, S.-H. Cho, K.-R. Lee, J.-H. Lim, S.-S. Bae, Permeation flux of surface-modified hydrophilic polysulfone membrane, Korean Chemical Engineering Research, 42 (2004) 59-64.
[16] Y. Sui, Z. Wang, X. Gao, C. Gao, Antifouling PVDF ultrafiltration membranes incorporating PVDF-g-PHEMA additive via atom transfer radical graft polymerizations, Journal of Membrane Science, 413 (2012) 38-47.
[17] H. Zhang, M. Chiao, Anti-fouling coatings of poly (dimethylsiloxane) devices for biological and biomedical applications, Journal of Medical and Biological Engineering, 35 (2015) 143-155.
[18] T. McPherson, A. Kidane, I. Szleifer, K. Park, Prevention of protein adsorption by tethered poly (ethylene oxide) layers: experiments and single-chain mean-field analysis, Langmuir, 14 (1998) 176-186.
[19] Y. Chang, Y.-J. Shih, R.-C. Ruaan, A. Higuchi, W.-Y. Chen, J.-Y. Lai, Preparation of poly (vinylidene fluoride) microfiltration membrane with uniform surface-copolymerized poly (ethylene glycol) methacrylate and improvement of blood compatibility, Journal of Membrane Science, 309 (2008) 165-174.
[20] Y. Chang, T.-Y. Cheng, Y.-J. Shih, K.-R. Lee, J.-Y. Lai, Biofouling-resistance expanded poly (tetrafluoroethylene) membrane with a hydrogel-like layer of surface-immobilized poly (ethylene glycol) methacrylate for human plasma protein repulsions, Journal of Membrane Science, 323 (2008) 77-84.
[21] M. Ulbricht, H. Matuschewski, A. Oechel, H.-G. Hicke, Photo-induced graft polymerization surface modifications for the preparation of hydrophilic and low-proten-adsorbing ultrafiltration membranes, Journal of Membrane Science, 115 (1996) 31-47.
[22] S. Wang, T. Li, C. Chen, B. Liu, J.C. Crittenden, PVDF ultrafiltration membranes of controlled performance via blending PVDF-g-PEGMA copolymer synthesized under different

reaction times, Frontiers of Environmental Science & Engineering, 12 (2018) 3.
[23] S. Belfer, R. Fainshtain, Y. Purinson, J. Gilron, M. Nyström, M. Mänttäri, Modification of NF membrane properties by in situ redox initiated graft polymerization with hydrophilic monomers, Journal of Membrane Science, 239 (2004) 55-64.
[24] S. Belfer, Y. Purinson, R. Fainshtein, Y. Radchenko, O. Kedem, Surface modification of commercial composite polyamide reverse osmosis membranes, Journal of Membrane Science, 139 (1998) 175-181.
[25] V. Freger, J. Gilron, S. Belfer, TFC polyamide membranes modified by grafting of hydrophilic polymers: an FT-IR/AFM/TEM study, Journal of Membrane Science, 209 (2002) 283-292.
[26] G. Kang, M. Liu, B. Lin, Y. Cao, Q. Yuan, A novel method of surface modification on thin-film composite reverse osmosis membrane by grafting poly (ethylene glycol), Polymer, 48 (2007) 1165-1170.
[27] W. Zhang, Z. Yang, Y. Kaufman, R. Bernstein, Surface and anti-fouling properties of a polyampholyte hydrogel grafted onto a polyethersulfone membrane, Journal of Colloid and Interface Science, 517 (2018) 155-165.
[28] Z. Yang, D. Saeki, H. Matsuyama, Zwitterionic polymer modification of polyamide reverse-osmosis membranes via surface amination and atom transfer radical polymerization for anti-biofouling, Journal of Membrane Science, 550 (2018) 332-339.
[29] M. He, K. Gao, L. Zhou, Z. Jiao, M. Wu, J. Cao, X. You, Z. Cai, Y. Su, Z. Jiang, Zwitterionic materials for antifouling membrane surface construction, Acta Biomaterialia, 40 (2016) 142-152.
[30] B. Liu, X. Liu, S. Shi, R. Huang, R. Su, W. Qi, Z. He, Design and mechanisms of antifouling materials for surface plasmon resonance sensors, Acta Biomaterialia, 40 (2016) 100-118.
[31] G. Book, Compendium of chemical terminology, International Union of Pure and Applied Chemistry, 528 (2014).
[32] J.M.G. Cowie, V. Arrighi, Polymers: chemistry and physics of modern materials, CRC press, 2007.
[33] C. Liu, J. Lee, J. Ma, M. Elimelech, Antifouling thin-film composite membranes by controlled architecture of zwitterionic polymer brush layer, Environmental Science & Technology, 51 (2017) 2161-2169.
[34] P. Król, P. Chmielarz, Recent advances in ATRP methods in relation to the synthesis of copolymer coating materials, Progress in Organic Coatings, 77 (2014) 913-948.
[35] B. Tansel, J. Sager, J. Garland, S. Xu, L. Levine, P. Bisbee, Deposition of extracellular polymeric substances (EPS) and microtopographical changes on membrane surfaces during intermittent filtration conditions, Journal of Membrane Science, 285 (2006) 225-231.
[36] J.M. Veza, M. Ortiz, J.J. Sadhwani, J.E. Gonzalez, F.J. Santana, Measurement of biofouling

in seawater: some practical tests, Desalination, 220 (2008) 326-334.
[37] R. Bernstein, E. Antón, M. Ulbricht, UV-photo graft functionalization of polyethersulfone membrane with strong polyelectrolyte hydrogel and its application for nanofiltration, ACS Applied Materials & Interfaces, 4 (2012) 3438-3446.
[38] D. Saeki, T. Tanimoto, H. Matsuyama, Anti-biofouling of polyamide reverse osmosis membranes using phosphorylcholine polymer grafted by surface-initiated atom transfer radical polymerization, Desalination, 350 (2014) 21-27.
[39] S. Chen, L. Li, C. Zhao, J. Zheng, Surface hydration: principles and applications toward low-fouling/nonfouling biomaterials, Polymer, 51 (2010) 5283-5293.
[40] D. Saeki, S. Nagao, I. Sawada, Y. Ohmukai, T. Maruyama, H. Matsuyama, Development of antibacterial polyamide reverse osmosis membrane modified with a covalently immobilized enzyme, Journal of Membrane Science, 428 (2013) 403-409.
[41] C. Liu, D. Zhang, Y. He, X. Zhao, R. Bai, Modification of membrane surface for anti-biofouling performance: Effect of anti-adhesion and anti-bacteria approaches, Journal of Membrane Science, 346 (2010) 121-130.
[42] D. Saeki, H. Karkhanechi, H. Matsuura, H. Matsuyama, Effect of operating conditions on biofouling in reverse osmosis membrane processes: Bacterial adhesion, biofilm formation, and permeate flux decrease, Desalination, 378 (2016) 74-79.
[43] S. Jeon, J. Lee, J. Andrade, P. De Gennes, Protein—surface interactions in the presence of polyethylene oxide: I. Simplified theory, Journal of Colloid and Interface Science, 142 (1991) 149-158.
[44] S. Jeon, J. Andrade, Protein—surface interactions in the presence of polyethylene oxide: II. Effect of protein size, Journal of Colloid and Interface Science, 142 (1991) 159-166.
[45] S. Chen, F. Yu, Q. Yu, Y. He, S. Jiang, Strong resistance of a thin crystalline layer of balanced charged groups to protein adsorption, Langmuir, 22 (2006) 8186-8191.
[46] S. Chen, L. Li, C.L. Boozer, S. Jiang, Controlled chemical and structural properties of mixed self-assembled monolayers of alkanethiols on Au (111), Langmuir, 16 (2000) 9287-9293.
[47] S. Herrwerth, W. Eck, S. Reinhardt, M. Grunze, Factors that determine the protein resistance of oligoether self-assembled monolayers− internal hydrophilicity, terminal hydrophilicity, and lateral packing density, Journal of the American Chemical Society, 125 (2003) 9359-9366.
[48] J. Zheng, L. Li, H.-K. Tsao, Y.-J. Sheng, S. Chen, S. Jiang, Strong repulsive forces between protein and oligo (ethylene glycol) self-assembled monolayers: a molecular simulation study, Biophysical Journal, 89 (2005) 158-166.
[49] D. Rigby, H. Sun, B. Eichinger, Computer simulations of poly (ethylene oxide): force field, pvt diagram and cyclization behaviour, Polymer International, 44 (1997) 311-330.

[50] H. Sun, COMPASS: an ab initio force-field optimized for condensed-phase applications overview with details on alkane and benzene compounds, The Journal of Physical Chemistry B, 102 (1998) 7338-7364.
[51] H. Sun, P. Ren, J. Fried, The COMPASS force field: parameterization and validation for phosphazenes, Computational and Theoretical Polymer Science, 8 (1998) 229-246.

Chapter 4

Improved anti-biofouling performance of polyamide reverse osmosis membranes modified with a polyampholyte with effective carboxyl anion and quaternary ammonium cation ratio

4.1. Introduction

Clean water shortage has become a serious problem in the worldwide, due to population growth and the water source contamination [1, 2]. Reverse osmosis (RO) membrane processes are highly useful ways for both seawater desalination and wastewater treatment, due to their high energy efficiency [3, 4]. However, a membrane fouling (especially biofouling) is a challenging problem to address, because it is difficult to completely remove bacteria from a fouled RO membrane surface [5, 6]. Biofouling is associated with plugging of the membrane, as a result of bacterial attachment followed by the formation of a biofilm made from extracellular polymeric substance [7]. This phenomenon results in a significant decrease in water permeability and salt rejection, higher energy consumption for filtration, and shorter membrane lifetime [8].

Common strategies to reduce the biofouling of RO membranes involve avoiding the attachment of bacteria on the membrane surface [9], by modifying it with various hydrophilic

polymers such as polyethylene glycol [10], polydopamine [11, 12], polyelectrolytes [13-15], and zwitterionic polymers [16-19]. Among these polymers, zwitterionic materials have received much attention as one of the most promising materials to improve anti-biofouling performance, such as poly(2-methacryloyloxyethyl phosphorylcholine) (pMPC) [20, 21], poly[(2-methacryloyloxy)ethyl]dimethyl-(3-sulfopropyl)ammonium hydroxide (pMEDSAH) [22], and poly(carboxybetaine methacrylate) (pCBMA) [23-25]. A key factor in the anti-biofouling properties of zwitterionic polymers is that the polymer molecule has both positive and negative charge groups and the net charge of the whole molecule is zero, which could maximize the surface hydration and minimize the interaction between membrane surface and bacteria [26, 27]. However, polymers synthesized using zwitterionic monomers are very expensive because of the complicated synthesis of monomers, which results in the limited types of zwitterionic materials available on the market and the low production output to date [28].

As an alternative to zwitterionic polymers, polyampholyte materials, made of amphoteric polymers composed of positively and negatively charged moieties on different monomer units, have also demonstrate anti-biofouling characteristics because of their similarity to zwitterionic polymers [29-31]. For example, a series of polyampholytes composed of the cationic monomer with a quaternary ammonium cation and the anionic monomer with a sulfonic group exhibited low fouling properties [29, 30, 32-36]. Another type of synthetic polyampholytes prepared by the anionic monomer with a carboxyl group and the cationic monomer with an amide group showed high resistance to nonspecific protein adsorption [37, 38].

To fabricate a membrane with excellent anti-biofouling properties using a polyampholyte, it is essential to optimize the ratio between the anion and the cation monomers on the membrane surface. In other words, to achieve anti-biofouling properties, the charge densities of the anion and cation monomers on the membrane surface should be the same. However, the monomer ratio

in polyampholytes grafted on the membrane surface may differ from that in mixed monomer solution, because each monomer has different polymerization reaction kinetics [32]. Thus, analyzing the surface composition is a necessary task when polyampholytes are employed for surface modification. Nevertheless, this aspect has often been neglected in previous studies, in which the monomer ratio on the surface was considered the same as that in the mixed monomer solution, without any experimental evidence [39, 40]. One of the key tasks associated with the surface composition analysis is the selection of a suitable approach for analyzing the composition of the grafted polymers without any effects of the membrane components.

Modifying the RO membrane with a polyampholyte allows controlling the surface ratio of the polyampholyte and determining the relation between the monomer ratio in the polyampholyte grafted on the membrane and that in the mixed monomer solution. This relation can then be used to elucidate the correlation between the anti-biofouling properties and the surface composition. Controlling the monomer ratio in the polyampholyte grafted on the membrane will also enable varying the membrane charge from negative to positive, keeping the surface hydrophilicity almost constant by using cationic and anionic monomers with a similar structure. This would enable the separate evaluation of the effects of membrane charge and hydrophilicity of the membrane surface on the biofouling properties. Hydrophilicity, surface charge, and surface roughness are the main factors influencing the anti-biofouling properties of a membrane [41]. In general, the membranes with high hydrophilicity (i.e. low water contact angle(degree)) and neutral charge (i.e. near zero ζ-potential (mV)) are prone to show lower biofouling [42]. Because it is known that the hydrophilic layer prevents the adsorption of bacteria, while the neutral charged surface could reduce the electrostatic attraction between foulants and membrane surface [43]. However, only few studies have attempted to isolate the effect of the individual factors on the anti-biofouling mechanism.

In this work, a polyamide RO membrane was modified with a polyampholyte composed of anionic 2-carboxyethyl acrylate (CAA) and cationic [2-(acryloyloxy)ethyl] trimethyl ammonium chloride (TMA). In addition to showing a similar structure to pCBMA, this system allows controlling the composition of the p(CAA-co-TMA) polyampholyte on the membrane surface. Previous studies have demonstrated various unique characteristics of the p(CAA-co-TMA) polyampholyte such as pH responsive, fouling resistance, and protein conjugation [39, 40, 44], but there is few investigation about the effect of CAA/TMA monomer ratio on the membrane characterizations and anti-biofouling performance. Therefore, p(CAA-co-TMA) polyampholytes with different CAA/TMA monomer ratios were grafted on the surface of polyamide RO membranes by surface-initiated atom transfer radical polymerization (SI-ATRP); this method offers a unique route to construct a polymer with controlled architecture and well-defined composition [45-47]. First, the relationship between the CAA/TMA ratio of a mixed monomer solution and that of on the membrane surface was accurately determined. Secondly, the RO membranes with different net surface charges were fabricated by changing the CAA/TMA ratio in the mixed monomer solution. The net surface charge and hydrophilicity were evaluated by ζ-potential and water contact angle measurements, respectively. The anti-biofouling properties of the p(CAA-co-TMA)-grafted membranes were systematically investigated by protein adsorption and static bacterial attachment. Then, the effects of surface net charge and hydrophilicity of the membrane surface on the anti-biofouling properties were evaluated. Finally, the stability of the p(CAA-co-TMA)-grafted membranes that showed the best anti-biofouling properties among the membranes fabricated in this work was evaluated by a long-term dynamic biofouling filtration experiment. The anti-biofouling behavior in this experiment is a very important property of membranes used in water treatment applications, because biofilm growth is a slow and time-dependent process [48]; in addition, chemical treatments to remove biofilm are not preferable to

processes based on polyamide RO membranes, due to the polyamide decomposition [49]. However, most studies have focused on the bacterial resistance of polyampholytes in static and short-term conditions [29, 31], whereas the long-term stability of the anti-biofouling properties has hardly been investigated.

4.2. Theoretical and experimental

4.2.1. Theoretical

To possess the anti-biofouling properties, the membrane surface charge should be neutral in marine environments at pH 8.0 [50] and in physiological environments at pH 7.4 [51], because the polyamide RO membrane is mainly applied in seawater desalination and physiological wastewater treatment. First, the CAA/TMA molar ratio on the membrane surface that would generate a neutral membrane surface at a pH around 7–8 was estimated. The aromatic polyamide skin layer of pristine RO membranes has a negative charge at pH higher than 4 [52]. However, the extent to which the charge of the skin layer affects the net charge of a p(CAA-co-TMA)-grafted membrane surface is not clear. Thus, the net charge of the p(CAA-co-TMA)-grafted membrane surface was estimated using Eq. (A1) in the Appendix 2, neglecting the effect of the skin layer on the net charge. Figure 4.1 shows the charge of the membrane surface calculated by assuming that the acid dissociation constant (pKa) of the CAA carboxyl anion is 4.76 (corresponding to CH_3COOH) [53], and that TMA has a permanent positive charge originating from the quaternary ammonium cation, with no pH dependence. Figure 4.1 clearly shows that when the molar ratio between carboxyl anion and quaternary ammonium cation is 1:1, the net charge of p(CAA-co-TMA) is zero under at pH > 6. Therefore, a polyamide RO membrane with excellent anti-biofouling properties can be fabricated by grafting p(CAA-co-TMA) with a 1:1 CAA/TMA ratio. If the negative charge of the polyamide skin layer cannot be neglected, the

CAA/TMA ratio should be less than unity, for example of 0.5:1, to compensate the effect of the negative charge of the polyamide skin layer.

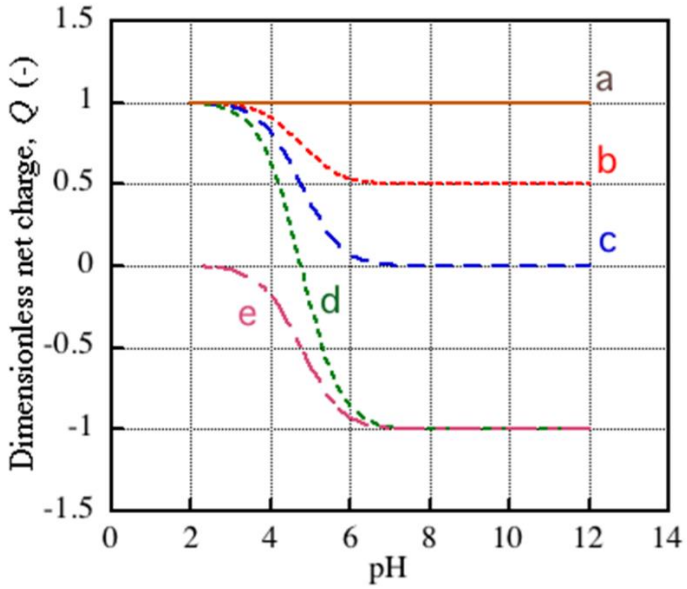

Fig. 4.1. Dimensionless net charge of p(CAA-co-TMA) as a function of pH. The CAA and TMA molar ratios in p(CAA-co-TMA) are CAA/TMA is (a) 0:1, (b) 0.5:1, (c) 1:1, (d) 2:1, and (e) 1:0.

4.2.2. Experimental

4.2.2.1. Materials

A commercial polyamide RO membrane, ES20 (Nitto, Osaka, Japan), was used as the membrane substrate. 3-Aminopropyltrimethoxysilane (APTS; Tokyo Chemical Industry, Tokyo, Japan) was used for membrane surface amination, and α-bromoisobutyryl bromide (BIBB; Sigma-Aldrich, St. Louis, MO, USA) was employed as the initiators of the SI-ATRP reaction. Ethyl-2-bromoisobutyrate (EBIB; Tokyo Chemical Industry) was used as SI-ATRP initiator to synthesize bulk polymers. Tris(2-pyridylmethyl)amine (TPMA; Wako Pure Chemical Industries, Osaka, Japan), L-ascorbic acid (Tokyo Chemical Industry), and copper (II) bromide (CuBr2;

Sigma-Aldrich) were used as a ligand, reductant, and catalyst of the SI-ATRP reaction, respectively. CAA (Sigma-Aldrich) and TMA (Sigma-Aldrich) were used as anionic and cationic monomers, respectively. 2,2,2-Trifluoroethanol (TFE; Sigma-Aldrich), pyridine (Sigma-Aldrich) and di-tert-butylcarbodiimide (Di-tBUC; Sigma-Aldrich) were used for the carboxyl derivatization reaction. Bovine serum albumin-fluorescein isothiocyanate conjugate (BSA; Sigma-Aldrich), lysozyme (LYZ; Wako Pure Chemical Industries), and fluorescein 5-isothiocyanate (Tokyo Chemical Industry) were used for the protein adsorption tests. Sphingomonas paucimobilis NBRC 13935 (NITE Biological Resource Center, Chiba, Japan) were used as the model bacteria. Tryptic soy broth (TSB; Becton, Dickinson and Company, Franklin Lakes, NJ, USA) was used as a medium culture. SYTO9 (Life Technologies, Carlsbad, CA, USA) was used to stain the bacteria. 25% Glutaraldehyde solution (Wako Pure Chemical Industry) was used to bacteria fixation on membrane surface. Deuterium oxide (D_2O; SCETI) was employed as solvent in the proton nuclear magnetic resonance (^{1}H-NMR) measurements. Milli-Q water (Merck Millipore, Darmstadt, Germany) was used in all the experiments.

4.2.2.2. Synthesis of bulk polyampholyte

First, 5 mL of mixed monomer aqueous solution containing CAA and TMA in a given molar ratio (total concentration 2.8 M) was placed into a 50-mL glass bottle, and the pH was adjusted at 6.0 using 3 M NaOH. Then, 7.4 mL of methanol, 1.6 mL of 0.5 M ascorbic acid, and 2 mL of 88 mM EBIB were added to the bottle. After 10 min of nitrogen bubbling, 4 mL of methanol containing 0.02 mmol of $CuBr_2$ and 0.04 mmol of TPMA were added with a syringe to initiate the SI-ATRP reaction. The mixed solution was then shaken (100 rpm) at 25 °C for 1 h. After that, the polymerization solution was diluted three times with Milli-Q water to terminate the reaction

and then dialyzed in a Fisherbrand dialysis tubing (MWCO 6000–8000) against Milli-Q water for 1 week, followed by freeze-drying.

The CAA/TMA molar ratio of the synthesized CAA/TMA bulk polyampholyte, p(CAA-co-TMA), was measured by a ^{1}H-NMR spectrometer (JEOL RESONANCE, Tokyo, Japan) according to the following procedure. First, 0.02 g of collected p(CAA-co-TMA) powder was dissolved in 0.5 mL D_2O for the ^{1}H-NMR measurements. The acquired ^{1}H-NMR spectra were analyzed by the Delta 5.1.3 software, which was used to calculate the peak area of the functional groups. Then, the CAA/TMA molar ratio was obtained as the peak area ratio of the functional groups originating from CAA and TMA.

The CAA/TMA molar ratios in the mixed monomer aqueous solution (hereafter referred to as the feed ratios) used in this work and the labels used to denote the resulting polyampholytes are shown in Table 4.1.

Table 4.1. Labels of mixed monomer aqueous solutions with various CAA/TMA feed ratios.

CAA/TMA feed ratio*	1:0	13:1	6:1	3:1	1:1	1:3	0:1
Polyampholyte	CAA	C13T1	C6T1	C3T1	C1T1	C1T3	TMA

*Total monomer concentration: 2.8 M.

4.2.2.3. Membrane surface modification

A schematic illustration of the SI-ATRP process employed for surface modification is shown in Fig. 4.2; the procedure is similar to that used in a previous study [22], and the p(CAA-co-TMA)-grafted membrane was fabricated using the same SI-ATRP conditions as for the synthesis of the bulk polyampholyte. First, 5 mL of mixed monomer aqueous solution at pH 6, containing

CAA and TMA in a given molar ratio (total concentration 2.8 M), was prepared. After a 10 min amination with 1 v/v% APTS and 1 min of immobilization with 3 wt% BIBB immobilization on a polyamide RO membrane, the membrane was placed in a 50-mL glass bottle. Then, the 5 mL of the prepared monomer solution, 9.4 mL of methanol, and 1.6 mL of 0.5 M ascorbic acid were added. After 10 min of nitrogen bubbling, 4 mL of methanol containing 0.02 mmol of $CuBr_2$ and 0.04 mmol of TPMA were added with a syringe to initiate the SI-ATRP reaction. The bottle was placed in a shaker (100 rpm) at 25 °C for 1 h. Finally, the modified membrane was removed from the bottle, washed overnight with Milli-Q water in a shaker (60 rpm) at 40 °C, and stored in Milli-Q water.

In the following, the p(CAA-co-TMA)-grafted membranes with different CAA/TMA feed ratios are represented by the corresponding polyampholyte labels shown in Table 1, such as CAA membrane, C13T1 membrane, etc.

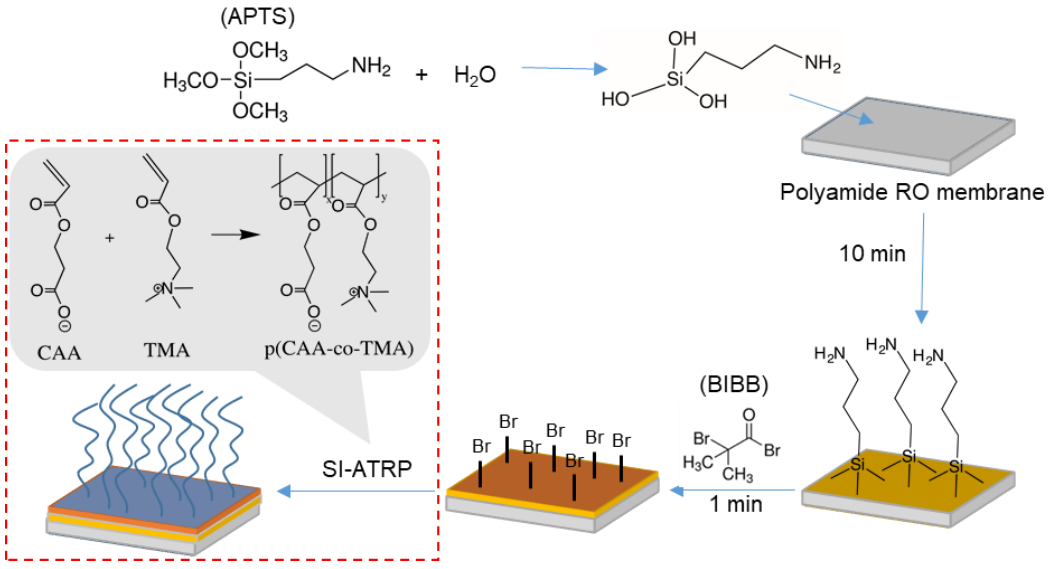

Fig. 4.2. Schematic illustration of the fabrication of the p(CAA-co-TMA)-grafted membranes by the SI-ATRP method.

4.2.2.4. Surface composition

The crucial tasks for membrane characterization involved confirming the grafting of p(CAA-co-TMA) and to quantifying the molar ratio between CAA and TMA grafted on the membrane surface (hereafter referred to as the surface ratio). In the case of TMA, the content of quaternary ammonium cations, which are present only on TMA but not exists on polyamide, was evaluated by X-ray photoelectron spectroscopy (XPS; JPS-9010MC, JEOL). The high-resolution N_{1s} spectra, obtained from the tested membranes, were separated into three peaks using the SpecSurf software in analysis mode; the peaks can be attributed to amine groups (399 eV), amide groups (400 eV), and quaternary ammonium cations (403 eV) [54].

In the case of CAA, the carboxyl anion is an analogue of the methyl acetate group of polyamide, CAA, and TMA. Therefore, it is difficult to directly confirm the CAA grafting on the surface by XPS directly. To solve this problem, a carboxyl derivatization reaction was carried out that enabled the conversion of the carboxyl anion to the trifluoromethyl (TFE) group. The reaction of the carboxyl anion with TFE is shown in Fig. 4.3 [55]. A membrane with 1 cm diameter was placed in a 5-mL glass bottle. TFE (0.9 mL), pyridine (0.4 mL), and Di-tBuC (0.3 mL) were sequentially added to the glass bottle at 15-min intervals. The glass bottle was then sealed with a screw cap, and the reaction was allowed to proceed at room temperature for ~12 h. Then, the membrane was removed from the glass bottle and washed with Milli-Q water to remove the unreacted reagents, followed by freeze-drying. The fluorine composition F_{1s} on the resulting membrane surfaces was evaluated by XPS. The high-resolution F_{1s} spectra were analyzed by the SpecSurf software in analysis mode.

The CAA/TMA surface ratio was calculated by Eq. (1) (the detailed derivation of this equation is shown in the section A2.2 of Appendix 2):

$$Ratio = \frac{x}{y} = \frac{27F}{3-24F} \quad (1)$$

where x and y are the molar contents of CAA and TMA monomers grafted on the surface, respectively, and F is the atomic ratio of fluorine (F_{1s}), corresponding to the peak area ratio of fluorine element obtained from the SpecSurf software in analysis mode.

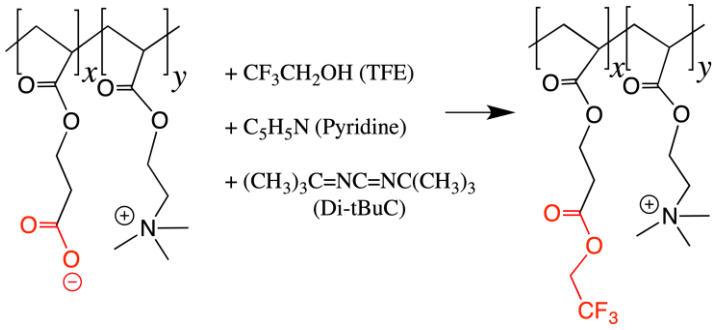

Fig. 4.3. Carboxyl derivatization reaction.

4.2.2.5. Surface characterizations

The surface charge of the polyamide RO and modified membranes was evaluated by the ζ-potential measurements (SurPASS™, Anton Paar, Graz, Austria). The surface hydrophilicity was evaluated by averaging 10 independent measurements of water contact angle on each membrane, performed using a contact angle meter (DM-300, Kyowa Interface Science, Saitama, Japan).

4.2.2.6. Protein adsorption

As the neutral polyampholyte shows high resistance to the adsorption of charged proteins, the protein adsorption of pristine and modified membranes was evaluated using two model proteins: negatively charged fluorescent BSA, and positively charged fluorescent LYZ (the synthesis protocol of fluorescent LYZ is described in the section A2.3 of Appendix 2). A 0.2 M phosphate buffer solution (PBS, pH=7) was used as solvent to dissolve the proteins. The membranes were soaked in a protein solution (20 mg/L in PBS) for 12 h. Then, the membranes

were removed from the protein solution and rinsed with PBS to remove the unbound protein molecules. All soaked membranes were observed by confocal laser scanning microscopy (CLSM; FV1000D, Olympus, Tokyo, Japan) and the relative fluorescence intensity was analyzed by the ImageJ software (National Institutes of Health, Bethesda, MD, USA).

4.2.2.7. Biofouling

The biofouling performance was investigated by 24-h static bacterial adhesion and 3-day dynamic biofouling filtration tests. The experimental protocols of these tests are the same as those used in a previous study [22]. *Sphingomonas paucimobilis* NBRC 13935 was selected as the model bacteria because these bacteria were known to cause a biofouling in RO membrane processes [56]. To prepare the bacterial suspension, first, a bacterial colony taken from an agar plate was precultured in 20 mL of 30 g/L TSB medium at 30 °C for 12 h. Then, the precultured bacterial suspension was diluted 50 times with 30 g/L TSB medium and cultured again for 4 h at 30 °C. By using 30 g/L TSB medium, the bacterial suspension was adjusted to a final optical density of 0.05 at 450 nm for the biofouling experiments. The optical density was measured using a spectrophotometer (V-650, Jasco, Tokyo, Japan).

For the static bacterial adhesion test, the membranes (0.5 cm × 1.0 cm) were soaked in 2 mL of prepared bacterial suspension (pH ≈ 7; the preparation protocol is described in the Supplementary Information.) and shaken at 120 rpm and 30 °C for 24 h. Then, the membranes were gently rinsed twice with aqueous 0.85 wt% NaCl solution and immersed in aqueous 0.85 wt% NaCl containing SYTO9 for 20 min to stain the bacteria adhered to the membrane surface. To fix the stained bacteria, the membranes were immersed in aqueous 2.5% glutaraldehyde for 3 min, rinsed, and kept in aqueous 0.85 wt% NaCl. The stained membranes were observed by CLSM, and the coverage of the adhered bacteria was calculated with the ImageJ software.

For the dynamic biofouling filtration test, the prepared bacterial suspension was poured on the surface of the fabricated membrane and incubated at 30 °C for 1 h to allow bacterial adhesion on the membrane surface. The membrane was briefly washed with aqueous 0.85 wt% NaCl and set in a cross-flow membrane test unit (effective membrane area: 8.07 cm^2). An aqueous medium containing 3 g/L TSB medium and 7.65 g/L NaCl was fed to the membrane cell at 2.0 mL/min and 1.5 MPa for 3 days. The feed water side of the membrane surface was magnetically stirred at 200 rpm, and the entire membrane cell was incubated at 30 °C. The weight of accumulated permeate weight was then recorded to calculate the changes in the water permeability. The membrane surfaces were observed by CLSM after the filtration test.

4.2.2.8. Water permeability and salt rejection

Water permeability and salt rejection are the important performance of RO membrane process. It is considered that the surface modification will affect the water permeability and/or salt rejection. Thus, we measured these properties of modified membranes to confirm the effect of surface modification. First, a membrane was set in a crossflow filtration cell (effective membrane area was 8.07 cm^2). The operation pressure and flow rate in the system were 0.75 MPa and 10 mL/min, respectively. Secondly, the test membrane was pre-compacted by Milli-Q water for 30 min. Then the accumulated weight of permeate water was recorded by using RsWeight software (A&D company, Tokyo, Japan) for 1h. The water permeability, L (L/(m^2·h·MPa) (LMH/MPa)) was calculated as follow:

$$L = \frac{Q}{A \times t \times P} \quad (2)$$

where Q is the volume of permeate water (L), A is the effective membrane surface area (m^2), t is the time (h), and P is the applied pressure (MPa).

To measure the salt rejection, 500 ppm NaCl solution was filtered to the membrane under the same operation conditions of water permeability measurement. The salt rejection, R (%) was calculated as follows:

$$R = \frac{c_0 - c_p}{c_0} \times 100\% \quad (3)$$

where c_0 and c_p are the NaCl concentration in feed and permeate, respectively, which were obtained from a conductivity of each solution measured with conductivity meter (B-771, Horiba, Kyoto, Japan)

4.3. Results and discussion

4.3.1. Polyampholyte synthesis

^{1}H-NMR spectroscopy measurements were carried out to confirm the successful synthesis and to identify the CAA/TMA ratio of the p(CAA-co-TMA) bulk polyampholytes. In the ^{1}H-NMR analysis shown in Fig. 4.4, the peak labeled "a" at 2.7 ppm is attributed to the methylene unit of CAA bonded to the carboxyl anion. The two peaks at 3.1 ppm and 3.7 ppm (labeled "c" and "b" in Fig. 4.4, respectively) are assigned to the methylene and methyl groups, respectively, of the quaternary ammonium cation of TMA. These three peaks appeared in the ^{1}H-NMR spectra of all p(CAA-co-TMA) polyampholytes with different monomer feed ratios, which indicates that the polyampholyte can be formed from the CAA and TMA components.

The obtained monomer ratios of the synthesized bulk p(CAA-co-TMA) polyampholytes are shown in Table 4.2. The value of the b/c ratio between peak area of the corresponding peaks was close to 1 in all synthesized p(CAA-co-TMA) compounds, indicating the accuracy of the ^{1}H-NMR spectra. Figure 4.5 shows the CAA/TMA ratios (averages of the values of a/c and a/b values) of the p(CAA-co-TMA) bulk polyampholytes as a function of the CAA/TMA feed ratio. The figure clearly shows that the CAA/TMA ratio of the bulk polyampholyte is directly proportional

to the feed ratio, although the two values are not the same. A bulk polyampholyte with 1:1 CAA/TMA ratio can be synthesized from the mixed monomer solution with a CAA/TMA feed ratio of approximately 2. In the fabrication of p(CAA-co-TMA)-grafted membranes, the polymerization and grafting processes take place simultaneously. Thus, the optimum feed ratio to fabricate p(CAA-co-TMA)-grafted membranes with a 1:1 surface ratio may differ from that of the bulk polymers; however, p(CAA-co-TMA)-grafted membranes with a 1:1 surface ratio can be fabricated using a mixed monomer solution with a feed ratio of approximately 2.

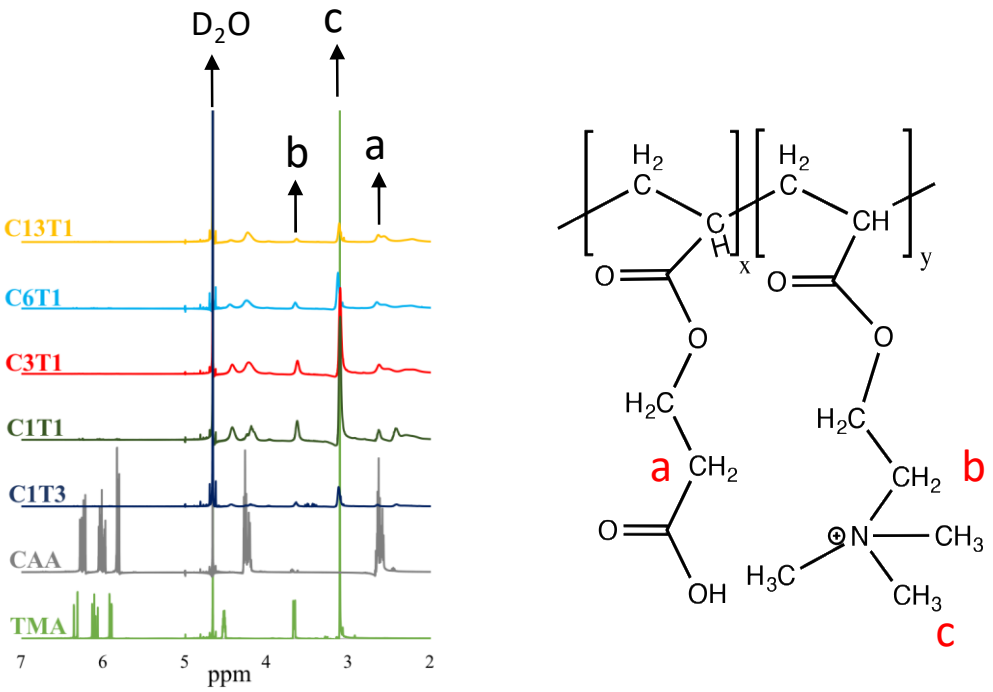

Fig. 4.4. ^{1}H-NMR spectra of CAA, TMA, and p(CAA-co-TMA) compounds with various CAA/TMA feed ratios.

Table 4.2. CAA/TMA ratios of the synthesized polyampholytes in the bulk state and on membrane surfaces, as determined by ^{1}H-NMR and XPS measurements, respectively.

Samples	CAA/TMA feed ratio	Bulk polyampholyte p(CAA-co-TMA)				Modified membrane	
		^{1}H-NMR				XPS	
		b/c	a/c	a/b	CAA/TMA (average of a/c and a/b)	F (%)	CAA/TMA surface ratio
C13T1	13	0.79	5.82	7.37	6.60	10.36	5.45
C6T1	6	0.77	2.06	2.71	2.39	8.21	2.15
C3T1	3	0.75	1.04	1.38	1.21	6.14	1.08
C1T1	1	0.92	0.40	0.43	0.42	3.79	0.49
C1T3	0.33	0.86	0.22	0.26	0.24	1.67	0.17

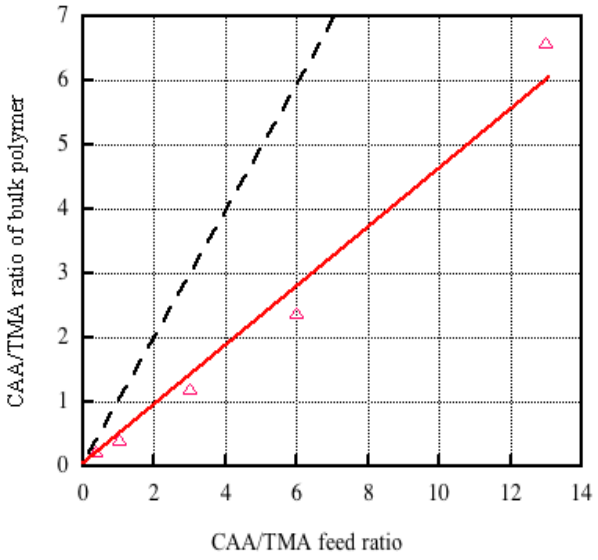

Fig. 4.5. CAA/TMA ratio as a function of CAA/TMA feed ratio. △: experimental data; solid line: smoothed line of experimental data; dotted line: in the case where CAA/TMA ratio of bulk polymer is equal to CAA/TMA feed ratio.

4.3.2. Membrane surface characterization

4.3.2.1. Surface composition

In order to confirm the grafting of the p(CAA-co-TMA) polyampholyte and quantify the CAA/TMA surface ratio, the surface compositions of the p(CAA-co-TMA)-grafted membranes were analyzed by XPS. Quaternary ammonium cations are only present in the TMA membrane, but not in the polyamide RO membrane, BIBB-immobilized membrane, or CAA membranes. Thus, the peak separation was conducted on the N_{1s} high-resolution spectra acquired from the surface of the p(CAA-co-TMA)-grafted membranes, to probe the grafting of TMA. Figure 4.6 shows the appearance of a peak at 403 eV, attributed to the quaternary ammonium cation of TMA, when the polymerization solution contained TMA. However, TMA can be adsorbed on the membrane surface due to the electrostatic interaction between quaternary ammonium cation of TMA and carboxyl group of polyamide, causing the peak at 403 eV to appear in the spectra. As shown in Fig. 4.7, as the pristine polyamide RO membrane adsorbs TMA, and the peak at 403 eV (due to adsorbed TMA) appears in the XPS spectra, whereas the BIBB-immobilized RO membrane does not adsorb TMA. Because all the p(CAA-co-TMA)-grafted membranes are of the BIBB-immobilized RO type, the 403 eV peak of p(CAA-co-TMA)-grafted membranes indicates that the TMA was successfully grafted on the membrane surface by SI-ATRP.

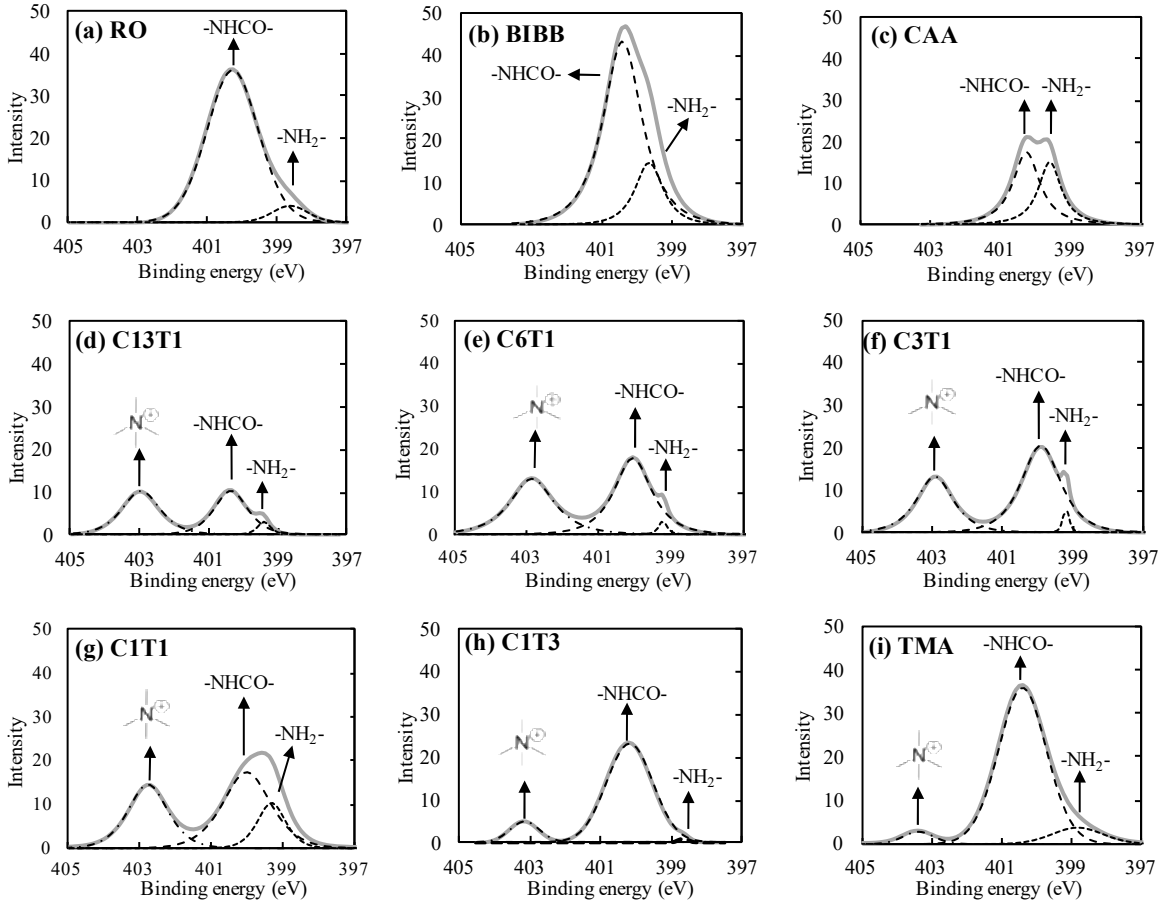

Fig. 4.6. Peak separation of the N_{1s} high-resolution spectrum of (a) pristine RO, (b) BIBB-immobilized, and p(CAA-co-TMA)-grafted membranes ((c) CAA, (d) C13T1, (e) C6T1, (f) C3T1, (g) C1T1, (h) C1T3, (i) TMA).

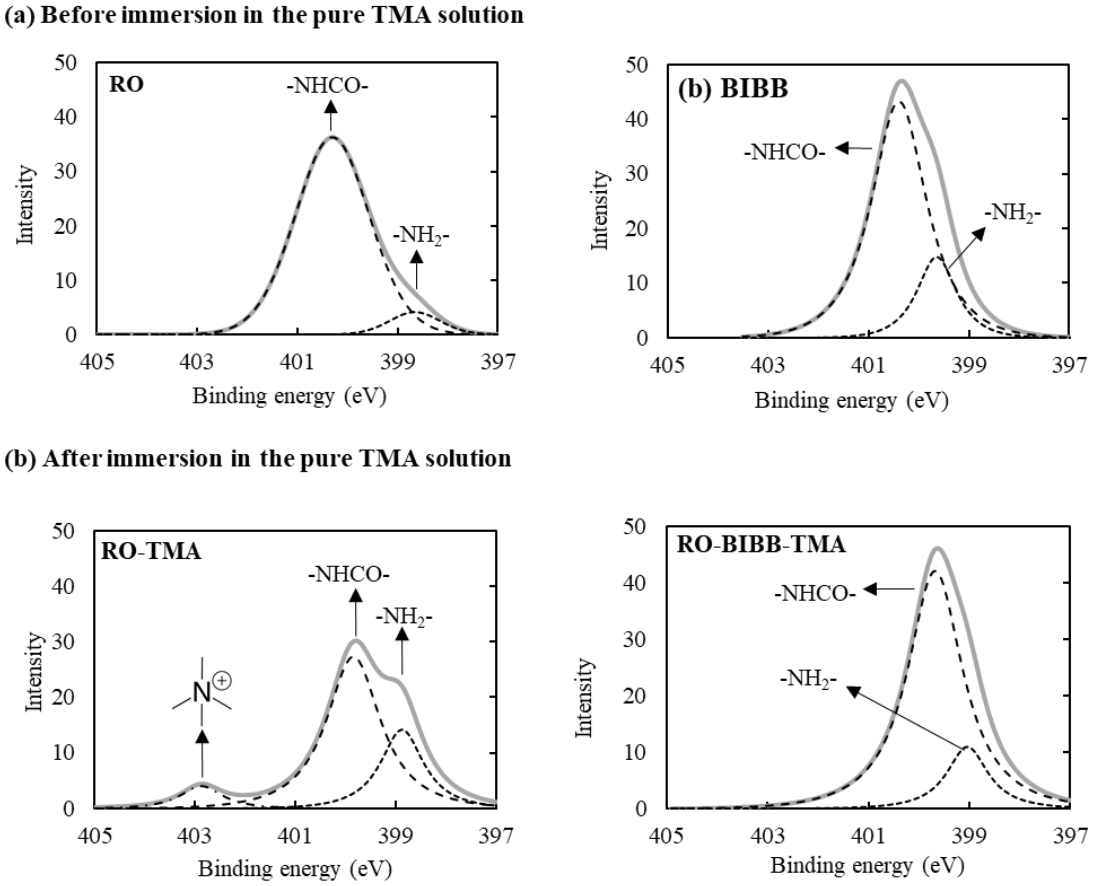

Fig. 4.7. Quaternary ammonium cation composition of pristine RO and BIBB-immobilized membranes (a) before and (b) after immersion in the pure TMA solution.

The carboxyl anion of CAA is an analogue of the methyl acetate group of polyamide, CAA, and TMA. Therefore, it is difficult to confirm the grafting of CAA grafting on the surface by common methods such as the attenuated total reflection Fourier transform infrared spectroscopy and XPS. To solve this problem, as described above, a carboxyl derivatization reaction was carried out to convert the carboxyl anion to the trifluoromethyl group (Fig. 4.3). According to the XPS spectra of pristine RO and modified membranes (Fig. 4.8) treated by the carboxyl derivatization reaction, the elemental fluorine (F_{1s}) was detected only in the p(CAA-co-TMA)-grafted membranes, while no F_{1s} peak was observed in the spectra of pristine polyamide RO,

BIBB-immobilized, and TMA membranes, probably because the carboxyl group of the polyamide is much less reactive in the carboxyl derivatization reaction. These results indicate that CAA was also successfully grafted on the membrane surface. Therefore, it is reasonable to conclude that the atomic percentage of fluorine measured by XPS merely expresses the composition of the carboxyl anion of CAA, which can be used to quantify the CAA/TMA surface ratio by Eq. (1).

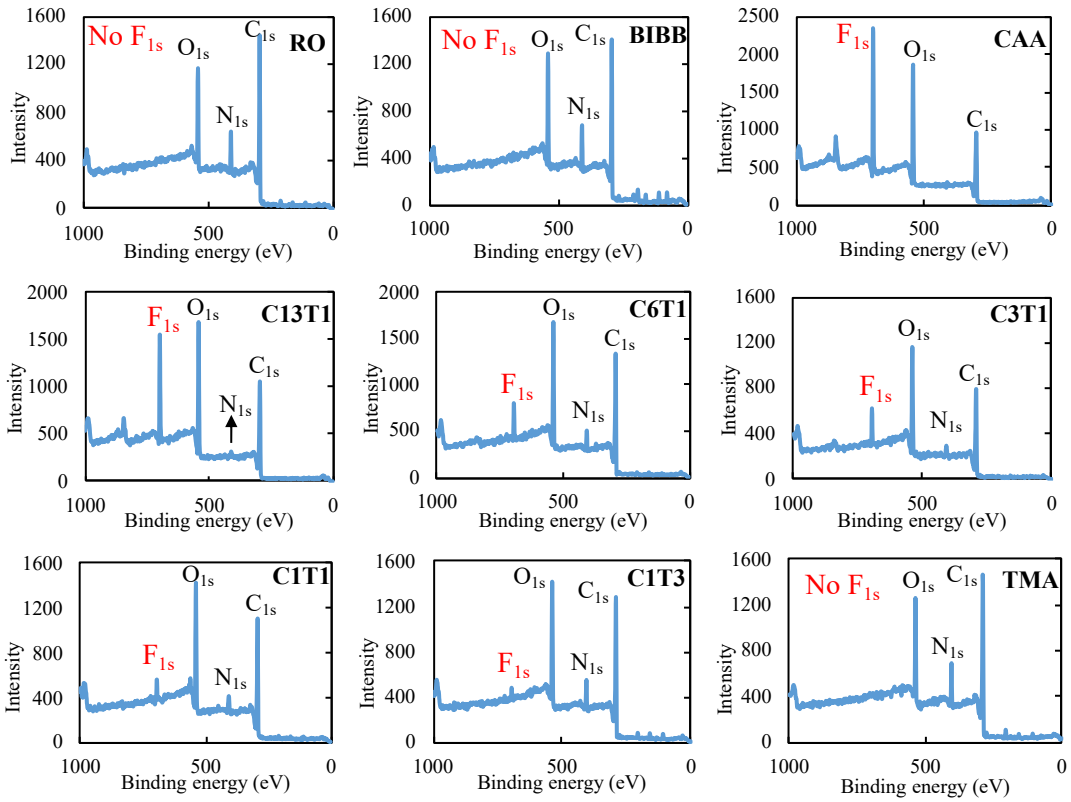

Fig. 4.8. XPS spectra of pristine RO, BIBB-immobilized, and p(CAA-co-TMA)-grafted membranes after carboxyl derivatization reaction.

As shown in Table 4.2, the atomic percentage of F_{1s} on the membrane surface increased with increasing CAA content. Figure 4.9 shows the CAA/TMA surface ratios as a function of the feed ratio, together with the CAA/TMA ratios of the bulk polymers shown in Fig. 4.5. The figure reveals that the CAA/TMA surface ratio is directly proportional to the feed ratio as well as to the

CAA/TMA ratio of the bulk polyampholyte. However, the proportionality constant of the membrane is somewhat lower than that of the bulk polyampholytes. This is probably because the polymerization reaction kinetics of the individual monomers on the skin layer of the polyamide RO membranes were different from those in the mixed monomer solution. In any case, Fig. 4.9 shows that a neutral modified membrane with 1:1 CAA/TMA surface ratio would be obtained with a feed ratio of approximately 3:1, which is similar to the results for bulk polymers obtained from ^{1}H-NMR measurements as discussed in Section 4.3.1. In previous studies, the CAA/TMA surface ratio was considered the same as the feed ratio, without any experimental evidence [39, 40]. However, the results reveal that the surface ratio is not always the same as the feed ratio. The synthesis of copolymers may depend on the polymerization reaction kinetics of the individual monomers [32], because each monomer has an inherent polymerization kinetics. In general, the experimental determination of the surface ratio is an essential task when a polyampholyte is grafted on the membrane surface.

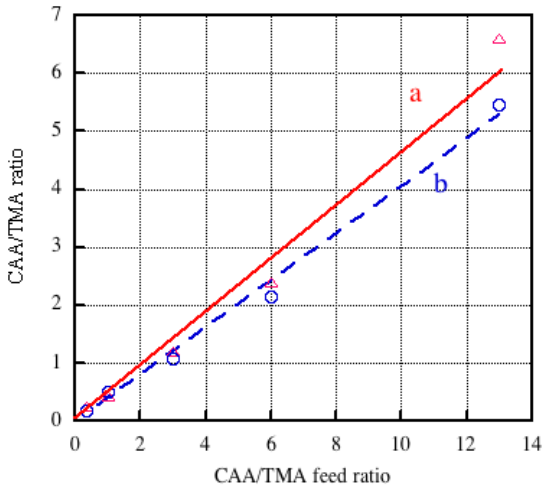

Fig. 4.9. Relationship between the CAA/TMA ratio and the feed ratio: (a) in bulk polyampholytes, (b) on the surface of p(CAA-co-TMA)-grafted membranes.

4.3.2.2. Surface charge

The surface charge of the pristine and modified membranes was evaluated by ζ–potential measurements in a pH range from 3 to 9. The results for the pristine RO and p(CAA-co-TMA)-grafted membranes are shown in Fig. 4.10(a). The pristine RO membrane was negatively charged above pH 3. The CAA membrane exhibited a negative surface charge over the measured pH range, because the carboxyl anion of CAA has a pKa value of 4.76. In contrast, the ζ–potential of the TMA membrane showed an obvious decreased from 72 mV to 30 mV in the pH range from 3 to 5, and then became constant at ~30 mV at a pH values from 5 to 9, which is inconsistent with the theoretical result that the quaternary ammonium cation of TMA maintains a positive charge at any pH value (Fig. 4.1). This is because the XPS intensity of quaternary ammonium cation is much lower than that of amide group on the surface of the TMA membrane, as shown in Fig. 4.6(i). In other words, the TMA membrane surface was not completely covered by polyTMA. Thus, it is impossible to neglect the influence of the polyamide RO membrane, whose ζ–potential decreased from 0 mV to −41 mV in the pH range from 3 to 5, and remained near −40 mV at pH value from 5 to 9. The combination effect of quaternary ammonium cation and polyamide leads to the resulting ζ–potential of the TMA membrane.

In Fig. 4.10(a), the isoelectric point (IEP) of the p(CAA-co-TMA)-grafted membranes gradually shifts to the higher pH with the increasing amount of TMA in the polymerization solution, indicating that the surface charge becomes more positive. The ζ–potential of the p(CAA-co-TMA)-grafted membranes shifts from positive to negative with increasing pH, and becomes almost constant above pH 7. The CAA/TMA surface ratio of the C6T1 membrane is 2.15 and corresponds to curve d in Fig. 4.1, while the C3T1 (surface ratio 1.08) and C1T1 (surface ratio 0.49) membranes correspond to curve c and b in Fig. 4.1, respectively. The comparison of Figs. 4.1 and 4.10(a) clearly shows that the pH dependency of the surface net charge obtained

experimentally is consistent with the theoretical prediction shown in Fig. 4.1. This means that the surface charge of the p(CAA-co-TMA)-grafted membranes is well explained by the dissociation of ionic groups on the membrane surface.

To evaluate the anti-biofouling characteristics of p(CAA-co-TMA)-grafted membranes for treating waste water above pH 7, Fig. 4.10(b) clearly shows the relationship between ζ–potential above pH 7 and surface ratios. With larger surface ratio values, the ζ–potential of the surface of the p(CAA-co-TMA)-grafted membranes become more negative, due to the increased content of anionic CAA. In particular, the C3T1 membrane with surface ratio of 1.08, shows a nearly zero (slightly negative) ζ–potential above pH 7. Therefore, the C3T1 membrane is expected to possess excellent anti-biofouling properties for the treatment of the sea water with pH 8.0 or wastewater with pH 7.4.

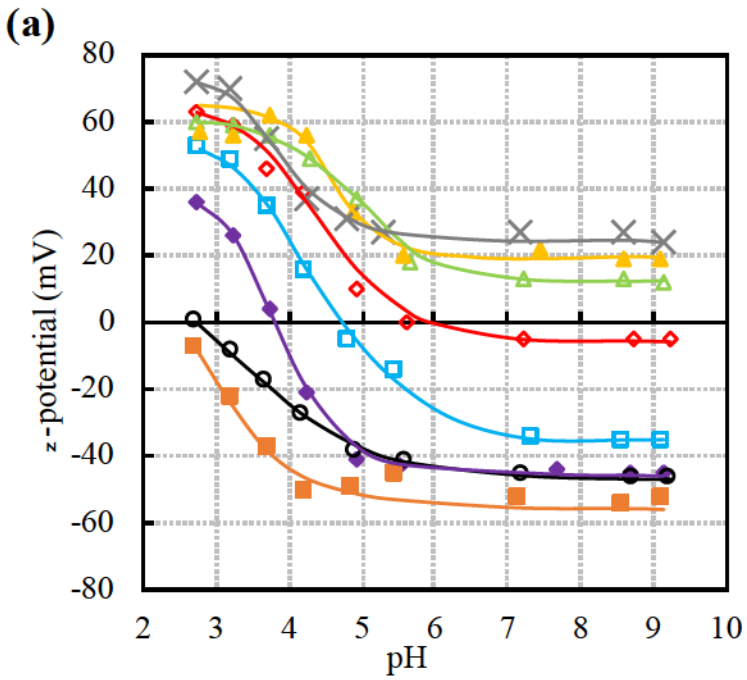

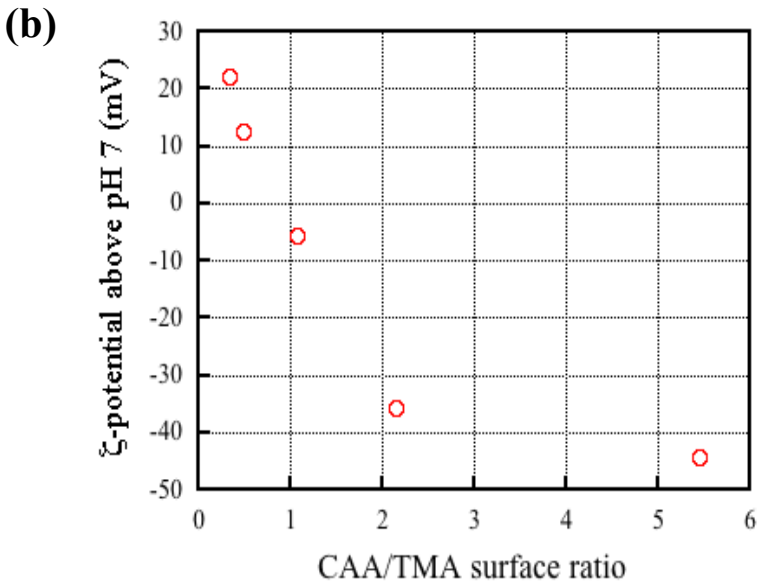

Fig. 4.10. (a) ζ–potential as a function of pH. ○: RO, ■: CAA, ◆: C13T1, □: C6T1, ◇: C3T1, △: C1T1, ▲: C1T3, ×: TMA. (b) ζ–potential of p(CAA-co-TMA)-grafted membranes above pH 7 as a function of CAA/TMA surface ratios.

4.3.3. Anti-biofouling performance

4.3.3.1. Protein adsorption

In order to characterize the protein adsorption properties of the p(CAA-co-TMA)-grafted membranes, the adsorption of proteins was measured at pH 7 using BSA (IEP = 5.0) and LYZ (IEP = 9.6) as models of negatively and positively charged proteins, respectively [57]. Protein adsorption is known to be correlated with biofouling (bacterial attachment) [18, 58, 59].

The relative fluorescence intensities of pristine and modified membranes after the adsorption of BSA and LYZ are shown in Fig. 4.11(a), and the corresponding CLSM images are shown in Fig. 4.12. The pristine RO membranes adsorbed a large amount of both LYZ and BSA, although these membranes have a negative net surface charge above pH 7, probably because of their low hydrophilicity (high water contact angle), as shown in Fig. 4.11(b). The hydrophilicity of the

p(CAA-co-TMA)-grafted membranes is much higher (lower water contact angle) than that of the pristine RO ones, except for the TMA membrane, whose hydrophilicity is lower than that of the other p(CAA-co-TMA)-grafted membranes, but still higher than that of the pristine RO membranes.

The net surface charge of the CAA, C13T1, C6T1, and C3T1 membranes is negative above pH 7, and the negative charge density estimated from the ζ–potential decreases in the order CAA > C13T1 > C6T1 > C3T1, as shown in Fig. 4.10. On the other hand, the net surface charge of the C1T1, C1T3, and TMA membranes is positive above pH 7, and the positive charge density follows the order C1T1 < C1T3 < TMA. Figure 4.11(c) shows the relationship between protein adsorption (BSA and LYZ) and ζ–potential above pH 7 of p(CAA-co-TMA)-grafted membranes. The figure reveals that when the membrane surface and the foulants have opposite charges there is a strong electrostatic attraction between them, and proteins are easily adsorbed on the membrane surface even if its hydrophilicity is very high. It is well established that a higher hydrophilic surface exhibits better anti-biofouling properties [60-62]. However, these findings indicate that, in the presence of a strong electrostatic attraction between membrane surface and foulants, biofouling takes place even when the hydrophilicity of the membrane surface is very high. On the other hand, when the membrane surface and the foulants have the same charge, an electrostatic repulsion is established between them, and proteins are scarcely adsorbed on the membrane. Interestingly, in the region where electrostatic repulsion is present, the anti-biofouling properties are scarcely affected by the increase in the degree of surface charge repulsion.

The relative fluorescence intensity of C3T1 is only about 20 % for both BSA and LYZ, which is the lowest value among all tested membranes. This is due to the high hydrophilicity of the C3T1 surface (originating from its large number of ionic groups), as well as to its almost

complete lack of electrostatic attraction with charged proteins. Thus, the C3T1 membrane is expected to exhibit excellent anti-biofouling performances.

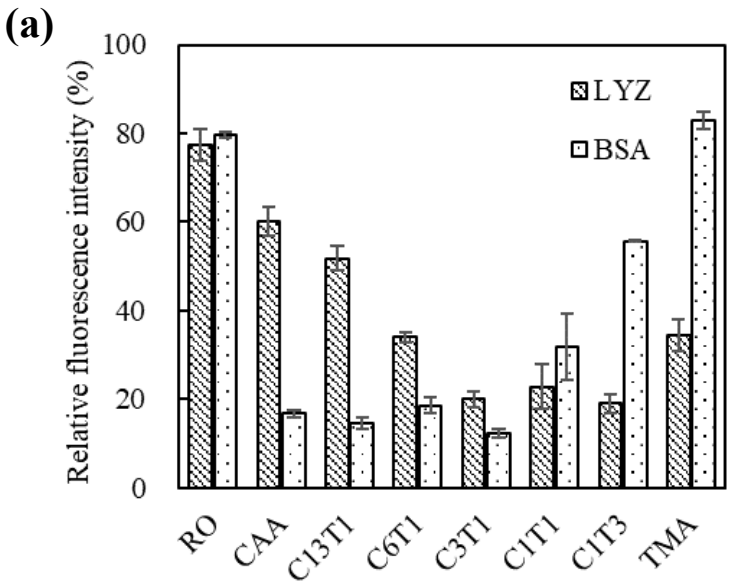

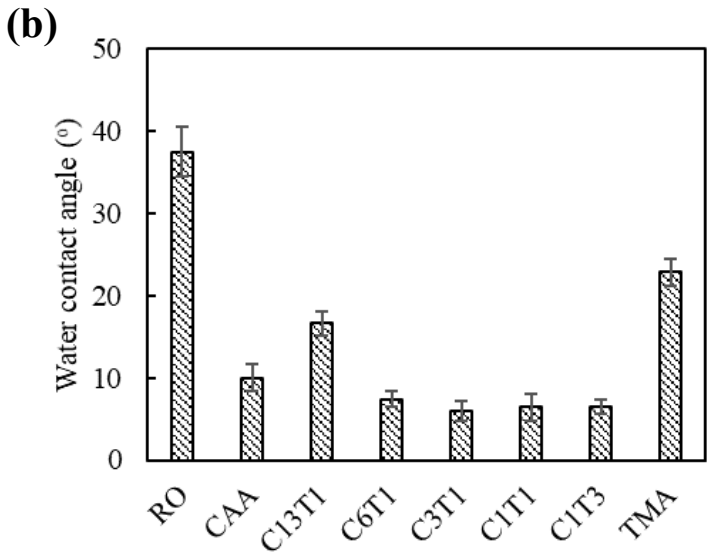

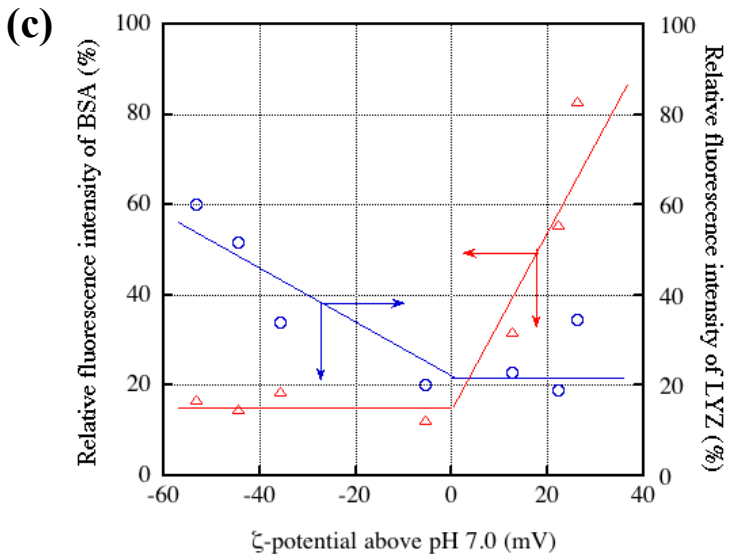

Fig. 4.11. (a) Protein adsorption of pristine RO and p(CAA-co-TMA)-grafted membranes; (b) water contact angle of pristine RO and p(CAA-co-TMA)-grafted membranes; (c) effect of ζ-potential above pH 7 on protein adsorption of p(CAA-co-TMA)-grafted membranes. ○: LYZ, △: BSA.

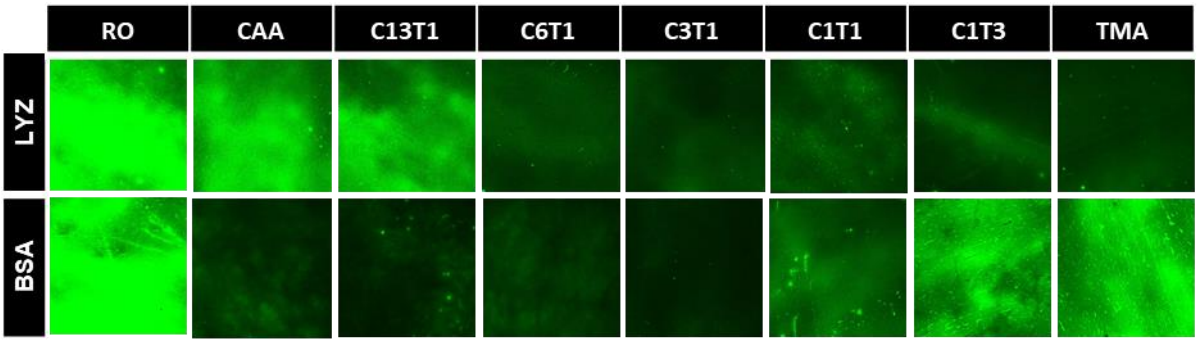

Fig. 4.12. CLSM images of pristine RO and p(CAA-co-TMA)-grafted membranes after protein adsorption.

4.3.3.2. Biofouling

Biofouling tests, including static bacterial adhesion and dynamic biofouling filtration, were also conducted to confirm the findings of section 4.3.3.1, suggesting that the non-biofouling characteristics are a result of the neutral nature of polyampholytes with a high hydrophilic surface.

Sphingomonas paucimobilis NBRC 13935 strains were selected for the biofouling tests; the pH of the bacterial suspension was approximately 7.0. Figure 4.14 shows the CLSM images of static bacterial adhesion, while Fig. 4.13(a) displays the bacterial coverage on the tested membrane surfaces, obtained from Fig. 4.14. A large number of bacteria was adhered on the pristine polyamide RO membrane because of its low surface hydrophilicity. For the p(CAA-co-TMA)-grafted membranes, as expected from the electrostatic interactions involved, significant bacterial attachment was observed on the positively charged membranes (C1T3 and TMA); however, no bacterial attachment was detected on the negatively charged membranes (CAA, C13T1, C6T1, and C3T1 membranes), because the *Sphingomonas paucimobilis* NBRC 13935 strains have negatively charged cell walls [63]. The C1T1 membrane, with a CAA/TMA surface ratio of 0.49, also showed no bacterial adhesion, despite having a positive net surface charge. On the other hand, the C1T3 membrane adsorbed a large number of bacteria. This is probably because that the anti-biofouling properties due to high surface hydrophilicity dominates the electrostatic attraction between surface charge and bacteria in the case of the C1T1 membrane. In contrast, for the CIT3 membrane, the electrostatic attraction prevails over the anti-biofouling properties due to the high surface hydrophilicity. As expected, based on the analysis of section 4.3.3.1, the bacteria adsorption onto the C3T1 membrane was negligibly low, because the CAA/TMA surface ratio of the C3T1 membrane is near 1:1 and its net surface charge is close to zero (slightly negative).

Figure 4.13 (b) shows the relationship between bacterial coverage, water contact angle, and surface charge. In the region where the ζ–potential over pH 7 is positive, the bacterial attachment

increased with the net surface charge of the membranes, even if the hydrophilicity of the membrane surface is very high (corresponding to a very low water contact angle). On the other hand, when the ζ–potential above pH 7 is negative, the surface net charge had no significant effect on the bacterial resistance. This phenomenon is consistent with Fig. 4.11(c). The closed symbols in Fig. 4.13(b) correspond to the pristine RO membrane. The bacterial coverage of the pristine RO membrane is 1.9%, and higher than that of other membranes with negative ζ-potential above pH 7, even though the ζ-potential of the pristine RO membrane is also around -46 mV. This is because its water contact angle of pristine RO is 37.4°, denoting a low hydrophilicity compared with that of p(CAA-co-TMA)-grafted membranes with negative ζ-potential. This suggests that, even in the presence of an electrostatic repulsion between the foulant and membrane charges, a low hydrophilicity of the membrane surface promotes an adhesion. A similar phenomenon was reported for anion exchange membranes [64]

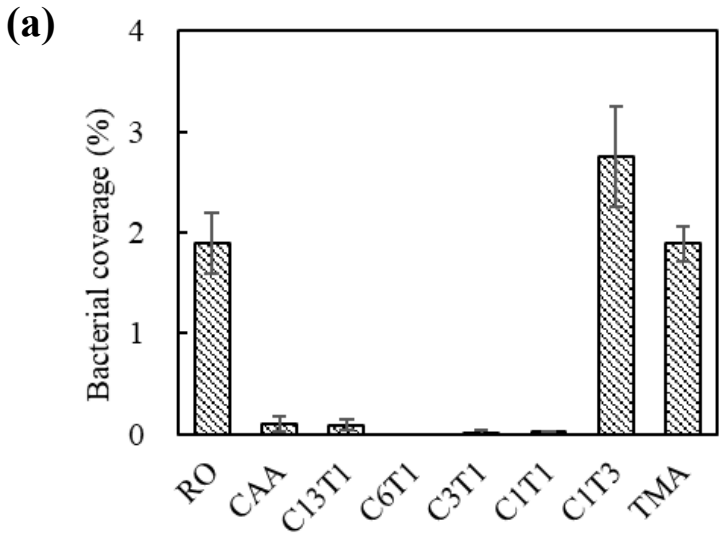

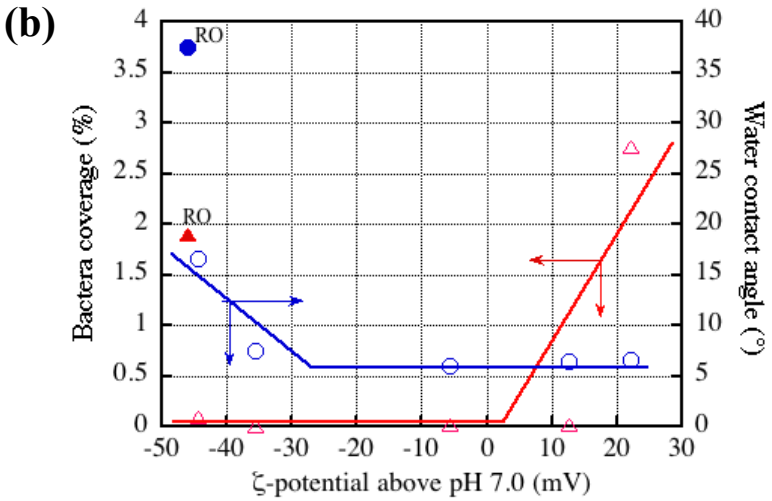

Fig. 4.13. (a) Static bacterial adhesion of pristine RO and p(CAA-co-TMA)-grafted membranes. (b) Relationship between bacterial coverage (△), water contact angle (○), and surface charge of p(CAA-co-TMA)-grafted membranes. Closed symbols represent the data corresponding to the pristine RO membrane.

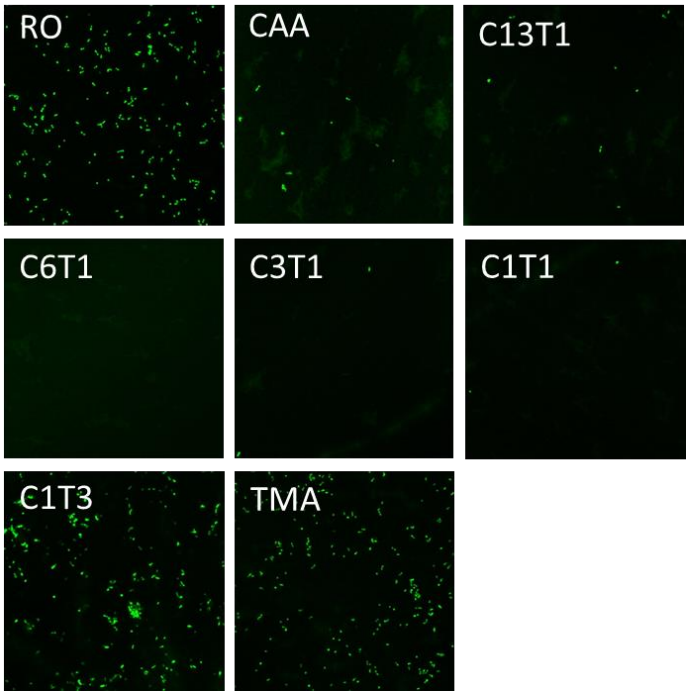

Fig. 4.14. CLSM images of pristine RO and p(CAA-co-TMA)-grafted membranes after static bacterial adhesion.

The static tests of protein and bacterial adhesion are not sufficient to predict the biofouling behavior in practical membrane processes, because these adhesion tests fail to reproduce several conditions relevant to biofilm growth. Thus, in order to further confirm the anti-biofouling properties of the membrane with 1:1 CAA/TMA surface ratio (C3T1), a dynamic biofouling filtration test was carried out over a period much longer than that of the static bacterial adhesion tests. The corresponding data, shown in Fig. 4.15(a), reveal that the C3T1 membrane had much better anti-biofouling performance than the pristine polyamide RO one. The permeability of the C3T1 membrane decreased by only ~20% after filtration for more than 60 h filtration, whereas that of the pristine polyamide RO membrane decreased by ~70%. The membrane surfaces were observed by CLSM after the dynamic biofouling filtration test as shown in Fig. 4.15(b). These data indicate that, during the dynamic biofouling filtration, higher amount of biofilm was formed on the surface of pristine RO membrane compared to the C3T1 membrane, which suggested that larger amount of bacteria adhered on the pristine RO membrane surface in the initial bacterial adhesion stage. This further confirms the assumption that a polyamide RO membrane with excellent anti-biofouling performance can be prepared by grafting p(CAA-co-TMA) with a CAA/TMA surface ratio of approximately 1:1.

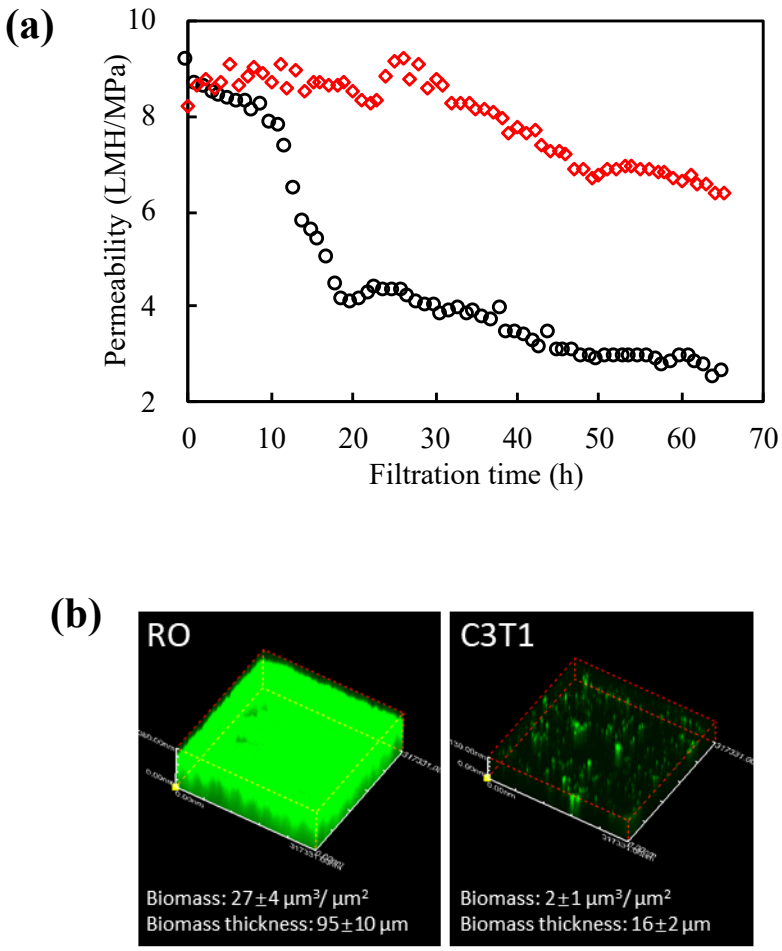

Fig. 4.15. (a) Water permeability of pristine RO and C3T1 membranes as a function of filtration time in the dynamic biofouling filtration tests. ○: RO, ◇: C3T1. (b) CLSM images and biofilm quantification (green area) of pristine RO and C3T1 membranes after the dynamic biofouling filtration tests.

4.3.4. Water permeability and salt rejection

It is reasonable to consider that the surface modification will affect the water permeability and/or salt rejection. Figure 4.16 shows the water permeability and salt rejection of pristine and modified RO membranes. It is found from Fig. 4.16 that the surface modification affected on both water permeability and salt rejection. The water permeability of modified membrane increased

with the increase of TMA portion of modified layer, while the salt rejection decreased with the increase of TMA portion. Compared with the pristine membrane, the decrease of water permeability of modified membrane is probably resulted from the increase of water flux resistance due to the increase of surface layer thickness. The reason of the decrease in salt rejection is not clear at this moment. However, one possible reason will be the increase of pore size of skin layer due to the modification with TMA. If the surface modification with TMA increases the pore size of skin layer, it is possible to explain the increase of water permeability and the decrease of salt rejection with the increase of TMA portion in the modified layer.

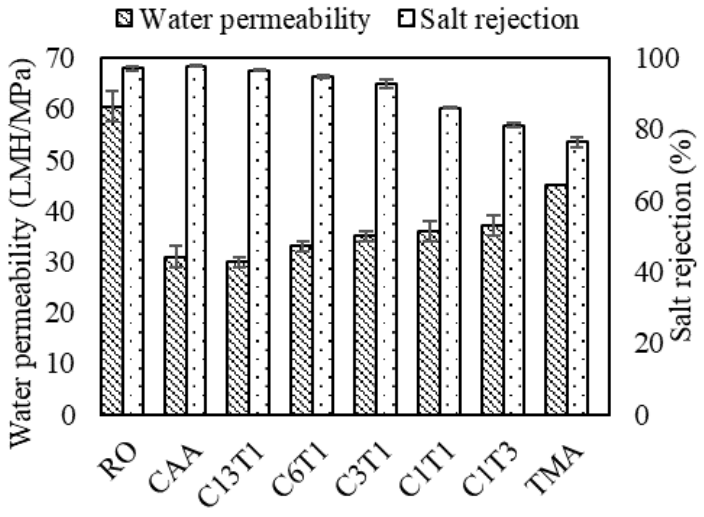

Fig. 4.16. Water permeability and salt rejection of pristine and modified membranes

4.4. Conclusion

SI-ATRP was used to graft CAA/TMA polyampholytes on the surface of polyamide RO membranes, in order to improve their anti-biofouling properties. To elucidate the effect of the monomer ratio of the grafted polyampholyte, several types of p(CAA-co-TMA) polyampholytes were grafted on the RO membrane surface, and the anti-biofouling properties were evaluated by

protein adsorption, static bacterial attachment, and long-term dynamic biofouling filtration experiments.

First, it was found that the CAA/TMA surface ratio was directly proportional but not identical to the feed ratio. Thus, the anti-biofouling properties of the modified membranes were evaluated as a function of the CAA/TMA ratio of the membrane surface. Based on the consistency between the pH dependence of the experimentally obtained ζ-potential and the theoretical prediction, it was concluded that the surface charge of the polyampholyte is determined by the dissociation of the ionic groups of the polyampholyte. Moreover, it can be found that, in the presence of a strong electrostatic attraction between membrane surface and foulants, biofouling took place even for a membrane surface with very high hydrophilicity. On the other hand, in the absence of electrostatic attraction between membrane surface and foulants, the anti-biofouling properties were determined by the hydrophilicity of the membrane.

Finally, it was found that the modified RO membrane with 1:1 CAA/TMA surface ratio, fabricated from a mixed monomer solution with 3:1 CAA/TMA ratio, had nearly zero net surface charge above pH 6 and showed an excellent anti-biofouling performance even in long-term dynamic biofouling filtration tests. This is due to the highly hydrophilic character of the surface (originating from its large content of ionic groups) and also to the almost complete absence of electrostatic attraction with charged bacteria, because the net surface charge is close to zero.

Appendix 2

A2.1. Net charge calculation

Herein, the calculation of the net charge of the p(CAA-co-TMA) polyampholytes was discussed. As shown in Fig. 4.1, TMA is a strong base (quaternary ammonium cation) and its charge does not depend on the pH value. On the other hand, CAA is a weak acid and its charge is

pH-dependent. The dissociation of CAA can be described as follows:

$\text{R-COOH} \leftrightarrows \text{R-COO}^- + \text{H}^+$

$$K_a = \frac{[\text{R}-\text{COO}^-]\ [\text{H}^+]}{[\text{R}-\text{COOH}]} = \frac{\alpha[\text{H}^+]}{1-\alpha}$$

where K_a is the dissociation constant and α is the degree of dissociation. By denoting the charge of 1 mol CAA at full dissociation ($\alpha = 1$) as q^- (eq), the charge of 1 mol TMA as q^+ (eq), and the CAA/TMA molar ratio of p(CAA-co-TMA) as $\left(\frac{x}{y}\right)$, the net charge of p(CAA-co-TMA) containing $\left(\frac{x}{y}\right)$ mol CAA and 1 mol TMA, q (eq), is given by the following equation:

$$q(\text{eq}) = \alpha\left(\frac{x}{y}\right)q^- + q^+ = \frac{K_a}{[\text{H}^+]+K_a} \cdot \left(\frac{x}{y}\right) \cdot q^- + q^+$$

Then, the dimensionless net charge of p(CAA-co-TMA), Q, is given by Eq. (A1), because $-q^- = q^+$ in p(CAA-co-TMA).

$$Q = \frac{q}{q^+} = -\frac{K_a}{[\text{H}^+]+K_a} \cdot \left(\frac{x}{y}\right) + 1 \qquad \text{(A1)}$$

In Eq. (A1), pK_a was set to 4.76 (corresponding to CH_3COOH, $K_a = 10^{-pKa}$).

A2.2. Derivation of Eq. (1)

The fluorine atomic ratio F, as determined by XPS, was calculated as:

$$F = \frac{N_f}{N_{total}} = \frac{3x}{24x+27y}$$

where N_f and N_{total} are the fluorine and total atomic numbers in p(CAA-co-TMA), respectively, whereas x and y are the numbers of CAA and TMA monomers grafted on the surface of p(CAA-co-TMA)-grafted membranes, respectively. As shown in Fig. A2.1, on the basis of the chemical structure of the resulting polymer, N_f and N_{total} are equal to $3x$ and $(24x + 27y)$, respectively. Thus, the monomer ratio is given by:

$$\frac{x}{y} = \frac{27F}{3-24F}$$

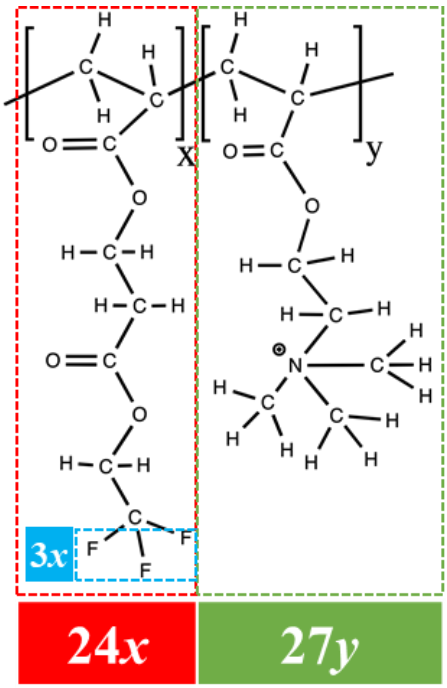

Fig. A2.1. Polymer structure of p(CAA-co-TMA) after the carboxyl derivatization reaction.

A2.3. Fluorescein labeling

First, 0.2 M NaH_2PO_4 and 0.2 M Na_2HPO_4 solutions were mixed to prepare a phosphate buffer solution (PBS) with pH 8.6. Then, 0.01 g of fluorescein 5-isothiocyanate and 0.1 g of lysozyme (LYZ) were dissolved in 100 mL of PBS. The mixed solution was then stirred for 3 h at 25 °C. The labeling reaction occurred between fluorescein and LYZ took place during this period. Afterwards, the reacted solution was poured into a dialysis tubing (MWCO 6000-8000) against the PBS buffer. After 72 h, the resulting solution was treated by a filter (0.45 μm). Finally, a 400-ppm LYZ solution labeled with fluorescein was obtained and kept in a dark place. Notably, the entire experiment must be conducted in a dark location.

References

[1] M. Falkenmark, J. Lundqvist, Comprehensive assessment of the freshwater resources of the world. World freshwater problems--call for a new realism, (1997).
[2] T.R. Malthus, An Essay on the Principle of Population. Reprint 2004. Edited with an introduction and notes by Geoffrey Gilbert, in, Oxford, UK: Oxford University Press, 1798.
[3] L.M. Fry, J.R. Mihelcic, D.W. Watkins, Water and nonwater-related challenges of achieving global sanitation coverage, Environmental Science & Technology, 42 (2008) 4298-4304.
[4] M.A. Montgomery, M. Elimelech, Water and sanitation in developing countries: including health in the equation, ACS Publications, 2007.
[5] C. Jarusutthirak, G. Amy, Role of soluble microbial products (SMP) in membrane fouling and flux decline, Environmental Science & Technology, 40 (2006) 969-974.
[6] C.M. Pang, P. Hong, H. Guo, W.-T. Liu, Biofilm formation characteristics of bacterial isolates retrieved from a reverse osmosis membrane, Environmental Science & Technology, 39 (2005) 7541-7550.
[7] Y. Miura, Y. Watanabe, S. Okabe, Membrane biofouling in pilot-scale membrane bioreactors (MBRs) treating municipal wastewater: impact of biofilm formation, Environmental Science & Technology, 41 (2007) 632-638.
[8] A. Matin, Z. Khan, S. Zaidi, M. Boyce, Biofouling in reverse osmosis membranes for seawater desalination: phenomena and prevention, Desalination, 281 (2011) 1-16.
[9] G.-R. Xu, J.-N. Wang, C.-J. Li, Strategies for improving the performance of the polyamide thin film composite (PA-TFC) reverse osmosis (RO) membranes: Surface modifications and nanoparticles incorporations, Desalination, 328 (2013) 83-100.
[10] D.J. Miller, P.A. Araujo, P.B. Correia, M.M. Ramsey, J.C. Kruithof, M.C. van Loosdrecht, B.D. Freeman, D.R. Paul, M. Whiteley, J.S. Vrouwenvelder, Short-term adhesion and long-term biofouling testing of polydopamine and poly (ethylene glycol) surface modifications of membranes and feed spacers for biofouling control, Water Research, 46 (2012) 3737-3753.
[11] S. Kasemset, A. Lee, D.J. Miller, B.D. Freeman, M.M. Sharma, Effect of polydopamine deposition conditions on fouling resistance, physical properties, and permeation properties of reverse osmosis membranes in oil/water separation, Journal of Membrane Science, 425 (2013) 208-216.
[12] B.D. McCloskey, H.B. Park, H. Ju, B.W. Rowe, D.J. Miller, B.J. Chun, K. Kin, B.D. Freeman, Influence of polydopamine deposition conditions on pure water flux and foulant adhesion resistance of reverse osmosis, ultrafiltration, and microfiltration membranes, Polymer, 51 (2010) 3472-3485.

[13] T. Ishigami, K. Amano, A. Fujii, Y. Ohmukai, E. Kamio, T. Maruyama, H. Matsuyama, Fouling reduction of reverse osmosis membrane by surface modification via layer-by-layer assembly, Separation and Purification Technology, 99 (2012) 1-7.
[14] J. Nikkola, X. Liu, Y. Li, M. Raulio, H.-L. Alakomi, J. Wei, C.Y. Tang, Surface modification of thin film composite RO membrane for enhanced anti-biofouling performance, Journal of Membrane Science, 444 (2013) 192-200.
[15] Y. Zhou, S. Yu, C. Gao, X. Feng, Surface modification of thin film composite polyamide membranes by electrostatic self deposition of polycations for improved fouling resistance, Separation and Purification Technology, 66 (2009) 287-294.
[16] W.K. Cho, B. Kong, I.S. Choi, Highly efficient non-biofouling coating of zwitterionic polymers: Poly ((3-(methacryloylamino) propyl)-dimethyl (3-sulfopropyl) ammonium hydroxide), Langmuir, 23 (2007) 5678-5682.
[17] Y.-F. Yang, Y. Li, Q.-L. Li, L.-S. Wan, Z.-K. Xu, Surface hydrophilization of microporous polypropylene membrane by grafting zwitterionic polymer for anti-biofouling, Journal of Membrane Science, 362 (2010) 255-264.
[18] J. Wang, Z. Wang, J. Wang, S. Wang, Improving the water flux and bio-fouling resistance of reverse osmosis (RO) membrane through surface modification by zwitterionic polymer, Journal of Membrane Science, 493 (2015) 188-199.
[19] M.L.M. Tirado, M. Bass, M. Piatkovsky, M. Ulbricht, M. Herzberg, V. Freger, Assessing biofouling resistance of a polyamide reverse osmosis membrane surface-modified with a zwitterionic polymer, Journal of Membrane Science, 520 (2016) 490-498.
[20] D. Saeki, T. Tanimoto, H. Matsuyama, Anti-biofouling of polyamide reverse osmosis membranes using phosphorylcholine polymer grafted by surface-initiated atom transfer radical polymerization, Desalination, 350 (2014) 21-27.
[21] L.-F. Fang, S. Jeon, Y. Kakihana, J.-i. Kakehi, B.-K. Zhu, H. Matsuyama, S. Zhao, Improved antifouling properties of polyvinyl chloride blend membranes by novel phosphate based-zwitterionic polymer additive, Journal of Membrane Science, 528 (2017) 326-335.
[22] Z. Yang, D. Saeki, H. Matsuyama, Zwitterionic polymer modification of polyamide reverse-osmosis membranes via surface amination and atom transfer radical polymerization for anti-biofouling, Journal of Membrane Science, (2018).
[23] G. Cheng, Z. Zhang, S. Chen, J.D. Bryers, S. Jiang, Inhibition of bacterial adhesion and biofilm formation on zwitterionic surfaces, Biomaterials, 28 (2007) 4192-4199.
[24] G. Cheng, G. Li, H. Xue, S. Chen, J.D. Bryers, S. Jiang, Zwitterionic carboxybetaine polymer surfaces and their resistance to long-term biofilm formation, Biomaterials, 30 (2009) 5234-5240.
[25] Z. Zhang, T. Chao, S. Chen, S. Jiang, Superlow fouling sulfobetaine and carboxybetaine polymers on glass slides, Langmuir, 22 (2006) 10072-10077.

[26] S. Chen, L. Li, C. Zhao, J. Zheng, Surface hydration: Principles and applications toward low-fouling/nonfouling biomaterials, Polymer, 51 (2010) 5283-5293.
[27] S. Chen, J. Zheng, L. Li, S. Jiang, Strong resistance of phosphorylcholine self-assembled monolayers to protein adsorption: insights into nonfouling properties of zwitterionic materials, Journal of the American Chemical Society, 127 (2005) 14473-14478.
[28] A. Laschewsky, Structures and synthesis of zwitterionic polymers, Polymers, 6 (2014) 1544-1601.
[29] A. Venault, T.-C. Wei, H.-L. Shih, C.-C. Yeh, A. Chinnathambi, S.A. Alharbi, S. Carretier, P. Aimar, J.-Y. Lai, Y. Chang, Antifouling pseudo-zwitterionic poly (vinylidene fluoride) membranes with efficient mixed-charge surface grafting via glow dielectric barrier discharge plasma-induced copolymerization, Journal of Membrane Science, 516 (2016) 13-25.
[30] W. Zhang, Z. Yang, Y. Kaufman, R. Bernstein, Surface and anti-fouling properties of a polyampholyte hydrogel grafted onto a polyethersulfone membrane, Journal of Colloid and Interface Science, 517 (2018) 155-165.
[31] Y.-H. Zhao, X.-Y. Zhu, K.-H. Wee, R. Bai, Achieving highly effective non-biofouling performance for polypropylene membranes modified by UV-induced surface graft polymerization of two oppositely charged monomers, The Journal of Physical Chemistry B, 114 (2010) 2422-2429.
[32] M.T. Bernards, G. Cheng, Z. Zhang, S. Chen, S. Jiang, Nonfouling polymer brushes via surface-initiated, two-component atom transfer radical polymerization, Macromolecules, 41 (2008) 4216-4219.
[33] X. Peng, L. Zhao, G. Du, X. Wei, J. Guo, X. Wang, G. Guo, Q. Pu, Charge tunable zwitterionic polyampholyte layers formed in cyclic olefin copolymer microchannels through photochemical graft polymerization, ACS Applied Materials & Interfaces, 5 (2013) 1017-1023.
[34] Y.-J. Shih, Y. Chang, D. Quemener, H.-S. Yang, J.-F. Jhong, F.-M. Ho, A. Higuchi, Y. Chang, Hemocompatibility of polyampholyte copolymers with well-defined charge bias in human blood, Langmuir, 30 (2014) 6489-6496.
[35] C. Leng, H. Huang, K. Zhang, H.-C. Hung, Y. Xu, Y. Li, S. Jiang, Z. Chen, Effect of surface hydration on antifouling properties of mixed charged polymers, Langmuir, 34 (2018) 6538-6545.
[36] S. Lin, Y. Li, L. Zhang, S. Chen, L.a. Hou, Zwitterion-like, charge-balanced ultrathin layers on polymeric membranes for antifouling property, Environmental Science & Technology, 52 (2018) 4457-4463.
[37] C. Chou, S. Syu, J.-H. Chang, P. Aimar, Y. Chang, Bioinspired Pseudozwitterionic Hydrogels with Bioactive Enzyme Immobilization via pH-Responsive Regulation, Langmuir, 35 (2018) 1909-1918.

[38] J. Zhao, M. Johnson, R. Fisher, N. Burke, H. Stöver, Synthetic Polyampholytes as Macromolecular Cryoprotective Agents, Langmuir, 35 (2018) 1807-1817.
[39] L. Mi, M.T. Bernards, G. Cheng, Q. Yu, S. Jiang, pH responsive properties of non-fouling mixed-charge polymer brushes based on quaternary amine and carboxylic acid monomers, Biomaterials, 31 (2010) 2919-2925.
[40] T. Tah, M.T. Bernards, Nonfouling polyampholyte polymer brushes with protein conjugation capacity, Colloids and Surfaces B: Biointerfaces, 93 (2012) 195-201.
[41] J.S. Louie, I. Pinnau, I. Ciobanu, K.P. Ishida, A. Ng, M. Reinhard, Effects of polyether–polyamide block copolymer coating on performance and fouling of reverse osmosis membranes, Journal of Membrane Science, 280 (2006) 762-770.
[42] R. Bernstein, S. Belfer, V. Freger, Bacterial attachment to RO membranes surface-modified by concentration-polarization-enhanced graft polymerization, Environmental Science & Technology, 45 (2011) 5973-5980.
[43] D. Rana, T. Matsuura, Surface modifications for antifouling membranes, Chemical Reviews, 110 (2010) 2448-2471.
[44] M.E. Schroeder, K.M. Zurick, D.E. McGrath, M.T. Bernards, Multifunctional polyampholyte hydrogels with fouling resistance and protein conjugation capacity, Biomacromolecules, 14 (2013) 3112-3122.
[45] R. Barbey, L. Lavanant, D. Paripovic, N. Schuwer, C. Sugnaux, S. Tugulu, H.-A. Klok, Polymer brushes via surface-initiated controlled radical polymerization: synthesis, characterization, properties, and applications, Chemical Reviews, 109 (2009) 5437-5527.
[46] J.-S. Wang, K. Matyjaszewski, Controlled/" living" radical polymerization. Halogen atom transfer radical polymerization promoted by a Cu (I)/Cu (II) redox process, Macromolecules, 28 (1995) 7901-7910.
[47] J. Xia, K. Matyjaszewski, Controlled/“living” radical polymerization. Atom transfer radical polymerization catalyzed by copper (I) and picolylamine complexes, Macromolecules, 32 (1999) 2434-2437.
[48] M. Herzberg, M. Elimelech, Biofouling of reverse osmosis membranes: role of biofilm-enhanced osmotic pressure, Journal of Membrane Science, 295 (2007) 11-20.
[49] J. Glater, S.-k. Hong, M. Elimelech, The search for a chlorine-resistant reverse osmosis membrane, Desalination, 95 (1994) 325-345.
[50] A.I. Catarino, M. Bauwens, P. Dubois, Acid–base balance and metabolic response of the sea urchin Paracentrotus lividus to different seawater pH and temperatures, Environmental Science and Pollution Research, 19 (2012) 2344-2353.
[51] S. Jiang, Z. Cao, Ultralow-fouling, functionalizable, and hydrolyzable zwitterionic materials and their derivatives for biological applications, Advanced Materials, 22 (2010) 920-932.

[52] M. Hirose, Trend of recent reverse osomosis membrane. Bulletin of the Society of Sea Water Science, Japan, 52 (1998) 86-91.
[53] The Chemical Society of Japan, Handbook of Chemistry: Pure Chemistry, 5th ed., Maruzen, Japan.
[54] N. Tawil, E. Sacher, E. Boulais, R. Mandeville, M. Meunier, X-ray photoelectron spectroscopic and transmission electron microscopic characterizations of bacteriophage–nanoparticle complexes for pathogen detection, The Journal of Physical Chemistry C, 117 (2013) 20656-20665.
[55] A. Chilkoti, B.D. Ratner, D. Briggs, Plasma-deposited polymeric films prepared from carbonyl-containing volatile precursors: XPS chemical derivatization and static SIMS surface characterization, Chemistry of Materials, 3 (1991) 51-61.
[56] L. Bereschenko, G. Heilig, M. Nederlof, M. Van Loosdrecht, A. Stams, G. Euverink, Molecular characterization of the bacterial communities in the different compartments of a full-scale reverse-osmosis water purification plant, Applied and Environmental Microbiology, 74 (2008) 5297-5304.
[57] R. Al-Shakhshir, F. Regnier, J.L. White, S.L. Hem, Effect of protein adsorption on the surface charge characteristics of aluminium-containing adjuvants, Vaccine, 12 (1994) 472-474.
[58] Y. Chang, S.-H. Shu, Y.-J. Shih, C.-W. Chu, R.-C. Ruaan, W.-Y. Chen, Hemocompatible mixed-charge copolymer brushes of pseudozwitterionic surfaces resistant to nonspecific plasma protein fouling, Langmuir, 26 (2009) 3522-3530.
[59] Y.-J. Shih, Y. Chang, Tunable blood compatibility of polysulfobetaine from controllable molecular-weight dependence of zwitterionic nonfouling nature in aqueous solution, Langmuir, 26 (2010) 17286-17294.
[60] A.U.H. Khan, Z. Khan, I.H. Aljundi, Improved hydrophilicity and anti-fouling properties of polyamide TFN membrane comprising carbide derived carbon, Desalination, 420 (2017) 125-135.
[61] L.-J. Zhu, L.-P. Zhu, J.-H. Jiang, Z. Yi, Y.-F. Zhao, B.-K. Zhu, Y.-Y. Xu, Hydrophilic and anti-fouling polyethersulfone ultrafiltration membranes with poly (2-hydroxyethyl methacrylate) grafted silica nanoparticles as additive, Journal of Membrane Science, 451 (2014) 157-168.
[62] L. Zou, I. Vidalis, D. Steele, A. Michelmore, S. Low, J. Verberk, Surface hydrophilic modification of RO membranes by plasma polymerization for low organic fouling, Journal of Membrane Science, 369 (2011) 420-428.
[63] W.W. Wilson, M.M. Wade, S.C. Holman, F.R. Champlin, Status of methods for assessing bacterial cell surface charge properties based on zeta potential measurements, Journal of Microbiological Methods, 43 (2001) 153-164.
[64] S. Mulyati, R. Takagi, A. Fujii, Y. Ohmukai, H. Matsuyama, Simultaneous improvement of the monovalent anion selectivity and antifouling properties of an anion exchange membrane in an

electrodialysis process, using polyelectrolyte multilayer deposition, Journal of Membrane Science, 431 (2013) 113-120.

Chapter 5

Antifouling polyamide reverse osmosis membranes with multi-defense properties by controllably constructing amphiphilic diblock copolymer brush layer

5.1. Introduction

Thin film composite (TFC) polyamide membranes represent state-of-the-art materials for reverse osmosis (RO), nanofiltration (NF), and forward osmosis (FO) applications [1-3]. Specifically, the TFC RO membranes contain a polyamide-selective layer interfacial polymerized on an underlying porous support, and they achieve higher level of both solute selectivity and water permeability [4-6]. However, membrane fouling of TFC polyamide RO (hereafter, cited as polyamide RO) membranes remains as a serious problem due to the relative intrinsic hydrophobicity of the polyamide layer, which could compromise the membrane water flux, increase the consumption of energy, and shorten the membrane life [7-9]. Consequently, significant efforts have been made to enhance membrane antifouling performance.

Surface modification with hydrophilic polymers such as poly[poly(ethyleneglycol)methacrylate] (pPEG), has been considered to control membrane fouling induced by organic foulants and microorganisms [10-12]. Zwitterionic polymers are novel antifouling materials that have been applied to increase the hydrophilicity of polyamide RO

membrane [13-16]. Unlike non-ionic pPEG, zwitterionic polymers have a balanced charge that forms a more stable and tighter hydration layer on the membrane surface via electrostatic interactions [17-19]. This hydration layer could potentially avoid close contact between the foulants and the membrane surface, and this so-called "fouling resistant" strategy may delay the occurrence of membrane fouling [13, 17, 20, 21]. Foulants attached onto modified membrane surfaces would do great damage to the antifouling hydration layer, while not always be completely removed by physical flushing under long-term operation, which would gradually deteriorate the membrane performance [22, 23]. In practice, chemical cleaning has been required to maintain the performance of fouled membranes. However, the chemical cleaning method not only increases the operational costs, but also reduces the membrane service lifespan [22, 23]. Therefore, the development of antifouling membranes with broader applicability is critical to energy-efficient and sustainable membrane processes.

Constructing amphiphilic surfaces, which contained both hydrophilic and low surface energy segments, was proposed to fabricate next generation antifouling membranes [24-28]. In addition to providing a simple "fouling resistant" strategy by using hydrophilic segments, amphiphilic surfaces could also take advantage of low surface energy segments to weaken the interfacial bonds. In other words, the deposited foulants would easily slip from the amphiphilic surfaces with weak hydraulic washing [29-31], which is referred to as a ''fouling release'' strategy. Under the guidance of this principle, a large number of ultrafiltration (UF) membranes with amphiphilic surfaces have already been successfully prepared. The optimal membranes often exhibit excellent antifouling properties, which will be attributed to the fouling release ability of polydimethylsiloxane (PDMS) or perfluoropolyether-based polymer segments, as well as the fouling resistant ability of hydrophilic polyethylene glycol (PEO)-based segments [26, 32, 33].

In this work, a controllable architecture of amphiphilic diblock copolymer on polyamide RO membranes was fabricated to integrate both "fouling resistant" and "fouling release" antifouling strategies. This work described sequentially grafting two materials on polyamide RO membrane surfaces via dual surface-initiated atom transfer radical polymerization (SI-ATRP): zwitterionic polymer, poly[2-(methacryloyloxy)ethyl-dimethyl-(3-sulfopropyl) ammonium hydroxide] (pMEDSAH) with strong hydrophilicity and poly(2,2,2-trifluoroethyl methacrylate) (pTFEMA) with low surface energy. To characterize the amphiphilic diblock copolymer modified membranes, contact angle, ζ-potential, X-ray photoelectron spectroscopy (XPS), and energy dispersive X-ray spectrometry (EDS) mapping were measured. The fouling resistant and fouling release properties of these modified membranes were extensively investigated by static bacterial adhesion and long-term dynamic filtration tests using sodium alginate for organic fouling, and bacterial suspension for biofouling.

5.2. Materials and methods

5.2.1. Materials

Commercial ES20 purchased from Nitto Denko (Osaka, Japan) was used as the pristine polyamide RO membrane. Membrane surface amination was accomplished using 3-aminopropyltrimethoxysilane (APTS; Tokyo Chemical Industry, Tokyo, Japan). α-Bromoisobutyryl bromide (BIBB; Sigma-Aldrich, St. Louis, MO, USA) was the initiator of the SI-ATRP reaction. Tris(2-pyridylmethyl)amine (TPMA; Wako Pure Chemical Industry, Osaka, Japan), ascorbic acid (Tokyo Chemical Industry), and copper (II) bromide ($CuBr_2$; Sigma-Aldrich) were used as a ligand, reducer, and catalyst of the SI-ATRP reaction, respectively. MEDSAH (EMD Millipore Co., Ltd., Germany) and TFEMA (stabilized with MEHQ, Tokyo Chemical Industry) were used as the monomers. Sodium alginate (Nacalai Tesque Inc., Kyoto, Japan) and

Sphingomonas paucimobilis NBRC 13935 (*S. paucimobilis* NBRC 13935; NITE Biological Resource Center, Chiba, Japan) were employed as the model foulants. Tryptic soy broth (TSB; Becton, Dickinson and Company, Franklin Lakes, NJ, USA) was used as a medium culture. SYTO9 (Life Technologies) was used to stain the bacteria and 25% glutaraldehyde solution (Wako Pure Chemical Industry) was used to fix the bacteria. Calcium chloride ($CaCl_2$) was bought from Wako Pure Chemical Industry. Milli-Q water (Merck Millipore, Darmstadt, Germany) was used for all solutions preparations.

5.2.2. Preparation of poly(MEDSAH-block-TFEMA)-grafted membranes

The membrane preparation process is illustrated in Fig. 5.1. A pristine RO membrane with diameter of 3.6 cm was immersed in a 20 mL 1 v/v% APTS aqueous solution for 10 min and then transferred into a 10 mL hexane solution containing 3 wt% BIBB for 1 min. The BIBB-immobilized membrane was stored in Milli-Q water for further modification.

MEDSAH solution (5 mmol) dissolved in a Milli-Q water: methanol mixture (1:1, 14.4 mL, v/v) was added into a 50-mL glass bottle with a BIBB-immobilized membrane. Then a 1.6 mL solution of 0.5 M ascorbic acid in methanol was injected into the bottle as well. After 10 min degassing by N_2, for initiating the SI-ATRP reaction, a 4 mL methanol solution containing $CuBr_2$ (5 mM) and TPMA (10 mM) was syringed into the bottle. This polymerization was undertaken for 10 min. Afterwards, the pMEDSAH-grafted membrane was thoroughly rinsed with Milli-Q water to remove the monomers that were unreacted, and then the membrane was stored in methanol for the next SI-ATRP reaction.

The pMEDSAH-grafted membrane was placed in a 50-mL glass containing a TFEMA solution (5 mmol) dissolved in pure methanol (14.4 mL) and a 1.6 mL solution of 0.5 M ascorbic acid in methanol. After 10 min of degassing by N_2, a 4 mL methanol solution containing $CuBr_2$

(5 mM) and TPMA (10 mM) was injected into the bottle and polymerized for 2 h. The p(MEDSAH)-*block*-p(TFEMA) (abbreviated as "p(MEDSAH-*b*-TFEMA)")-grafted membrane was rinsed with methanol and Milli-Q water and kept in Milli-Q water for further use. Herein, pMEDSAH- and p(MEDSAH-*b*-TFEMA)- grafted membranes are designated as hydrophilic RO membrane and amphiphilic RO membrane, respectively.

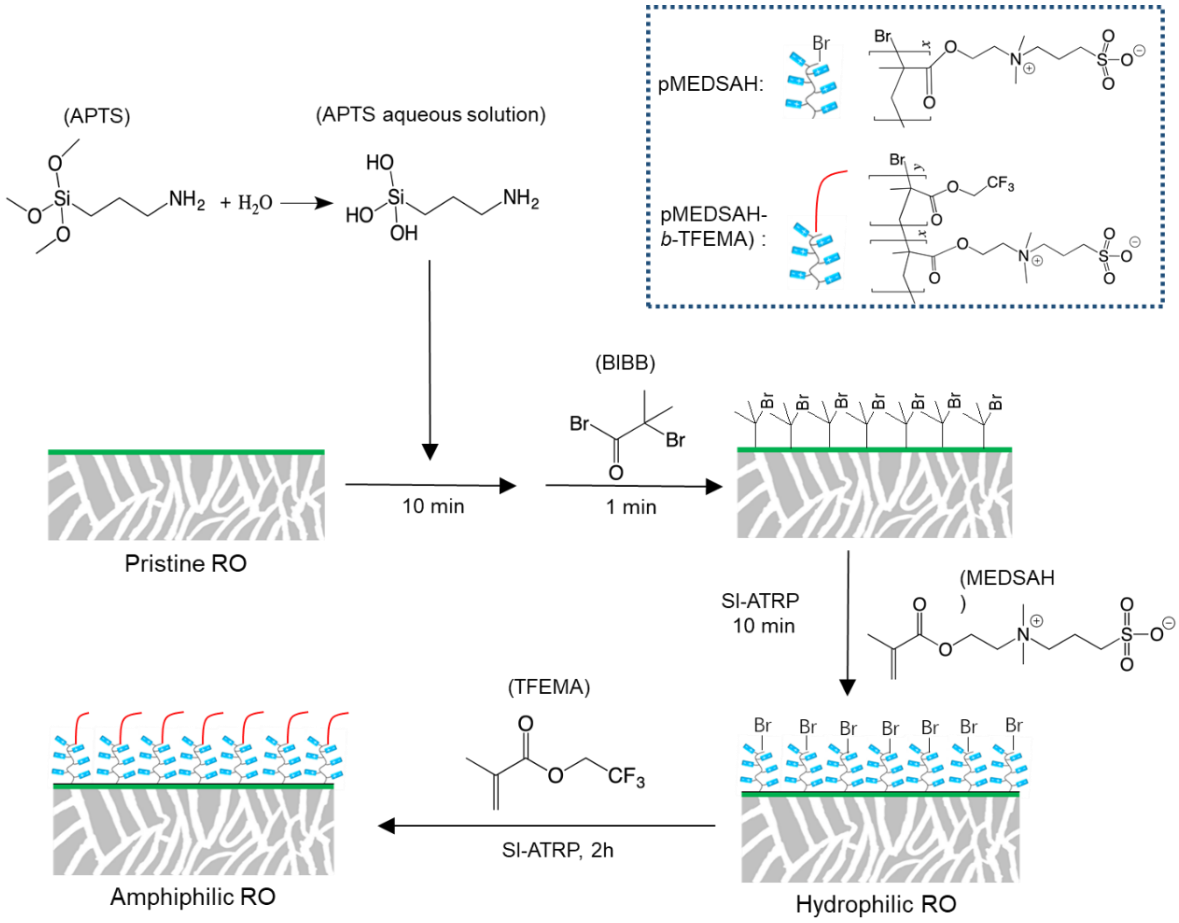

Fig. 5.1. Schematic illustration for the amphiphilic p(MEDSAH-*b*-TFEMA)-grafted membrane fabrication (i.e., amphiphilic RO membrane) via dual SI-ATRP.

5.2.3. Degree of grafting

Degree of grafting was investigated to evaluate the efficiency of the dual SI-ATRP reaction. Pristine 10.2 cm^2 RO membrane were modified with pMEDSAH and p(MEDSAH-*b*-TFEMA) as descripted in the section for the preparation of poly(MEDSAH-*block*-TFEMA)-grafted membranes in the manuscript. After that, the pristine RO, pMEDSAH-grafted, and p(MEDSAH-*b*-TFEMA)-grafted membranes were freeze-dried for 24 hours. Then the pristine RO and modified membranes were weighed and the degree of grafting was calculated using Eq. (1).

$$Degree\ \ of\ \ grafting = \frac{W_2 - W_1}{S} \quad (1)$$

where W_1 and W_2 are the weight of pristine RO and modified membranes, respectively. The value of W_1 was 0.97 mg, which is the average weight of five pristine RO membranes. S is the membrane area, which was 10.2 cm^2.

5.2.4. Membrane surface characterizations

Membrane surface hydrophilicity was assessed by the water contact angle measurement with a goniometer (DM-300, Kyowa Interface Science, Saitama, Japan). Surface charge of membranes was measured by the ζ-potential (SurPASSTM3, Anton Paar, Graz, Austria). Membrane surface composition was characterized by XPS (JPS-9010MC, JEOL) and each elemental content was analyzed using SpecSurf software in the analysis mode. The elemental distributions of carbon, oxygen, nitrogen, sulfur, and fluorine on the membrane surfaces were analyzed by EDS (JSF-7500, JEOL, Tokyo, Japan). Field emission scanning electron microscopy (FE-SEM; JSF-7500, JEOL) and atomic force microscopy (AFM; SPA-400, Hitachi High-Technologies, Tokyo, Japan) were employed to observe the membrane surface morphology and to quantify the surface roughness, respectively.

5.2.5. Static bacterial adhesion tests

Membrane antifouling properties were assessed via static bacterial adhesion tests by using gram-negative bacillus *S. paucimobilis* NBRC 13935 as the model bacteria. The experimental procedure was described in a previous study [15]. First, the bacteria was precultured in 20 mL 30 g/L TSB medium for 12 h at 30 ºC. A 0.4 mL precultured bacterial suspension was cultured again in a fresh 20 mL 30 g/L TSB medium for 4 h at 30 ºC, and was then adjusted to an optical density at 450 nm of 0.05. Second, a membrane sample (1 cm × 0.5 cm) was soaked in the 2 mL bacterial suspension. After shaking for 24 h at 30 ºC, the resultant membrane was rinsed twice with 0.85 wt% NaCl aqueous solution to remove nonadherent bacteria. The adhered bacteria on the membrane surface was stained with SYTO9 for 20 min and fixed with 2.5% glutaraldehyde for 3 min. Finally, the membrane was washed again by 0.85 wt% NaCl, and kept in a 0.85 wt% NaCl aqueous solution for confocal laser scanning microscopy (CLSM; FV1000D, Olympus, Tokyo, Japan) observation. All the CLSM images of membrane samples were taken at a magnification of 40 times under the Alexa Fluor® 488 mode. Bacterial coverage was quantified using ImageJ software (National Institutes of Health, Bethesda, MD, USA) from CLSM images.

5.2.6. Dynamic filtration tests

In dynamic filtration tests, a cross-flow filtration unit with 8.07 cm^2 of effective membrane area was employed to evaluate the antifouling properties of the amphiphilic membrane. Sodium alginate and bacteria (*S. paucimobilis* NBRC 13935) were selected as the model foulants.

The dynamic sodium alginate filtration was begun by feeding 50 mM of NaCl aqueous solution to adjust the initial flux (J_0) of each membrane to ~30 LMH (L/(m^2•h) under an applied

pressure of approximately 1.0 ~ 1.5 MPa. Next, a feed solution containing 100 ppm sodium alginate, 0.5 mM $CaCl_2$, and 50 mM NaCl was fed at 10 mL/min for 6 h to initiate fouling. Then, the fouled membrane was flushed with Milli-Q water at 10 mL/min for 1 h. The water flux of this cleaned membrane was measured again using 50 mM NaCl aqueous solution without foulants as the feed solution. The long-time stability of the membranes was assessed by performing three cycles of the above-mentioned fouling experiments. The flux recovery ratio (*FRR*) of each cycle was calculated as shown in Eq. (2).

$$FRR = \frac{J_n}{J_0} \times 100\% \quad (2)$$

where J_0 is the initial flux and J_n is the flux recovery after each fouling stage (n=1, 2, 3).

The experimental condition of the dynamic biofouling filtration tests using the bacterial suspension was analogous to that of the dynamic sodium alginate filtration tests except for the composition of the feed solution. To obtain the bacterial feed solution, a cultured bacterial suspension was prepared as described in the static bacterial adhesion test, and then it was added into the 50 mM NaCl aqueous solution until the bacterial feed solution was adjusted to an optical density at 450 nm of 0.05. Also, each cycle of biofouling experiment ran 20 h and the entire biofouling experiment was processed at 30 ºC. After the dynamic biofouling tests, the morphologies of biofilm on the resultant membrane surfaces were observed by SEM and the biofilm formation was quantified by CLSM.

5.2.7. Surface energy and Interaction energy

According to the three-liquid Lifshitz-van der Waals acid-base model (abbreviated as "three-liquid model"), surface energy ($\gamma_s{}^{total}$) at a surface is the sum of the apolar electrodynamic Lifshitz-van der Waals (LW) interaction ($\gamma_s{}^{LW}$) and the polar (Lewis) acid-base (AB) interaction

($\gamma_s{}^{AB}$). The former interaction involves the dispersion, orientation, and the induction interaction, while the latter interaction is designated as an electron-acceptor ($\gamma_s{}^{+}$) / electron-donor ($\gamma_s{}^{-}$) interaction, depending on the hydrogen-bonding number of a surface [34, 35]. Here, diiodomethane (apolar), water (polar), and glycerol (polar) were selected as the test liquids. The contact angles (θ) of the membrane samples in the test liquids were determined in order to calculate the surface energy ($\gamma_s{}^{total}$) as shown in Eqs. (3) and (4) [35].

$$\gamma_s{}^{total} = \gamma_s{}^{LW} + \gamma_s{}^{AB} = \gamma_s{}^{LW} + 2\sqrt{\gamma_s{}^{+}\gamma_s{}^{-}} \quad (3)$$

$$(1 + \cos\theta)\gamma_l{}^{total} = 2(\sqrt{\gamma_s{}^{LW}\gamma_l{}^{LW}} + \sqrt{\gamma_s{}^{+}\gamma_l{}^{-}} + \sqrt{\gamma_s{}^{-}\gamma_l{}^{+}}) \quad (4)$$

where $\gamma_s{}^{total}$ and $\gamma_l{}^{total}$ are the surface energy of the membrane surface and the test liquid, respectively; *LW* and *AB* are the components of apolar and polar interactions, respectively; $^{+}$ and $^{-}$ are the electron-acceptor and electron-donor components of polar interactions, respectively; and, θ is the contact angle of the membrane samples in the test liquids. The surface energy components ($\gamma_l{}^{total}$ $\gamma_l{}^{LW}$, $\gamma_l{}^{+}$ and $\gamma_l{}^{-}$) of the test liquids have been reported and are listed in Table 5.1 [36].

Table 5.1. Surface energy components (mJ/m^2) of various liquids.

Liquid	$\gamma_l{}^{LW}$	$\gamma_l{}^{+}$	$\gamma_l{}^{-}$	$\gamma_l{}^{AB}$	$\gamma_l{}^{total}$
diiodomethane	50.80	0.00	0.00	0.00	50.80
glycerol	34.00	3.92	57.40	30.00	64.00
water	21.80	25.50	25.50	51.00	72.80

Interaction energy between the foulant and the membrane surface was quantified to further understand the antifouling mechanism of the amphiphilic RO membrane [37]. Bacteria (*S. paucimobilis* NBRC 13935) was chosen as the studied foulant. Interaction energy (ΔG_{12}^{total}),

comprising LW (ΔG_{12}^{LW}) and AB (ΔG_{12}^{AB}) adhesion energies, was determined using Eqs. (5) - (7) [35].

$$\Delta G_{12}^{total} = \Delta G_{12}^{LW} + \Delta G_{12}^{AB} \quad (5)$$

$$\Delta G_{12}^{LW} = 2(\sqrt{\gamma_w{}^{LW}} - \sqrt{\gamma_2{}^{LW}})(\sqrt{\gamma_1{}^{LW}} - \sqrt{\gamma_w{}^{LW}}) \quad (6)$$

$$\Delta G_{12}^{AB} = 2[\sqrt{\gamma_w{}^{+}}(\sqrt{\gamma_1{}^{-}} + \sqrt{\gamma_2{}^{-}} - \sqrt{\gamma_w{}^{-}}) + \sqrt{\gamma_w{}^{-}}(\sqrt{\gamma_1{}^{+}} + \sqrt{\gamma_2{}^{+}} - \sqrt{\gamma_w{}^{+}}) - \sqrt{\gamma_1{}^{-}\gamma_2{}^{+}} - \sqrt{\gamma_1{}^{+}\gamma_2{}^{-}}] \quad (7)$$

where ΔG_{12}^{total} is the interaction energy between the membrane surface 1 (i.e. pristine RO, hydrophilic RO, and amphiphilic RO membranes) and the foulant 2 (i.e. bacteria-coated RO membranes), in the water *w*. To obtain the surface energy components of the bacteria (i.e. $\gamma_s{}^{LW}$, $\gamma_s{}^{+}$, and $\gamma_s{}^{-}$) for ΔG_{12}^{total} calculation, first, a bacterial aqueous solution with an optical density at 450 nm of 0.05 (the detailed preparation method can be found in the section titled "static bacterial adhesion tests") was fed to pristine RO membranes by dead-end cell filtration for 24 h. The contact angle (θ) of the fabricated bacteria-coated RO membrane was evaluated using water, glycerol, and diiodomethane, which could be used for calculating the surface energy components of the bacteria ($\gamma_s{}^{LW}$, $\gamma_s{}^{+}$, and $\gamma_s{}^{-}$) via Eqs. (3) and (4).

5.2.8. Hydration energy calculated using molecular dynamic simulation

Hydration energy of three given materials (i.e. polyamide, pMEDSAH, and p(MEDSAH-*b*-TFEMA)) was evaluated by molecular dynamic (MD) simulation. Through the Amorphous Cell module, three types of simulation models were built, and each model contained a given material and made up of 800 water molecules. All simulation models had similar atomic numbers and the density values were set at 1 g/cm^3 at the outset [38-40]. In the simulation models, polyamide and pMEDSAH were built with fine corresponding repeat units, respectively; while p(MEDSAH-*b*-TFEMA) model included fine MEDSAH repeat units and one TFEMA repeat units. First, the

energy of the simulation models was optimized via a geometry optimization step. Then, molecular structures under an equilibrium state were adopted to simulate the water-materials interactions in an MD process with an NVT ensemble (fixed temperature, system volume, and atom number) at 298 K for 500-ps. In this work, the BIOVIA Materials Studio® software was employed to carry out the energy minimization and MD calculation processes, in which a COMPASS force field was applied.

5.3. Results and discussion

5.3.1. Membrane characterizations

The aim of this study was to construct a polyamide RO membrane with both fouling resistance and fouling release properties by sequentially grafting a zwitterionic polymer (pMEDSAH, first-stage SI-ATRP) and a low surface energy polymer (pTFEMA, second-stage SI-ATRP) on a polyamide layer. The degrees of grafting for the pristine RO, hydrophilic RO, and amphiphilic RO membranes are presented in Fig. 5.2, and were 0, 0.10, 0.17 mg/cm^2, respectively. Therefore, the degree of grafting for the pMEDSAH and pTFEMA brushes in the p(MEDSAH-*b*-TFEMA) could be quantified at 0.10 and 0.07 mg/cm^2, respectively. The resultant modified membranes were comprehensively characterized to confirm the grafting of the amphiphilic diblock copolymer on the polyamide layer and to verify the corresponding surface characteristics for antifouling.

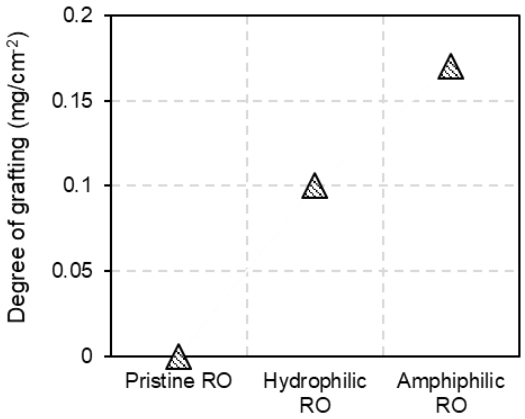

Fig.5.2. Degree of grafting for pristine RO, hydrophilic RO, and amphiphilic RO membranes.

Water contact angles is an evaluation of the membrane surface hydrophilicity. A lower water contact angle equates to a higher level of surface hydrophilicity. As shown in Fig. 5.3A, after grafting zwitterionic pMEDSAH brushes, the water contact angle of the hydrophilic RO membrane decreased from 37º to 14º, which could be attributed to the strong hydrating capability of pMEDSAH. Compared with the pMEDSAH-grafted membrane, the p(MEDSAH-*b*-TFEMA)-grafted membrane (i.e. amphiphilic RO membrane) has a slightly increased water contact angle of 23º due to the grafting of hydrophobic pTFEMA brushes. These changes on water contact angle exhibited the amphiphilic characteristic of p(MEDSAH-*b*-TFEMA)-grafted membrane.

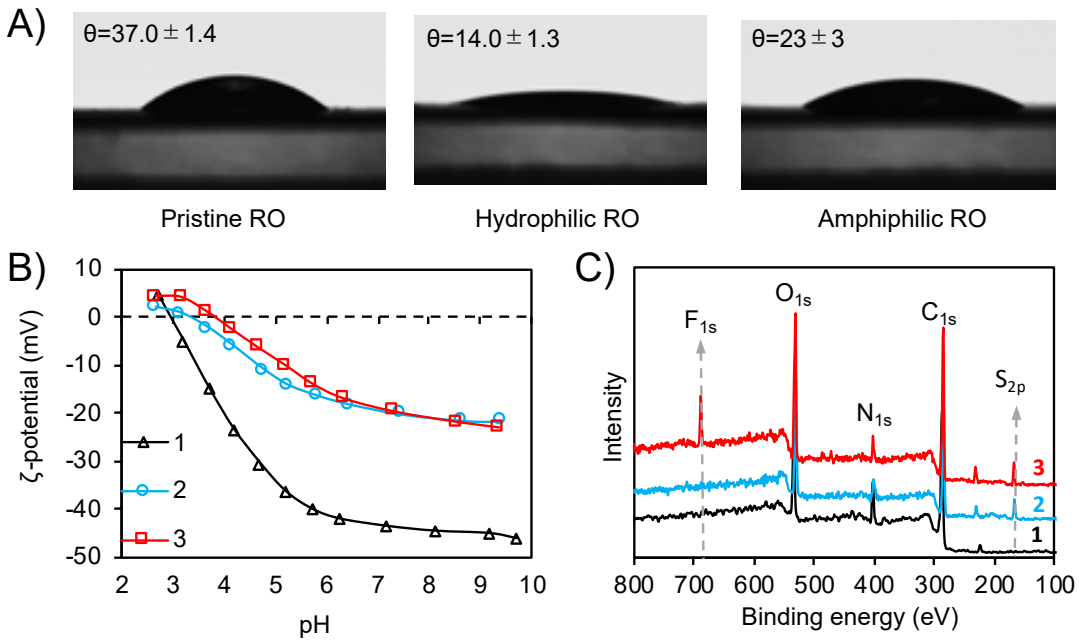

Fig. 5.3. Key membrane characteristics: Water contact angle (A), ζ-potential (B), and XPS spectra (C) of pristine RO (1), hydrophilic RO (2), and amphiphilic RO (3) membranes.

Membrane surface charge was further studied by the ζ-potential measurement. The ζ-potential data and isoelectrical point (IEP) of pristine RO, hydrophilic RO, and amphiphilic RO membranes are displayed in Fig. 5.3B and in Table 5.2, respectively. In Fig. 5.3B, the pristine RO membrane shows a negative charge at pH values ranging from 3 to 9 with an IEP at pH 2.8. After pMEDSAH grafting, the IEP was shifted to the right at pH 3.2, and the surface charge became less negative within the entire pH range, probably because the grafted neutral pMEDSAH brushes would have shielded the anionic carboxyl group on the polyamide layer surface. The ζ-potential of the amphiphilic RO membrane presented a trend similar to that of the hydrophilic RO membrane.

Table 5.2. Elemental composition and isoelectrical point (IEP) of pristine RO, hydrophilic RO, and amphiphilic RO membranes.

Membranes	Elemental composition (%)					IEP (pH)
	C_{1s}	N_{1s}	O_{1s}	S_{2p}	F_{1s}	
Pristine RO	77.3	10.0	12.6	/	/	2.8
Hydrophilic RO	64.7	5.3	24.2	5.8	/	3.2
Amphiphilic RO	60.3	5.0	23.9	6.8	4.1	3.7

Chemical composition of the membrane surfaces was analyzed by XPS technology. The XPS spectra of pristine RO hydrophilic RO, and amphiphilic RO membranes are displayed in Fig. 5.3C and the elemental percentages obtained from XPS spectra are shown in Table 5.2. The pristine RO membrane mainly consisted of carbon (C_{1s}, 77.3%), nitrogen (N_{1s}, 10%), and oxygen (O_{1s}, 12.6%), which were responsible for the binding energy at 280 eV, 400 eV, and 530 eV, respectively. After the grafting of pMEDSAH, a new peak at 169 eV attributed to the sulfur element (S_{2p}) appeared, which was assigned to the pMEDSAH brushes on hydrophilic RO membrane. In the spectra of the amphiphilic RO membrane, two peaks associated with sulfur (S_{2p}) and fluorine (F_{1s}) elements were observed, and their atomic percentages were 6.8% and 4.1%, respectively, which verified the successful surface modification with the amphiphilic diblock copolymer, p(MEDSAH-*b*-TFEMA). The distributions of sulfur (S) and fluorine (F) elements on the membrane surfaces were visualized by EDS mapping, and the images are displayed in Fig. 5.4. Compared with the pristine RO membrane, the S element (blue color in Fig. 5.4B) appeared on the surface of the hydrophilic RO membrane because of the grafting of pMEDSAH brushes. On the other hand, the entire amphiphilic RO membranes surface was uniformly covered with not only the S element (blue color in Fig. 5.4C) but also the F element (red color in Fig. 5.4F), which demonstrates a homogenous distribution of pMEDSAH segments and pTFEMA segments of p(MEDSAH-*b*-TFEMA) brushes on the surface of the modified membrane. Besides, the homogeneous distribution of S and F elements on the amphiphilic RO membrane surface further

indicates that the construction of p(MEDSAH-*b*-TFEMA) brush layers on the membrane surface was controllable via dual SI-ATRP reaction.

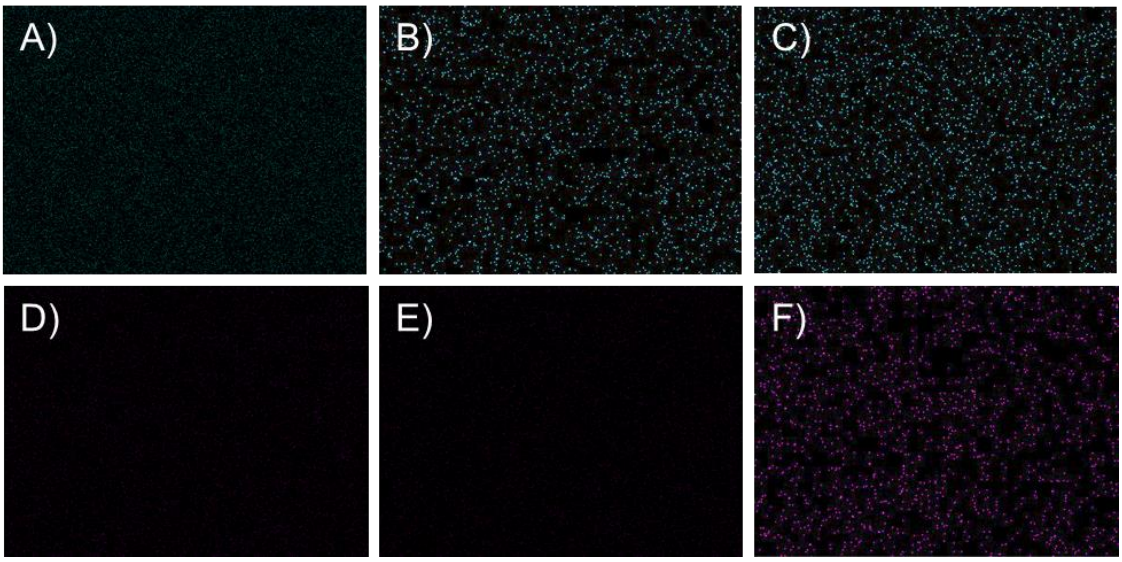

Fig. 5.4. Sulfur (S) and fluorine (F) elemental distributions on the surfaces of pristine RO (A and D), hydrophilic RO (B and E), and amphiphilic RO (C and F) membranes, respectively. **Note**: the blue and red colored areas represent the relevant S and F elements, respectively.

Effects of modification with p(MEDSAH-*b*-TFEMA) brushes on the membrane surface morphologies were also investigated, and the results are presented in Fig. 5.5. The polyamide layer of the pristine RO membrane possesses a typical ridge-and-valley structure (Fig. 5.5 A). After surface functionalization with pMEDSAH and p(MEDSAH-*b*-TFEMA) brushes, similar surface morphology to the pristine membrane surface can be observed in the SEM images (Figures 5.5B and 5.5C), AFM results also demonstrated almost no change in the surface roughness (Figure 5.5(D)-(F) and Table 5.3) after surface modifications (e.g. R_a=82.5, 80.4 and 79.0 nm for pristine RO, hydrophilic RO, and amphiphilic RO membranes, respectively).

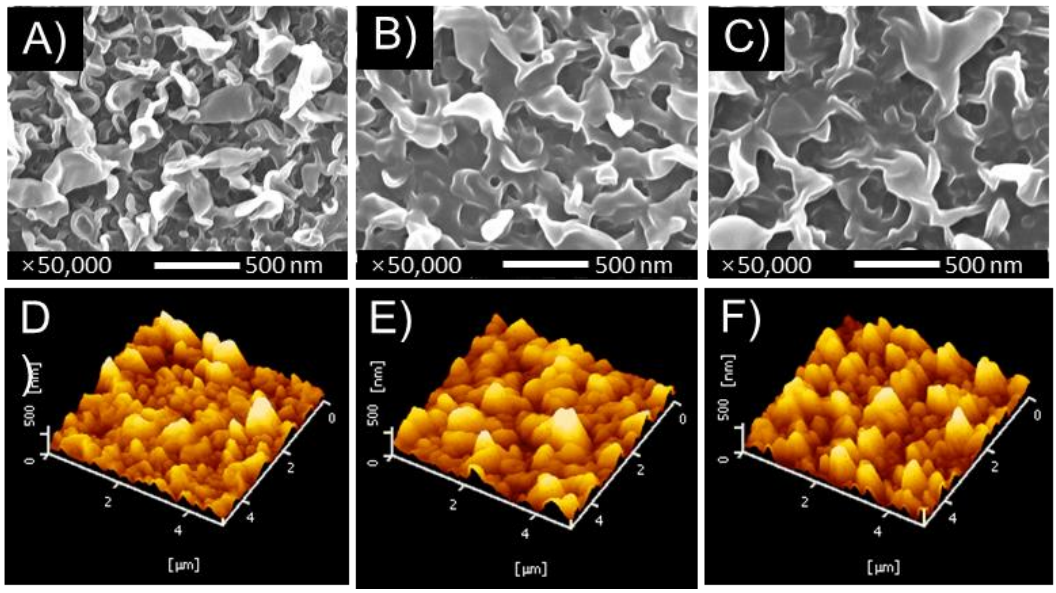

Fig. 5.5. Surface morphologies of pristine RO (A and D), hydrophilic RO (B and E), and amphiphilic RO (C and F) membranes, as observed by SEM (A-C) and AFM (D-F), respectively.

Table 5.3. Surface roughness of pristine RO, hydrophilic RO, and amphiphilic RO membranes.

Membranes	Surface roughness		
	Ra (nm)	RMS (nm)	Rz (nm)
Pristine RO	82.5	101.6	290.2
Hydrophilic RO	80.4	100.4	249.2
Amphiphilic RO	79.0	99.2	296.7

5.3.2. Bacterial adhesion tests

Membrane antifouling capabilities were studied by static tests using bacteria as the model foulant (Fig. 5.6). After exposure to the bacterial solution for 24 h, the pristine RO membrane had the largest green area (Fig. 5.6A), indicating largest amount of adhered bacteria. The adhesion of bacteria onto the pristine RO membrane was employed as a control to normalize those of modified membranes. By contrast, the hydrophilic RO membrane exhibited a smaller green area (Fig. 5.6B), which demonstrated significantly suppressed bacterial adsorption due to the strong hydration of

the pMEDSAH brushes. The relative bacterial coverage for the amphiphilic RO membrane (4%) was lower than that of the hydrophilic RO membrane (9%) (Fig. 5.6D). This difference will be ascribed to the low surface energy segments (i.e. pTFEMA) of the p(MEDSAH-*b*-TFEMA) brushes, which could weaken the interaction between the membrane surface and the foulant.

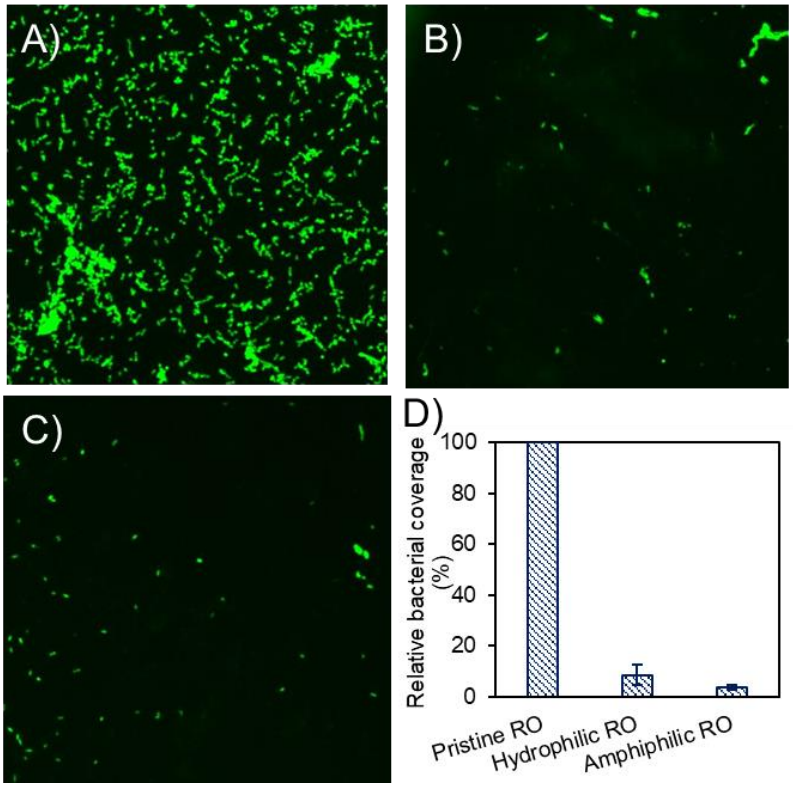

Fig. 5.6. Static bacterial adhesion results of pristine RO (A), hydrophilic RO (B), and amphiphilic RO (C) membranes. Relative coverage of bacteria (D) adhered onto the surfaces of pristine and modified membranes. The adhesion of bacteria on each membrane sample was normalized by that of the pristine RO membrane.

5.3.3. Antifouling performances in the RO process

Biofouling is triggered by an initial bacterial adhesion and the subsequent biofilm formation, which causes water flux decline, higher energy consumption, and limited life span of the RO

membrane [41-44]. Therefore, biofouling mitigation on the membrane surface is critical for effective antifouling functionality. Herein, dynamic biofouling filtration tests were performed by using the bacterial solution to assess the anti-biofouling properties of membranes. The obtained data are presented in Figures 5.7(A and C). In these figures, the flux is normalized by using the initial water flux. During the dynamic biofouling filtration, the water flux recovery performance of fouled membranes was evaluated with *FRR* by physical cleaning (rinsing) with Milli-Q water at the end of each fouling cycle.

As shown in Fig. 5.7A, the pristine RO membrane recorded the sharpest flux declines to 51%, 37%, and 28% of its initial permeate for the three cycles, respectively, due to the relative hydrophobic surface. By contrast, the hydrophilic RO membrane exhibited milder flux declines to 58% and 45% for the first two cycles, respectively, which verified the effective antifouling properties of hydrophilic modification. Unfortunately, the water flux of the hydrophilic RO membrane continued to decline and displayed 31% of its initial water flux at the end of the 3rd cycle, which was comparable with that of the pristine RO membrane. As the results show, the antifouling properties of hydrophilic membranes could gradually lose due to the defective hydration layer induced by the attached foulants on the membrane surfaces. These phenomena also occurred in previous studies [45]. By contrast, the amphiphilic RO membrane demonstrated the excellent antifouling properties against bacteria, and had the lowest water flux declines (72%, 57%, and 49% of initial water flux for the three cycles, respectively) than those of the other two membranes. These enhanced antifouling properties were attributed not only to the fouling resistant properties of the pMEDSAH segments, but also to the fouling release properties of the pTFEMA segments. The hydrophilic pMEDSAH segments could prevent contact between the foulants and the membrane surface by forming a strong hydrating layer via electrostatic interaction [46]. At the same time, the pTFEMA segments with low surface energy could loosen

the interaction between foulants and membrane surfaces, leading to a higher release rate of foulants from the membrane surface [47]. Therefore, during the dynamic filtration on cross flow mode, the fouling resistant properties significantly prevent water flux decline. In addition, the fouling release properties make the foulant attachment unstable, further eliminating the water flux decline and enhancing water flux recovery.

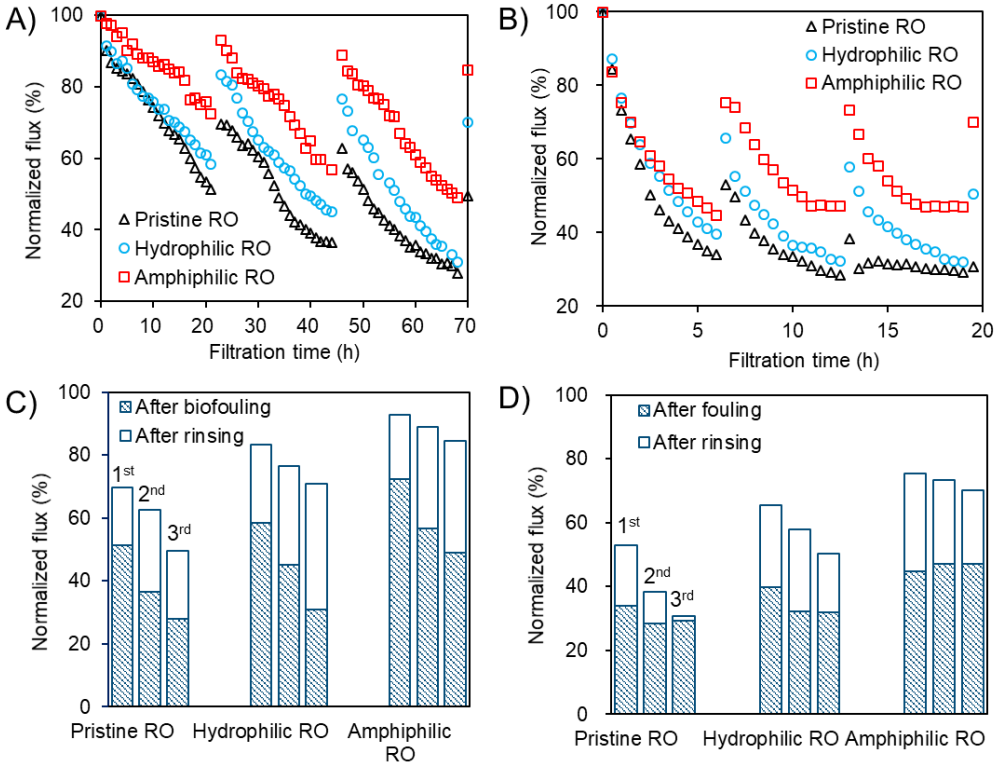

Fig. 5.7. Representative normalized flux of pristine RO hydrophilic RO, and amphiphilic RO membranes as a function of filtration time during (A) biofouling and (B) sodium alginate filtrations; Normalized flux of pristine RO, hydrophilic RO, and amphiphilic RO membranes after each of the (C) biofouling and (D) sodium alginate stages.

The antifouling properties of the modified membranes against an organic foulant (i.e. sodium alginate) in a dynamic mode were further evaluated. The corresponding dynamic fouling curves

are shown in Fig. 5.7B. Compared to the biofouling, alginate fouling led to severer water flux decline. That is because the presence of Ca^{2+} in the sodium alginate solution acts as a bridge between sodium alginate molecules and results in a cross-linked alginate-gel on the membrane surface [48, 49]. At the end of the 3rd cycle of filtration, the pristine RO and hydrophilic RO membranes had a comparable water flux decline to 30%, which was the highest decline among all the tested membranes, because of the hydraulic resistance of the alginate-gel formation on the membrane surface. Nevertheless, the amphiphilic RO membrane maintained a mild water flux decline to 47%. These results were further verified by the photo images of the fouled membranes after the 3rd cycle of filtration. As shown in Fig. 5.8, both the pristine RO and hydrophilic RO membranes were fully covered by a thicker sodium alginate gel, but only a limited sodium alginate gel layer was formed on the amphiphilic RO membrane. These results also indicate that the surface of the amphiphilic RO membrane is likely to have some non-cohesive dominants with sodium alginate releasing ability, which may be a result of the relatively weak interaction between sodium alginate molecules and low surface free energy dominants (i.e. pTFEMA segments).

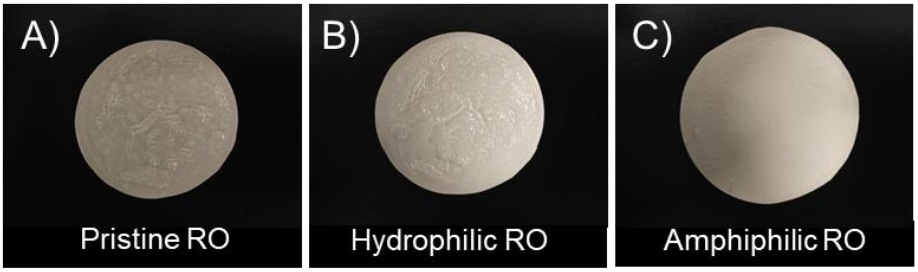

Fig. 5.8. Membrane surface morphology of pristine RO, hydrophilic RO, and amphiphilic RO membranes after a 3rd cycle of sodium alginate fouling filtration.

The aforementioned synergetic antifouling properties can be further verified by the obvious distinctions in the physical cleaning efficiencies between pristine and modified RO membranes.

As shown in Figures 5.7C and 5.7D, the cleaning efficiencies for these three membranes trended as follows: pristine RO membrane < hydrophilic RO membrane < amphiphilic RO membrane. Although the hydrophilic RO membrane was relatively more efficient at cleaning compared with the pristine RO membrane, irreversible fouling remained obvious and the recovered water flux after cleaning was about 30% of the initial water flux after three cycles of filtration (Figures 5.7C and 5.7D). That result suggests that a zwitterionic polymer cannot maintain its antifouling properties for prolonged periods of operation time. By contrast, because of the synergetic effects of fouling resistant and fouling release properties, the water flux of amphiphilic RO membranes could be satisfactorily recovered after simple physical cleaning as shown in Figures 5.7C and 5.7D. These antifouling properties were further confirmed by SEM and CLSM images of the cleaned membranes after the 3rd cycle of biofouling filtration. Figure 5.8 shows that the cleaned pristine RO membrane was fully covered by biofilm with a biomass of 48 $\mu m^3/\mu m^2$ and a thickness of 74 μm. On the cleaned hydrophilic RO membrane surface, a significant amount of biofilm could still be observed with a biomass of 34 $\mu m^3/\mu m^2$ and a thickness of 55 μm. However, almost no biofilm nor bacteria aggregation appeared on the cleaned amphiphilic RO membrane with the lowest biomass of 24 $\mu m^3/\mu m^2$ and thickness of 36 μm. In short, integrating fouling resistant and fouling release strategies against fouling provides a versatile solution for designing novel antifouling membranes.

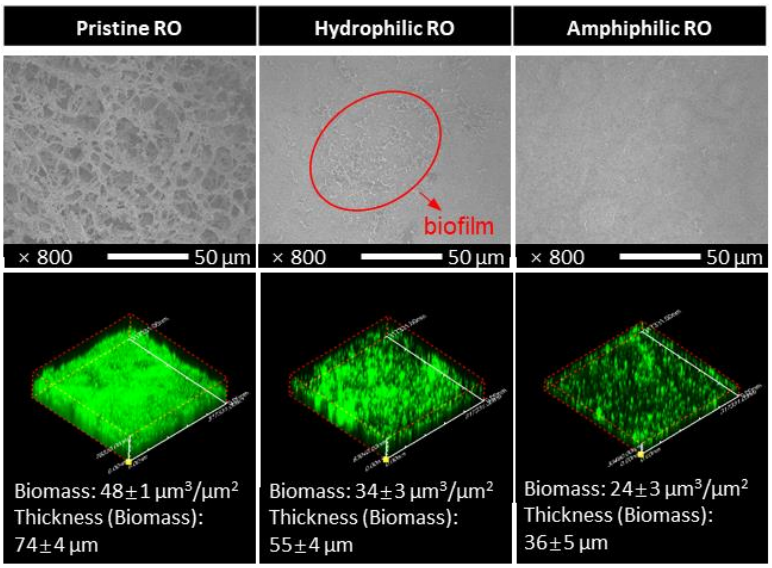

Fig. 5.8. Surface morphologies of the cleaned pristine RO, hydrophilic RO, and amphiphilic RO membranes were observed by SEM and CLSM. The biomass and biomass thicknesses were analyzed using ImageJ software from CLSM images.

5.3.4. Proposed multi-defense mechanism for antifouling

Hydration energy and surface energy of membrane surfaces could be manipulated by sequentially constructing the pMEDSAH and pTFEMA segments via dual SI-ATRP, and thus provided the multi-defense properties. Lower level of both hydration energy and surface energy are favorable, which implies a tighter hydration layer and a weaker intermolecular force between surfaces and foulants, respectively. Table 5.5 presents the surface energy (γ_s^{total}, mJ/m^2) as determined by the three-liquid model using the measured intrinsic liquid (diiodomethane, glycerol, and water) contact angles (Table 5.4). Table 5.6 summarizes the hydrogen (H)-bond number and hydration energy (ΔG_H, kcal/mol) between the given materials and water molecules calculated from the MD simulation. Lower hydration energy corresponds to higher H-bond number, meaning stronger hydration of the material. As illustrated in Table 5.6, the strong hydrophilicity of pMEDSAH segments imparted a lower hydration energy of -3707 kJ/mol compared with that of

the polyamide (-1197 kJ/mol) to the modified membrane surfaces. It indicated that a tighter hydration layer was formed on the surface of hydrophilic RO membrane, avoiding nonspecific foulant adsorption and effectively enhancing the fouling resistant properties. However, modification with pMEDSAH segments increased the surface energy from 59.6 mJ/m^2 of the pristine RO membrane to 65.8 mJ/m^2 of the hydrophilic RO membrane (Table 5.5). This meant once the foulant broken the hydration layer and touched the membrane surface, the adhered foulants were difficult to be removed from the hydrophilic membrane surfaces. On the other hand, the surface energy of the amphiphilic RO membrane was substantially decreased with pTFEMA segments to 55.4 mJ/m^2, which were lower than that of the hydrophilic RO membrane (65.8 mJ/m^2); while this amphiphilic RO membrane still maintained a much lower hydration energy (-2674 kJ/mol) than that of the pristine RO membrane (-1197 kJ/mol). Besides the strong hydration capacity of pMEDSAH segments, tightly binding electron pairs surrounding $-CF_3$ groups could supply a low surface energy layer barrier, which would prevent the dispersion interactions between the foulants and the membrane surfaces and avoid the damage of antifouling hydration layer due to foulants. The rational construction of pMEDSAH and pTFEMA segments could confer both fouling resistant and the fouling release properties to the membrane surfaces.

Table 5.4. Contact angle, θ, of pristine RO, hydrophilic RO, amphiphilic RO, and bacteria-coated RO membranes in three liquids including water, glycerol, and diiodomethane.

Surfaces	Contact angle θ (°)		
	Water	Glycerol	Diiodomethane
Pristine RO	37.0	33.6	9.3
Hydrophilic RO	14.0	10.9	14.9
Amphiphilic RO	23.0	33.8	33.0
Bacteria-coated RO	68.0	44.1	63.0

Table 5.5. Surface energy (mJ/m^2) components of pristine RO, hydrophilic RO, amphiphilic RO, and bacteria-coated RO membranes calculated from the three-liquid model.

	Pristine RO	Hydrophilic RO	Amphiphilic RO	Bacteria-coated RO
γ_s^{LW}	50.1	49.1	42.9	26.8
γ_s^+	0.7	1.7	0.8	6.8
γ_s^-	31.0	41.3	48.9	6.3
γ_s^{AB}	9.5	16.7	12.4	13.1
γ_s^{total}	59.6	65.8	55.4	39.9

Table 5.6. Hydrogen (H)-bond number and hydration energy (kJ/mol) of polyamide, pMEDSAH, and p(MEDSAH-*b*-TFEMA) calculated from molecular dynamics simulation.

	Polyamide	pMEDSAH	p(MEDSAH-*b*-TFEMA)
H-bound Number	23	43	30
Hydration Energy, ΔG_H	-1197	-3707	-2674

The initial fouling mechanism was governed by the membrane-foulant interactions [45, 50]. Therefore, a better understanding of the antifouling abilities via quantitative analysis of the membrane-foulant interactions becomes very critical. Table 5.7 lists the interaction energies ($\triangle G^{total}$, mJ/m^2) between the bacteria and the membrane surfaces, which were calculated using the surface energy components of the membrane surface (Table 5.5) and the bacteria (bacteria-coated RO in Table 5.5). If $\triangle G^{total}$ becomes more negative, the foulant is prone to approaching the membrane surface [51]. Among three membranes, the pristine RO membrane showed the highest negative interaction energy of -21.3 mJ/m^2, leading to the most serious membrane fouling. After the modification with pMEDSAH brushes, the interaction energy became less negative (-

14.8 mJ/m^2) owing to the strong hydration layer, which indicated better antifouling properties against bacteria. Moreover, subsequently grafted pTFEMA segments further reduced the interaction energy to -13.6 mJ/m^2 on the basis of the pMEDSAH-modified membrane. This difference between hydrophilic RO and amphiphilic RO membranes was attributed to the low surface energy layer created by the pTFEMA segments. Indeed, this tendency for interaction energy between the bacteria and the membranes matched well with the dynamic fouling performance (Fig. 5.7), which suggests that the multi-defense mechanisms, i.e., the fouling resistant properties as well as the fouling release properties, were responsible for the improved antifouling abilities.

Table 5.7. Interaction energy (mJ/m^2) between membrane surfaces and bacteria calculated from Eqs. (4)-(6).

	Pristine RO	Hydrophilic RO	Amphiphilic RO
ΔG^{LW}	-2.5	-2.4	-1.9
ΔG^{AB}	-18.9	-12.4	-11.7
ΔG^{total}	-21.3	-14.8	-13.6

5.4. Conclusion

A controllable architecture of amphiphilic diblock copolymer was well constructed for the polyamide RO membranes to integrate both “fouling resistance” and “fouling release” properties. To prepare this amphiphilic RO membrane, a hydrophilic segment of pMEDSAH and a low surface energy segment of pTFEMA were sequentially grafted on a membrane surface by dual SI-ATRP reaction. On the one hand, the resultant amphiphilic RO membrane effectively resisted the foulants of the sodium alginate and bacteria, because the strong hydrophilicity of pMEDSAH segments imparted the modified membrane surfaces with a lower hydration energy, which thereby

facilitated the formation of a tighter hydration layer to avoid nonspecific foulant adsorption on membrane surfaces. On the other hand, because the pTFEMA segment could decrease the surface energy and weaken the interaction between the foulant and the membrane surface, the amphiphilic RO membranes not only further eliminate the water flux decline during dynamic fouling filtration compared with the hydrophilic TFC membrane, but also could be satisfactorily recovered the water flux after simple physical cleaning. Therefore, the rational construction of pMEDSAH and pTFEMA segments could confer both fouling resistant and the fouling release properties to the membrane surfaces, providing a versatile solution for designing novel antifouling membranes.

References

[1] R.J. Petersen, Composite reverse osmosis and nanofiltration membranes, Journal of Membrane Science, 83 (1993) 81-150.
[2] N.Y. Yip, A. Tiraferri, W.A. Phillip, J.D. Schiffman, M. Elimelech, High performance thin-film composite forward osmosis membrane, Environmental Science & Technology, 44 (2010) 3812-3818.
[3] Z. Jiang, S. Karan, A.G. Livingston, Water transport through ultrathin polyamide nanofilms used for reverse osmosis, Advanced Materials, 30 (2018) 1705973.
[4] W. Lau, A. Ismail, N. Misdan, M. Kassim, A recent progress in thin film composite membrane: a review, Desalination, 287 (2012) 190-199.
[5] A. Ismail, M. Padaki, N. Hilal, T. Matsuura, W. Lau, Thin film composite membrane—Recent development and future potential, Desalination, 356 (2015) 140-148.
[6] J.-E. Gu, B.-M. Jun, Y.-N. Kwon, Effect of chlorination condition and permeability of chlorine species on the chlorination of a polyamide membrane, Water Research, 46 (2012) 5389-5400.
[7] G.-d. Kang, Y.-m. Cao, Development of antifouling reverse osmosis membranes for water treatment: a review, Water Research, 46 (2012) 584-600.
[8] X. Zhu, M. Elimelech, Colloidal fouling of reverse osmosis membranes: measurements and fouling mechanisms, Environmental Science & Technology, 31 (1997) 3654-3662.
[9] T.-V. Nguyen, M.M. Pendergast, M.T. Phong, X. Jin, F. Peng, M.L. Lind, E.M. Hoek, Relating fouling behavior and cake layer formation of alginic acid to the physiochemical

properties of thin film composite and nanocomposite seawater RO membranes, Desalination, 338 (2014) 1-9.
[10] F.-Q. Nie, Z.-K. Xu, X.-J. Huang, P. Ye, J. Wu, Acrylonitrile-based copolymer membranes containing reactive groups: surface modification by the immobilization of poly (ethylene glycol) for improving antifouling property and biocompatibility, Langmuir, 19 (2003) 9889-9895.
[11] C. Yang, X. Ding, R.J. Ono, H. Lee, L.Y. Hsu, Y.W. Tong, J. Hedrick, Y.Y. Yang, Brush-like polycarbonates containing dopamine, cations, and PEG providing a broad-spectrum, antibacterial, and antifouling surface via one-step coating, Advanced Materials, 26 (2014) 7346-7351.
[12] Z. Zhou, S. Rajabzadeh, A.R. Shaikh, Y. Kakihana, W. Ma, H. Matsuyama, Effect of surface properties on antifouling performance of poly (vinyl chloride-co-poly (ethylene glycol) methyl ether methacrylate)/PVC blend membrane, Journal of Membrane Science, 514 (2016) 537-546.
[13] L.-F. Fang, S. Jeon, Y. Kakihana, J.-i. Kakehi, B.-K. Zhu, H. Matsuyama, S. Zhao, Improved antifouling properties of polyvinyl chloride blend membranes by novel phosphate based-zwitterionic polymer additive, Journal of Membrane Science, 528 (2017) 326-335.
[14] D. Saeki, T. Tanimoto, H. Matsuyama, Anti-biofouling of polyamide reverse osmosis membranes using phosphorylcholine polymer grafted by surface-initiated atom transfer radical polymerization, Desalination, 350 (2014) 21-27.
[15] Z. Yang, D. Saeki, H. Matsuyama, Zwitterionic polymer modification of polyamide reverse-osmosis membranes via surface amination and atom transfer radical polymerization for anti-biofouling, Journal of Membrane Science, 550 (2018) 332-339.
[16] X. Zhang, J. Tian, S. Gao, W. Shi, Z. Zhang, F. Cui, S. Zhang, S. Guo, X. Yang, H. Xie, Surface functionalization of TFC FO membranes with zwitterionic polymers: Improvement of antifouling and salt-responsive cleaning properties, Journal of Membrane Science, 544 (2017) 368-377.
[17] S. Chen, J. Zheng, L. Li, S. Jiang, Strong resistance of phosphorylcholine self-assembled monolayers to protein adsorption: insights into nonfouling properties of zwitterionic materials, Journal of the American Chemical Society, 127 (2005) 14473-14478.
[18] C.J. Huang, N.D. Brault, Y. Li, Q. Yu, S. Jiang, Controlled Hierarchical Architecture in Surface-initiated Zwitterionic Polymer Brushes with Structurally Regulated Functionalities, Advanced Materials, 24 (2012) 1834-1837.
[19] R. Quintana, M. Gosa, D. Ja czewski, E. Kutnyanszky, G.J. Vancso, Enhanced stability of low fouling zwitterionic polymer brushes in seawater with diblock architecture, Langmuir, 29 (2013) 10859-10867.
[20] Q. Shao, S. Jiang, Molecular understanding and design of zwitterionic materials, Advanced Materials, 27 (2015) 15-26.

[21] S. Chen, L. Li, C. Zhao, J. Zheng, Surface hydration: Principles and applications toward low-fouling/nonfouling biomaterials, Polymer, 51 (2010) 5283-5293.
[22] X. Zhang, S. Gao, J. Tian, S. Shan, R. Takagi, F. Cui, L. Bai, H. Matsuyama, Investigation of Cleaning Strategies for an Antifouling Thin-Film Composite Forward Osmosis Membrane for Treatment of Polymer-Flooding Produced Water, Industrial & Engineering Chemistry Research, 58 (2019) 994-1003.
[23] X. Li, T. Cai, G.L. Amy, T.-S. Chung, Cleaning strategies and membrane flux recovery on anti-fouling membranes for pressure retarded osmosis, Journal of Membrane Science, 522 (2017) 116-123.
[24] W. Chen, Y. Su, J. Peng, X. Zhao, Z. Jiang, Y. Dong, Y. Zhang, Y. Liang, J. Liu, Efficient wastewater treatment by membranes through constructing tunable antifouling membrane surfaces, Environmental Science & Technology, 45 (2011) 6545-6552.
[25] W. Chen, Y. Su, J. Peng, Y. Dong, X. Zhao, Z. Jiang, Engineering a robust, versatile amphiphilic membrane surface through forced surface segregation for ultralow flux-decline, Advanced Functional Materials, 21 (2011) 191-198.
[26] A. Asatekin, S. Kang, M. Elimelech, A.M. Mayes, Anti-fouling ultrafiltration membranes containing polyacrylonitrile-graft-poly (ethylene oxide) comb copolymer additives, Journal of Membrane Science, 298 (2007) 136-146.
[27] S. Kang, A. Asatekin, A.M. Mayes, M. Elimelech, Protein antifouling mechanisms of PAN UF membranes incorporating PAN-g-PEO additive, Journal of Membrane Science, 296 (2007) 42-50.
[28] W. Ma, S. Rajabzadeh, A.R. Shaikh, Y. Kakihana, Y. Sun, H. Matsuyama, Effect of type of poly (ethylene glycol)(PEG) based amphiphilic copolymer on antifouling properties of copolymer/poly (vinylidene fluoride)(PVDF) blend membranes, Journal of Membrane Science, 514 (2016) 429-439.
[29] R.F. Brady Jr, I.L. Singer, Mechanical factors favoring release from fouling release coatings, Biofouling, 15 (2000) 73-81.
[30] R.B. Pernites, C.M. Santos, M. Maldonado, R.R. Ponnapati, D.F. Rodrigues, R.C. Advincula, Tunable protein and bacterial cell adsorption on colloidally templated superhydrophobic polythiophene films, Chemistry of Materials, 24 (2011) 870-880.
[31] M.P. Sousa, J.o.F. Mano, Superhydrophobic paper in the development of disposable labware and lab-on-paper devices, ACS Applied Materials & Interfaces, 5 (2013) 3731-3737.
[32] X. Zhao, Y. Su, Y. Li, R. Zhang, J. Zhao, Z. Jiang, Engineering amphiphilic membrane surfaces based on PEO and PDMS segments for improved antifouling performances, Journal of Membrane Science, 450 (2014) 111-123.

[33] R. Revanur, B. McCloskey, K. Breitenkamp, B.D. Freeman, T. Emrick, Reactive amphiphilic graft copolymer coatings applied to poly (vinylidene fluoride) ultrafiltration membranes, Macromolecules, 40 (2007) 3624-3630.
[34] C. Van Oss, R. Good, M. Chaudhury, Mechanism of DNA (Southern) and protein (Western) blotting on cellulose nitrate and other membranes, Journal of Chromatography A, 391 (1987) 53-65.
[35] C. Van Oss, R. Good, M. Chaudhury, Additive and nonadditive surface tension components and the interpretation of contact angles, Langmuir, 4 (1988) 884-891.
[36] C. Van Oss, Acid—base interfacial interactions in aqueous media, Colloids and Surfaces A: Physicochemical and Engineering Aspects, 78 (1993) 1-49.
[37] Q. Wang, Z. Wang, C. Zhu, X. Mei, Z. Wu, Assessment of SMP fouling by foulant–membrane interaction energy analysis, Journal of membrane science, 446 (2013) 154-163.
[38] H. Sun, COMPASS: an ab initio force-field optimized for condensed-phase applications overview with details on alkane and benzene compounds, The Journal of Physical Chemistry B, 102 (1998) 7338-7364.
[39] H. Sun, P. Ren, J. Fried, The COMPASS force field: parameterization and validation for phosphazenes, Computational and Theoretical Polymer Science, 8 (1998) 229-246.
[40] H. Sun, Z. Jin, C. Yang, R.L. Akkermans, S.H. Robertson, N.A. Spenley, S. Miller, S.M. Todd, COMPASS II: extended coverage for polymer and drug-like molecule databases, Journal of Molecular Modeling, 22 (2016) 47.
[41] H.-C. Flemming, Reverse osmosis membrane biofouling, Experimental Thermal and Fluid Science, 14 (1997) 382-391.
[42] H.-L. Yang, J. Chun-Te Lin, C. Huang, Application of nanosilver surface modification to RO membrane and spacer for mitigating biofouling in seawater desalination, Water Research, 43 (2009) 3777-3786.
[43] M.A. Saad, Biofouling prevention in RO polymeric membrane systems, Desalination, 88 (1992) 85-105.
[44] M.O. Saeed, A. Jamaluddin, I. Tisan, D. Lawrence, M. Al-Amri, K. Chida, Biofouling in a seawater reverse osmosis plant on the Red Sea coast, Saudi Arabia, Desalination, 128 (2000) 177-190.
[45] C. Liu, J. Lee, J. Ma, M. Elimelech, Antifouling thin-film composite membranes by controlled architecture of zwitterionic polymer brush layer, Environmental Science & Technology, 51 (2017) 2161-2169.
[46] M. He, K. Gao, L. Zhou, Z. Jiao, M. Wu, J. Cao, X. You, Z. Cai, Y. Su, Z. Jiang, Zwitterionic materials for antifouling membrane surface construction, Acta Biomaterialia, 40 (2016) 142-152.

[47] M.D. Dimitriou, Z. Zhou, H.-S. Yoo, K.L. Killops, J.A. Finlay, G. Cone, H.S. Sundaram, N.A. Lynd, K.P. Barteau, L.M. Campos, A general approach to controlling the surface composition of poly (ethylene oxide)-based block copolymers for antifouling coatings, Langmuir, 27 (2011) 13762-13772.
[48] A.E. Contreras, Z. Steiner, J. Miao, R. Kasher, Q. Li, Studying the role of common membrane surface functionalities on adsorption and cleaning of organic foulants using QCM-D, Environmental Science & Technology, 45 (2011) 6309-6315.
[49] J. Wu, A.E. Contreras, Q. Li, Studying the impact of RO membrane surface functional groups on alginate fouling in seawater desalination, Journal of Membrane Science, 458 (2014) 120-127.
[50] L.D. Nghiem, P.J. Coleman, C. Espendiller, Mechanisms underlying the effects of membrane fouling on the nanofiltration of trace organic contaminants, Desalination, 250 (2010) 682-687.
[51] S. Lee, S. Kim, J. Cho, E.M. Hoek, Natural organic matter fouling due to foulant–membrane physicochemical interactions, Desalination, 202 (2007) 377-384.

Chapter 6

Conclusion

Fresh water is absolutely imperative for living beings. Nevertheless, the fresh water which we can use is less than 1% of water on the earth. The demand for freshwater has been increasing owing to rapid increase of population, and increase of human activities. On the other hand, the fresh water resources have been decreasing due to the contamination of resources, the global warming and so on. Thus, it is emergent issue to produce fresh water from waste water and/or seawater in order to solve the water scarcity issues. Among various water treatment processes, membrane process is one of the potential methods for high quality wastewater treatment and reducing water scarcity. Especially, the reverse osmosis (RO) membrane technology is a promising technology for desalination and wastewater treatment, because of its simplicity, high efficiency, and relatively low energy consumption.

However, fouling, especially biofouling, is a major drawback of RO membrane, which causes the water flux decline, increased energy consumption, and shorter membrane life. Therefore, the objective of this thesis is to improve the anti-biofouling properties of polyamide RO membrane via surface modification using various novel materials. In this thesis, the commercial polyamide RO membrane, ES20 (Nitto Denko Co., Japan) was used as the pristine membrane. The modified membranes were characterized by ATR-FTIR, XPS, water contact angle, ζ-potential, SEM, and AFM. Further, the anti-biofouling properties were evaluated by

static bacterial adhesion and dynamic biofouling filtration tests. The results described in Chapters 2-5 are summarized as below.

6.1. Zwitterionic polymer modification of polyamide reverse osmosis membranes via surface amination and atom transfer radical polymerization for anti-biofouling

This chapter describes an effective pretreatment method to immobilize SI-ATRP initiators on the surface of polyamide RO membranes and the effect of the polymer main chain length on the biofouling behavior. Firstly, RO membrane surfaces were aminated with 3-aminopropyltrimethoxysilane (APTS). Then, α-bromoisobutyryl bromide (BIBB), an acyl halide-type SI-ATRP initiator, was reacted with the APTS layer. A zwitterionic polymer, poly[(2-methacryloyloxy)ethyl]dimethyl[3-sulfopropyl]ammonium hydroxide (pMEDSAH), was then grafted on the membrane surface via SI-ATRP.

The APTS treatment effectively introduced amino groups on the polyamide layer of the RO membrane and facilitated the immobilization of an SI-ATRP initiator (BIBB), while maintaining the water flux and salt rejection properties of the pristine membrane. A zwitterionic polymer, pMEDSAH, was grafted on the surface of BIBB-immobilized membranes and its main chain length was found to increase with the polymerization time. pMEDSAH grafting enhanced the surface hydrophilicity and changed the surface to a smoother and denser morphology. The hydrophilicity and static bacterial adhesion of the membranes was improved by increasing the polymerization time. The dynamic biofouling tests showed that biofilm formation and biofouling were effectively prevented by the pMEDSAH grafting and the increase of polymerization time.

The strategy using APTS treatment is applicable for facilitating the SI-ATRP initiator immobilization on less reactive surfaces of commercial RO membranes maintaining the permeation properties. Furthermore, this study not only demonstrated the great potential of the

zwitterionic polymer modification of RO membranes for the biofouling prevention, but also clarified that the control of the pMEDSAH main chain length was necessary to obtain the best performance for the improvement of the anti-biofouling property.

6.2. Effect of polymer structure modified on RO membrane surfaces via surface-initiated ATRP on dynamic biofouling behavior

In this chapter, the features of various hydrophilic polymers were systematically characterized and the effect of polymer structure on biofouling behavior of polyamide RO membranes was assessed. First, pHEMA, polyPEG (pPEG), and pMEDSAH were grafted on polyamide RO membranes surface via the SI-ATRP method. In order to isolate the effect of the main chain length, grafting density was fixed by using the same concentration of the initiator, and different SI-ATRP polymerization time was applied for merely controlling the main chain length of the grafted polymer on the membrane surfaces.

To assess the grafted polymer structure, the surface chemical properties of the modified membranes were analyzed by using ATR-FTIR and XPS. Thickness of the active layer and surface roughness were evaluated by SEM and AFM, respectively. Furthermore, molecular dynamics (MD) simulation was used for determining side chain length and hydrogen number of given polymers with water molecules. To evaluate biofouling behavior of grafted membranes, a static bacterial adhesion test and a dynamic biofouling filtration test were conducted.

As a result, the pHEMA-grafted membrane was relatively ineffective at preventing biofouling, due to the relatively weaker hydration and lower flexibility, while the combined features of pPEG with long side chains and a hydration layer effectively prevented biofouling even with short main chain length. The combination of strong hydration and proper main chain length is the main contribution to the anti-biofouling propensity of a zwitterionic polymer,

pMEDSAH. This research provides useful information on biofouling behavior on the surface of various polymers, that is, not only the main chain length but also the side chain and hydration state should be taken into account for developing anti-biofouling membranes.

6.3. Improved anti-biofouling performance of polyamide reverse osmosis membranes modified with a polyampholyte with effective carboxyl anion and quaternary ammonium cation ratio

A polyampholyte composed of anionic 2-carboxyethyl acrylate (CAA) and cationic [2-(acryloyloxy)ethyl] trimethyl ammonium chloride (TMA) was applied for improving the anti-biofouling properties of polyamide RO membranes. To elucidate the effect of the monomer ratio of the grafted polyampholyte, several types of p(CAA-co-TMA) polyampholytes were grafted on the RO membrane surface, and the anti-biofouling properties were evaluated by protein adsorption, static bacterial attachment, and long-term dynamic biofouling filtration experiments.

It was found that the CAA/TMA surface ratio was directly proportional but not identical to the feed ratio. The modified RO membrane with 1:1 CAA/ TMA surface ratio, fabricated from a mixed monomer solution with 3:1 CAA/TMA ratio, had nearly zero net surface charge above pH 6 and showed an excellent anti-biofouling performance even in long-term dynamic biofouling filtration tests. This is due to the highly hydrophilic character of the surface (originating from its large content of ionic groups) and also to the almost complete absence of electrostatic attraction with charged bacteria, because the net surface charge is close to zero.

Moreover, in the presence of a strong electrostatic attraction between membrane surface and foulants, biofouling took place even for a membrane surface with very high hydrophilicity. On the other hand, in the absence of electrostatic attraction between membrane surface and foulants, the anti-biofouling properties were determined by the hydrophilicity of the membrane.

6.4. Antifouling polyamide reverse osmosis membranes with multi-defense properties by controllably constructing amphiphilic diblock copolymer brush layer

A controllable architecture of amphiphilic diblock copolymer was well constructed for the polyamide RO membranes to integrate both "fouling resistance" and "fouling release" properties. To prepare this amphiphilic RO membrane, two materials were sequentially grafted on polyamide RO membrane surfaces via dual SI-ATRP: zwitterionic polymer, poly(2-(methacryloyloxy)ethyl-dimethyl-(3-sulfopropyl) ammonium hydroxide) (pMEDSAH) with strong hydrophilicity and poly(2,2,2-trifluoroethyl methacrylate) (pTFEMA) with low surface energy.

To characterize the amphiphilic diblock copolymer modified membranes, the measurements of contact angle, ζ-potential, XPS, and energy dispersive X-ray spectrometry (EDS) mapping were carried out. The fouling resistant and fouling release properties of these modified membranes were extensively investigated by static bacterial adhesion and long-term dynamic filtration tests using sodium alginate for organic fouling, and bacterial suspension for biofouling.

The resultant amphiphilic RO membrane effectively resisted the foulants of the sodium alginate and bacteria, because the strong hydrophilicity of pMEDSAH segments imparted the modified membrane surfaces with a lower hydration energy, which thereby facilitated the formation of a tighter hydration layer to avoid nonspecific foulant adsorption on membrane surfaces. Furthermore, the water flux through amphiphilic RO membrane could be satisfactorily recovered after simple physical cleaning because the pTFEMA segment could lower the surface energy, which weakened the interaction between the foulant and the membrane surface. Therefore, the rational construction of pMEDSAH and pTFEMA segments could confer both fouling resistant and the fouling release properties to the membrane surfaces, providing a versatile solution for designing novel antifouling membranes

Publication list

Chapter 2:

Z. Yang, D. Saeki, H. Matsuyama, Zwitterionic polymer modification of polyamide reverse-osmosis membranes via surface amination and atom transfer radical polymerization for anti-biofouling, Journal of Membrane Science, 550, 332-339, 2018, https://doi.org/10.1016/j.memsci.2018.01.001

Chapter 3:

Z. Yang, D. Saeki, H. C. Wu, T. Yoshioka, H. Matsuyama, Effect of polymer structure modified on RO membrane surfaces via surface-initiated ATRP on dynamic biofouling behavior. Journal of Membrane Science, 582, 111-119, 2019, https://doi.org/10.1016/j.memsci.2019.03.094

Chapter 4:

Z. Yang, D. Saeki, R. Takagi, H. Matsuyama, Improved anti-biofouling performance of polyamide reverse osmosis membranes modified with a polyampholyte with effective carboxyl anion and quaternary ammonium cation ratio. Journal of Membrane Science, 595, 117529, 2020, https://doi.org/10.1016/j.memsci.2019.117529

Chapter 5:

Z. Yang, X.Y. Zhang, M. Xie, H.C. Wu, T. Yoshioka, D. Saeki, H. Matsuyama, Antifouling polyamide reverse osmosis membranes with multi-defense properties by controllably constructing amphiphilic diblock copolymer brush layer. To be submitted.

Doctoral Dissertation, Kobe University
“Study on surface modification of RO membrane for improvement of anti-biofouling property (耐バイオファウリング性の向上を目的とした RO 膜の表面修飾に関する研究)”, 184 pages
Submitted on January, 21, 2020
The date of publication is printed in cover of repository version published in Kobe University Repository Kernel.